

THEORY OF SHIFTS, SHOCKS, AND THE INTIMATE CONNECTIONS TO L^2 -TYPE A POSTERIORI ERROR ANALYSIS OF NUMERICAL SCHEMES FOR HYPERBOLIC PROBLEMS

JAN GIESSELMANN AND SAM G. KRUPA

ABSTRACT. In this paper, we develop a posteriori error estimates for numerical approximations of scalar hyperbolic conservation laws in one space dimension. We develop novel quantitative partially L^2 -type estimates by using the theory of shifts, and in particular, the framework for proving stability first developed in [Krupa-Vasseur. On uniqueness of solutions to conservation laws verifying a single entropy condition. *J. Hyperbolic Differ. Equ.*, 2019]. In this paper, we solve two of the major obstacles to using the theory of shifts for quantitative estimates, including the change-of-variables problem and the loss of control on small shocks.

Our methods have no inherit small-data limitations. Thus, our hope is to apply our techniques to the systems case to understand the numerical stability of large data. There is hope for our results to generalize to systems: the stability framework [Krupa-Vasseur. On uniqueness of solutions to conservation laws verifying a single entropy condition. *J. Hyperbolic Differ. Equ.*, 2019] itself has been generalized to systems [Chen-Krupa-Vasseur. Uniqueness and weak-BV stability for 2×2 conservation laws. *Arch. Ration. Mech. Anal.*, 246(1):299–332, 2022]. Moreover, we are careful not to appeal to the Kruzhkov theory for scalar conservation laws. Instead, we work entirely within the context of the theory of shifts and a -contraction – and these theories apply equally to systems.

We present a MATLAB numerical implementation and numerical experiments. We also provide a brief introduction to the theory of shifts and a -contraction.

CONTENTS

1.	Introduction	2
2.	Statement of result and basic concepts	7
2.1.	A high-level overview of the proof of Theorem 2.2 (Main Theorem)	14
3.	A brief introduction to the theory of shifts, a -contraction, and an overview of our proof	16
3.1.	Shifts and a -contraction	16

Date: June 13, 2023.

2010 Mathematics Subject Classification. Primary 35L65; Secondary 35L45, 35L67, 65M15, 65M08.

Key words and phrases. Conservation laws, entropy conditions, entropy solutions, shocks, a posteriori error estimates, finite volume schemes, discontinuous Galerkin schemes.

Acknowledgment. This material is based upon work supported by the National Science Foundation under Grant No. DMS-1926686. The authors are grateful for financial support by the German Science Foundation (DFG) via grant TRR 154 (*Mathematical modelling, simulation and optimization using the example of gas networks*), project C05.

3.2.	Uniqueness via shifts	18
3.3.	More details on shifts in the scalar case	19
3.4.	Difficulties in deriving quantitative stability results	20
3.5.	A strategy for obtaining quantitative stability estimates	20
4.	Technical preliminary	23
4.1.	Front tracking estimate	24
4.2.	Control on Lipschitz constant of a smooth solution	27
4.3.	Extending the relative entropy inequality	28
4.4.	Control on shifts	29
4.5.	Pointwise difference between two solutions	29
4.6.	L^∞ -control on numerical solutions	30
5.	Construction of \hat{u} and $\hat{\psi}$	32
5.1.	Construction of \hat{u}	33
5.2.	Construction of $\hat{\psi}$	38
6.	Algorithm for controlling shifts	39
6.1.	Controlling Δ_i of ‘large’ shocks	39
6.2.	Algorithm for bounding (6.3) and (6.4)	41
6.3.	Determining when shocks have collided in $\hat{\psi}$	43
6.4.	Improved control on ‘front tracking’ shocks	46
6.5.	Control on the ‘boundary’ shocks	58
7.	The L^2 estimate and dissipation calculations	62
7.1.	Step 1: proof of (2.13)	62
7.2.	Step 2A: calculation of dissipation due to shifting	65
7.3.	Step 2B: proof that (6.1) is upper bound	66
8.	Proof of Theorem 2.3	69
9.	Expected convergence of estimator	70
9.1.	‘Large’ shocks	70
9.2.	‘Front tracking’ shocks	71
10.	Numerical experiments	73
10.1.	Experiment with ‘large’ shocks only	73
10.2.	Experiment including a rapidly decreasing piece	74
	Appendix A.	77
A.1.	Defining the extensions to make the v_i^0 .	77
A.2.	Proof of Lemma 4.3	81
	References	84

1. INTRODUCTION

In this paper, we study the scalar conservation law in one space dimension:

$$(1.1) \quad \begin{cases} \partial_t u + \partial_x A(u) = 0, & \text{for } x \in \mathbb{R}, t > 0, \\ u(x, 0) = u^0(x) \end{cases}$$

where $u: \mathbb{R} \times [0, T) \rightarrow \mathbb{R}$ is the unknown, $u^0 \in L^\infty(\mathbb{R})$ is the given initial data, and $A: \mathbb{R} \rightarrow \mathbb{R}$ is the given *flux function*. In this paper, we only consider $A \in C^2(\mathbb{R})$ which are strictly convex. A *classical* solution to (1.1) is a locally Lipschitz function $u: \mathbb{R} \times [0, T) \rightarrow \mathbb{R}$ which satisfies $\partial_t u + \partial_x A(u) = 0$ almost everywhere and verifies $u(x, 0) = u^0(x)$ for all $x \in \mathbb{R}$. We are also concerned with *weak solutions* to (1.1). A weak solution is a locally bounded and measurable function $u: \mathbb{R} \times [0, T) \rightarrow \mathbb{R}$ which verifies

$$(1.2) \quad \int_0^\infty \int_{-\infty}^\infty \partial_t \phi u + \partial_x \phi A(u) \, dx dt + \int_{-\infty}^\infty \phi(x, 0) u^0(x) \, dx = 0$$

for every Lipschitz-continuous function $\phi: \mathbb{R} \times [0, T) \rightarrow \mathbb{R}$ with compact support. In particular, every weak solution is a distributional solution to (1.1). Remark also that every classical solution is also a weak solution.

A pair of functions $\eta, q: \mathbb{R} \rightarrow \mathbb{R}$ are called an *entropy* and *entropy-flux*, respectively, for the system (1.1) if

$$(1.3) \quad q'(u) = \eta'(u)A'(u).$$

We say a weak solution to (1.1) is *entropic* for the entropy η if it satisfies the *entropy inequality*

$$(1.4) \quad \partial_t \eta(u) + \partial_x q(u) \leq 0$$

in the sense of distributions, where q is any corresponding entropy-flux. More precisely,

$$(1.5) \quad \int_0^\infty \int_{-\infty}^\infty \partial_t \phi \eta(u) + \partial_x \phi q(u) \, dx dt + \int_{-\infty}^\infty \phi(x, 0) \eta(u^0(x)) \, dx \geq 0$$

for every nonnegative Lipschitz-continuous function $\phi: \mathbb{R} \times [0, T) \rightarrow \mathbb{R}$ with compact support

We have in mind future applications to hyperbolic systems with multiple conserved quantities. Hyperbolic conservation laws are an important class of models in many physical and engineering applications. One example is the description of non-viscous compressible flows by the Euler equations. One particular feature of hyperbolic conservation laws that makes their analysis and the construction of reliable numerical schemes challenging is that they, in general, only have smooth solutions up to some finite time. Several successful schemes were developed so far and are mainly based on finite differences, finite volume and discontinuous Galerkin (dG) finite element schemes. For an overview on these schemes and the available convergence analysis we refer to [22, 30, 41, 27] and references therein.

For nonlinear hyperbolic conservation laws, analysis of systems is much more involved than the analysis of scalar problems. The main difference is that for scalar problems

there exist infinitely many entropies that gives rise to a rather restrictive class of entropy (weak) solutions for which existence and uniqueness of solutions as well as an L^1 contraction property can be shown. In contrast, systems are often only endowed with one entropy/entropy-flux pair due to the compatibility condition (1.3) being overdetermined in the systems case (for integrability conditions on the entropy, see [11, p. 13-14] and [11, p. 54-55]). For many physical systems only one entropy exists; therefore existence and uniqueness of entropy solutions are delicate issues.

Indeed, for systems in multiple space dimensions it can be shown via the technique of convex integration that for some set of initial data entropy solutions are not unique [6, 13]. On the other hand, in one space dimension Bressan and coworkers [1, 3] have shown that for small- BV initial data global entropy solutions exist and satisfy L^1 stability estimates in the class of small- BV solutions.

Given a classical solution \bar{u} to a conservation law, and a weak solution u which is entropic for a strictly convex entropy, the weak-strong stability theory of Dafermos [9, 10] and DiPerna [16] gives L^2 -type stability estimates between u and \bar{u} . Expanding on the theory of relative entropy, the theory of shifts [50] and a -contraction theory [29] have allowed for the method of relative entropy to consider the stability of solutions from a larger class. More recently, the theory of shifts and a -contraction theory have become sufficiently developed to allow for the stability of the well-known small- BV solutions [3] to be studied among solutions from the much larger class of solutions taking possibly very large values in L^2 [5]. The theory of shifts and a -contraction will be explained in more detail in Section 3.

In the convergence analysis of numerical schemes, two main classes of error estimates need to be distinguished: *a priori* and *a posteriori* estimates. *A priori* estimates aim at providing bounds for errors of numerical schemes that only depend on mesh width and features of the exact solution. In contrast, *a posteriori* estimates require computing the numerical solution but are independent of (usually unknown) quantities such as norms of exact solutions. In *a posteriori* estimates, it is desirable that the error estimate is *reliable* which means that the estimator is an upper bound of the error (i.e. of some norm of the difference of exact and numerical solution) and *efficient* which means that some (fixed) multiple of the error estimator is also a lower bound for the error. In the context of numerical schemes for hyperbolic conservation laws efficiency of estimators seems out of reach and we will settle for a weaker property – see the discussion in Section 9.

There are also some ‘intermediate’ classes of estimates where *a priori* convergence is guaranteed if some criterion that can only be verified *a posteriori*, i.e. once the numerical solution has been computed, is satisfied [2]. Indeed, interesting recent work by Bressan-Chiri-Shen [2] shows that if numerical solutions from a rather general class of numerical schemes satisfy an *a posteriori* stability condition and have bounded total variation then they converge in $L^\infty(0, T; L^1(\mathbb{R}))$ to the exact solution. Indeed, the results in [2] provide error bounds that are related to the consistency error in the $L^1(0, T; W^{-1,1}(\mathbb{R}))$ norm. Instead of providing *a priori* bounds for these consistency errors for specific schemes (as was done in [2]) one can also compute them *a posteriori* (for a wider variety of numerical

schemes) – which is being done in the recent preprint [21]. For a comparison of convergence rates of error estimators see Sections 9.1 and 9.2.

The first systematic a posteriori analysis for numerical approximations of scalar conservation laws, accompanied with corresponding adaptive algorithms, can be traced back to [31, 25] (see also [7, 15] and references therein). These estimates were derived by employing Kruzhkov’s doubling of variables technique using an infinite family of entropies [36]. A posteriori results for systems were derived in [38, 37] for front tracking and Glimm’s schemes. Goal oriented estimates, based on dual weighted residuals, have been investigated in [26]. However, the goal oriented estimates require the solving of dual problems that consist of advection equations with discontinuous velocity fields. Their well-posedness theory is only understood for scalar problems in one space dimension [48], so that for discontinuous numerical solutions to systems of conservation laws the well-posedness of dual problems is unclear and, therefore, dual weighted residual-type estimates cannot be proven to be reliable.

We would like to mention recent a priori convergence results on numerical schemes for systems of hyperbolic conservation laws: In [18] convergence of finite volume schemes to so-called dissipative solutions is shown while in [19] convergence to statistical solutions is proven. Both results are based on compactness arguments so that no quantitative information on the size of the error can be extracted. Indeed, quantitative information on the size of the error seems too much to ask for in this context since there is no uniqueness of solutions.

The goal of the work at hand is to provide reliable a posteriori error estimates for Runge-Kutta discontinuous Galerkin schemes for scalar conservation laws in one space dimension. We do not use the Kruzhkov stability theory for scalar conservation laws. Instead, we use the theory of shifts and a -contraction. These techniques naturally require only a single entropy condition and apply to scalar equations as well as systems. Thus, there is hope that the techniques developed in this paper will extend to systems. This is in contrast to the results in [31, 15] that use techniques that are systematically limited to scalar problems. Our approach follows the general ideas of reconstruction-based a posteriori error estimates as outlined in [43]. The fundamental idea is to compute a reconstruction of the numerical solution that satisfies all conditions necessary so that its difference to the exact solution can be bounded in terms of the residual, which is the non-zero right-hand side of (1.1) obtained as ‘error’ when the solution is inserted into the PDE, using some appropriate stability theory (that is the theory of shifts and a -contraction in our case). Our approach is similar to the one used in [14, 20] that was based on the original relative entropy stability estimates of Dafermos and DiPerna. *However, our results in the present paper improve upon those in [14, 20] as we provide an estimator that is convergent post shock formation.* This is intimately linked with the ability of the theory of shifts to consider solutions from a broader class than the original weak-strong theory. In particular, the theory of shifts is not restricted to studying the stability of a classical solution \bar{u} among the class of weak solutions u , but can in fact allow for arbitrarily many shocks to exist in the otherwise classical solution \bar{u} .

As discussed above, the methods of theory of shifts and a -contraction are well-known to have no small-data limitations, and in particular are able to study large shocks (see e.g. [40, 29]). Thus, the goal of future work is to push forward the ideas and results in the present paper to the systems case with multiple conserved quantities. In this way, we hope to study a posteriori stability of large-data solutions to hyperbolic systems. This is an exciting direction for research as the current state of the art for the numerical analysis of hyperbolic systems is largely limited to the case of small- BV solutions due to limitations in the current L^1 -based theory (e.g. [1, 3]).

Using the theory of shifts comes with some cost though. As mentioned above, the theory of shifts allows us to generalize the relative entropy theory to allow for shocks in an otherwise smooth solution \bar{u} . Thus, the core of our proof involves piecewise-smooth approximate solutions. However, the theory of shifts must allow for the discontinuities in \bar{u} to move in largely unpredictable ways, not necessarily following the Rankine-Hugoniot jump condition (see Section 3 for more on this). The cost is: due to the uncertainty in shock position, we are required to numerically simulate extensions for each of the continuous pieces of \bar{u} . These extensions are global in space and time.

As a consequence, we need to solve not one initial value problem numerically but as many as there are discontinuities in the initial data and we need to track approximate positions and position error bounds for each discontinuity so that we know which numerical solution might be revealed where and when, in comparison with the exact solution. This might seem like a huge computational burden severely increasing computational cost but since all the individual solutions will remain smooth we may use high order numerical schemes without stabilization mechanisms which mitigates the increase in computational costs. For each of the numerical solutions we will use reconstructions as described in [14, 20] since (for certain classes of numerical fluxes) they lead to residuals that scale optimally with mesh width for smooth solutions.

Indeed, for initial data that consists of smooth, increasing pieces with down jumps in between we obtain a posteriori error estimates where the estimators are $\mathcal{O}(h)$ for first order finite volume schemes on meshes with mesh width h . Then, let us for a moment consider numerical schemes on meshes that move such that any nondifferentiable points in our solution are always aligned with some cell boundary of the mesh. Then, for initial data that also contain (smooth) decreasing pieces our error estimators are $\mathcal{O}(h^{1/3})$. For more details, see Section 9. Known a posteriori error estimators (for first order finite volume schemes) are of order $\mathcal{O}(h^{1/2})$ for scalar problems [31]. Remark that for systems in one space dimension, Bressan-Chiri-Shen gives an a posteriori error estimator of order $\mathcal{O}(h^{1/3})$ [2].

The remainder of this paper is organized as follows: in Section 2 we introduce basic concepts and present our main results. In Section 3, we give a brief introduction to the key ideas behind the theory of shifts and a -contraction, and we present a more detailed overview of our proof. In Section 4, we give some technical lemmas we will need. Section 5 is devoted to the description of our numerical scheme and the construction of the key ancillary function $\hat{\psi}$. In Section 6 we describe our error estimator. In Section 7, we collect

the key calculations used in our error estimator (including the proof of our essential estimate (2.13), below). In Section 8, we prove Theorem 2.3. Section 9 is devoted to heuristics of the expected convergence behavior of our error estimator when using dG schemes with polynomials of degree 0 and an upwind type numerical flux. Finally, in Section 10 we introduce the MATLAB implementation of our numerical scheme and associated error estimator and give the results of numerical experiments.

2. STATEMENT OF RESULT AND BASIC CONCEPTS

We are concerned with approximate solutions \hat{u} to our conservation law, i.e. $\hat{u}: \mathbb{R} \times [0, T) \rightarrow \mathbb{R}$ for some $T > 0$ that are obtained by gluing together approximate solutions that are in turn obtained from Lipschitz-continuous reconstructions of numerical solutions (analogously to what was done in [20, 14]). The gluing process allows \hat{u} to have downward jumps and this is why we are able to obtain much stronger results than those that were obtained in [20, 14].

Throughout this paper, we will consider initial data in the following two forms. The first form is the one required for the exact initial data

$$(2.1) \quad \mathcal{S}^\epsilon := \{v \in L^\infty(\mathbb{R}) : \exists N \in \mathbb{N}, -\infty = x_0 < x_1 < \dots < x_N < x_{N+1} = +\infty : \text{for } i = 0, \dots, N, \\ v'(x) \text{ exists and is uniformly continuous for } x \in (x_i, x_{i+1}), v(x_i-) \geq v(x_i+) \\ \text{(when } i \neq 0), \text{ and exactly one of two cases hold: either for all } x \in (x_i, x_{i+1}), \\ \text{we have } \partial_x v|_{(x_i, x_{i+1})} > -\epsilon \text{ or for all } x \in (x_i, x_{i+1}), \text{ we have } \partial_x v|_{(x_i, x_{i+1})} \leq -\epsilon. \\ \text{Lastly, if } v|_{(x_i, x_{i+1})} > -\epsilon \text{ and } v|_{(x_{i+1}, x_{i+2})} > -\epsilon, \\ \text{then } v(x_{i+1}-) > v(x_{i+1}+) \text{ (for } i \neq N)\},$$

where $\epsilon > 0$ is a number that is fixed from now on and needs to be chosen such that up to a (fixed) time $T > 0$ no slopes form which are less than -1 , from any initial data with slope $> -\epsilon$. Notice there are no smallness assumptions for the class of functions \mathcal{S}^ϵ .

For a function $v \in \mathcal{S}^\epsilon$, we will call it *rapidly decreasing* on intervals (x_i, x_{i+1}) where $\partial_x v|_{(x_i, x_{i+1})} \leq -\epsilon$ and *nearly non-decreasing* on intervals where $\partial_x v|_{(x_i, x_{i+1})} > -\epsilon$. See Figure 1.

Remark that because $\mathcal{S}^\epsilon \subset L^\infty(\mathbb{R})$, we must have that for $v \in \mathcal{S}^\epsilon$, v is nearly non-decreasing on the intervals (x_0, x_1) and (x_N, x_{N+1}) (where the $x_0 < x_1 < \dots < x_{N+1}$ are in the context of (2.1)).

The second form is what we require for the initial data of the reconstructed numerical solution.

$$(2.2) \quad \mathcal{S}_d^\epsilon := \{v \in L^\infty(\mathbb{R}) : \exists N \in \mathbb{N}, -\infty = x_0 < x_1 < \dots < x_N < x_{N+1} = +\infty : \text{for } i = 0, \dots, N, \\ v'(x) \text{ exists and is uniformly continuous for } x \in (x_i, x_{i+1}), \\ \partial_x v|_{(x_i, x_{i+1})} > -\epsilon, \text{ and } v(x_i-) > v(x_i+)\}$$

This is closely related to the function space that is considered in [34] for sequences of approximate solutions.

Note that \mathcal{S}^ϵ is a larger space than \mathcal{S}_d^ϵ since some of the pieces are allowed to decrease strongly. Note also that functions in \mathcal{S}_d^ϵ are dense in \mathcal{S}^ϵ (in the L^p_{loc} topology, $1 \leq p < \infty$). This can be seen by approximating the rapidly decreasing parts by piecewise-constant functions.

Following the general theory of shifts and a -contraction, we study solutions to (1.1) among the class of functions verifying a Strong Trace Property (first introduced in [40]):

Definition 2.1 (Strong Trace Property). Fix $T > 0$. Let $u: \mathbb{R} \times [0, T) \rightarrow \mathbb{R}$ verify $u \in L^\infty(\mathbb{R} \times [0, T))$. We say u has the *Strong Trace Property* if for every fixed Lipschitz-continuous map $h: [0, T) \rightarrow \mathbb{R}$, there exists $u_+, u_-: [0, T) \rightarrow \mathbb{R}$ such that

$$(2.3) \quad \lim_{n \rightarrow \infty} \int_0^{t_0} \operatorname{ess\,sup}_{y \in (0, \frac{1}{n})} |u(h(t) + y, t) - u_+(t)| dt = \lim_{n \rightarrow \infty} \int_0^{t_0} \operatorname{ess\,sup}_{y \in (-\frac{1}{n}, 0)} |u(h(t) + y, t) - u_-(t)| dt = 0$$

for all $t_0 \in (0, T)$.

E.g., a function $u \in L^\infty(\mathbb{R} \times [0, T))$ satisfies the Strong Trace Property if, for each fixed h , the right and left limits

$$(2.4) \quad \lim_{y \rightarrow 0^+} u(h(t) + y, t) \quad \text{and} \quad \lim_{y \rightarrow 0^-} u(h(t) + y, t)$$

exist for almost every t . Specifically, a function $u \in L^\infty(\mathbb{R} \times [0, T))$ has the strong traces according to Definition 2.1 if u has a representative that is in BV_{loc} . However, the Strong Trace Property is weaker than BV_{loc} . Remark that if a weak solution u to (1.1) verifies the entropy inequality (1.5) for *every* convex entropy function η (and associated entropy-flux q), then classically it is known that $u(\cdot, t)$ instantaneously regularizes to BV_{loc} for every $t > 0$ (see e.g. [11, 46]), and thus the Strong Trace Property is verified. However, *nota bene*: in the present paper we are assuming very little on weak solutions u to (1.1), in particular only verifying (1.5) for one convex entropy, in analogy with the systems case, and thus *we do not have the classical theory available to us*.

We can now summarize some of our main results.

Theorem 2.2 (Main Theorem). *Fix $T > 0$. Then choose $\epsilon > 0$ such that smooth solutions to (1.1) with initial data whose slope is at least $-\epsilon$ do not form slopes less than -1 (and in particular do not form discontinuities) on the time interval $[0, T]$.*

Let \bar{u} be an exact solution to our conservation law (1.1) with initial data $\bar{u}^0 \in \mathcal{S}^\epsilon$. Assume \bar{u} verifies the entropy inequality (1.5) for the strictly convex entropy $\eta \in C^2(\mathbb{R})$. Assume also that \bar{u} verifies the Strong Trace Property (Definition 2.1).

Recalling that $\bar{u}^0 \in \mathcal{S}^\epsilon$, let $\bar{N} \in \mathbb{N}$ be the minimum integer required within the context of the definition of the space \mathcal{S}^ϵ (this prevents us from needlessly breaking the intervals (x_i, x_{i+1}) into smaller intervals). Then, let $x_1, \dots, x_{\bar{N}}$ denote the points from within the context of the definition of the space \mathcal{S}^ϵ .

Fix a (sufficiently small) parameter $\delta > 0$. Then, there exists $N^\delta \in \mathbb{N}$ and Lipschitz-continuous functions $v_1^\delta, \dots, v_{N^\delta+1}^\delta: \mathbb{R} \times [0, T] \rightarrow \mathbb{R}$ that verify $\partial_t v_i^\delta + \partial_x A(v_i^\delta) = 0$ (for $i = 1, \dots, N^\delta + 1$) and verify the ordering condition $v_i^\delta(x, 0) - v_{i+1}^\delta(x, 0) \geq \frac{1}{2}\epsilon\delta > 0 \forall i$ and $\forall x$.

Then, let the $v_1^\delta, \dots, v_{N^\delta+1}^\delta$ be simulated using a numerical scheme, giving reconstructed Lipschitz-continuous functions $\hat{v}_1^\delta, \dots, \hat{v}_{N^\delta+1}^\delta: \mathbb{R} \times [0, T] \rightarrow \mathbb{R}$. We assume the $\hat{v}_1^\delta, \dots, \hat{v}_{N^\delta+1}^\delta$ also satisfy the ordering condition

$$(2.5) \quad \hat{v}_i^\delta(x, t) > \hat{v}_{i+1}^\delta(x, t) \quad \forall i \text{ and } \forall (x, t),$$

which can be checked a posteriori.

There also exist Lipschitz-continuous curves $\hat{h}_1^\delta, \dots, \hat{h}_{N^\delta}^\delta: [0, T] \rightarrow \mathbb{R}$ that satisfy the ordering condition $\hat{h}_i^\delta(t) \leq \hat{h}_{i+1}^\delta(t) \forall i$ and $\forall t$ and also verify

$$\{x_1, \dots, x_N\} \subset \{\hat{h}_1^\delta(0), \dots, \hat{h}_{N^\delta}^\delta(0)\}.$$

Then, we define the numerical solution to our conservation law,

$$(2.6) \quad \hat{u}^\delta(x, t) := \begin{cases} \hat{v}_1^\delta(x, t) & \text{if } x < \hat{h}_1^\delta(t), \\ \hat{v}_2^\delta(x, t) & \text{if } \hat{h}_1^\delta(t) < x < \hat{h}_2^\delta(t), \\ \vdots & \\ \hat{v}_{N^\delta+1}^\delta(x, t) & \text{if } \hat{h}_{N^\delta}^\delta(t) < x. \end{cases}$$

We similarly define the ancillary function $\hat{\psi}^\delta: \mathbb{R} \times [0, T] \rightarrow \mathbb{R}$,

$$(2.7) \quad \hat{\psi}^\delta(x, t) := \begin{cases} \hat{v}_1^\delta(x, t) & \text{if } x < h_1^\delta(t), \\ \hat{v}_2^\delta(x, t) & \text{if } h_1^\delta(t) < x < h_2^\delta(t), \\ \vdots & \\ \hat{v}_{N^\delta+1}^\delta(x, t) & \text{if } h_{N^\delta}^\delta(t) < x, \end{cases}$$

for Lipschitz-continuous curves $h_1^\delta, \dots, h_{N^\delta}^\delta: [0, T] \rightarrow \mathbb{R}$ that satisfy the ordering condition $h_i^\delta(t) \leq h_{i+1}^\delta(t) \forall i$ and $\forall t$. Furthermore, $\hat{h}_i^\delta(0) = h_i^\delta(0) \forall i$ (and thus $\hat{u}^\delta(\cdot, 0) = \hat{\psi}^\delta(\cdot, 0)$). The h_i^δ are generalized characteristics of the exact solution \bar{u} .

Denote by \mathcal{I}^δ the set of indices belonging to curves \hat{h}_i^δ whose starting point coincides with one of the x_j .

We denote by \mathcal{D} the set of rapidly decreasing parts of \bar{u}^0 .

Then, the distance between \bar{u} and the approximate solution \hat{u}^δ is controlled as follows:

Fix $S > 0$ sufficiently large. First, we have the (obvious) estimate for every L^p space

$$(2.8) \quad \left\| \bar{u}(\cdot, t) - \hat{u}^\delta(\cdot, t) \right\|_{L^p(-S+st, S-st)} \\ \leq \left\| \bar{u}(\cdot, t) - \hat{\psi}^\delta(\cdot, t) \right\|_{L^p(-S+st, S-st)} + \left\| \hat{\psi}^\delta(\cdot, t) - \hat{u}^\delta(\cdot, t) \right\|_{L^p(-S+st, S-st)},$$

where $s > 0$ is the speed of information, a constant depending only on $\|\bar{u}\|_{L^\infty}$, the flux A , and the entropy η .

Furthermore,

$$(2.9) \quad \left\| \hat{\psi}^\delta(\cdot, t) - \hat{u}^\delta(\cdot, t) \right\|_{L^1(-S+st, S-st)} \leq \int_{\mathcal{B}(t)} |\hat{v}_{m(x,t)}^\delta - \hat{v}_{M(x,t)}^\delta| dx + \sum_{d \in \mathcal{D}} \left[\Gamma_d(t) + 2S\Upsilon_d(t) \right],$$

where $\Gamma_d(t)$ is a computable quantity defined in (6.21), $\Upsilon_d(t)$ is a computable quantity defined in (6.20),

$$\mathcal{B}(t) := \{x \in \mathbb{R} : \exists j \in \mathcal{I}^\delta : x \in [\hat{h}_j^\delta(t) - \Delta_j(t), \hat{h}_j^\delta(t) + \Delta_j(t)]\}$$

denotes regions (around the \hat{h}_j^δ , $j \in \mathcal{I}^\delta$) where it is unclear which part of the solution is revealed, and for $x \in \mathcal{B}(t)$

$$(2.10) \quad \mathcal{J}(x, t) := \{j : x \in [\hat{h}_j^\delta(t) - \Delta_j(t), \hat{h}_j^\delta(t) + \Delta_j(t)]\}$$

$$(2.11) \quad m(x, t) := \min\{i \in \mathcal{J}(x, t)\}$$

$$(2.12) \quad M(x, t) := \max\{i \in \mathcal{J}(x, t)\} + 1.$$

In all of the above $\Delta_i(t)$ is a (computable) bound on $|\hat{h}_i^\delta(t) - h_i^\delta(t)|$ (the uncertainty of the position of the i^{th} discontinuity at time t). For formulas for Δ_i , see (6.1), (6.39), and Section 6.4.4.

Finally,

$$(2.13) \quad \left\| \bar{u}(\cdot, t) - \hat{\psi}^\delta(\cdot, t) \right\|_{L^2(-S+st, S-st)}^2 \leq C \left(\left\| \bar{u}(\cdot, 0) - \hat{\psi}^\delta(\cdot, 0) \right\|_{L^2(-S, S)}^2 + \mathcal{R}(t) \right) e^{Ct},$$

with

$$(2.14) \quad \mathcal{R}(t) := \int_0^t \int_{-S+sr}^{S-sr} \max_{i \in \tilde{\mathcal{J}}(x, r)} (R_i^\delta(x, r))^2 dx dr$$

and where

$$(2.15) \quad \tilde{\mathcal{J}}(x, t) := \{j : \hat{h}_j^\delta(t) - \Delta_j(t) < x < \hat{h}_{j+1}^\delta(t) + \Delta_j(t)\}$$

is the set of potentially revealed solutions, and the residuals are defined by

$$(2.16) \quad R_i^\delta := \partial_t \hat{v}_i^\delta + \partial_x A(\hat{v}_i^\delta).$$

The constant $C > 0$ can be explicitly given in terms of $\|\bar{u}\|_{L^\infty}$, the flux A , entropy η and their derivatives and $\left\| \left[\partial_x \Big|_{(x,t)} \eta'(\hat{\psi}^\delta) \right]_- \right\|_{L^\infty(K)}$, where $[\cdot]_- := \min(0, \cdot)$ and $K := \{(x, t) : t \in [0, T), -S + st < x < S - st\}$.

We use the notation Δ_i to denote an upper bound on the difference $\left| \hat{h}_i^\delta(t) - h_i^\delta(t) \right|$ for a shock with position \hat{h}_i^δ in the computer and the corresponding generalized characteristic with position h_i^δ in the corresponding exact solution.

In fact, we are able to prove much more than Theorem 2.2. See Section 6 for a precise discussion of the various quantitative estimates we have on Δ_i for shocks of various sizes.

We implement our scheme (for the construction of \hat{u}) and our error estimator, following the analysis in the present paper, in MATLAB¹.

Remark 1. We will often drop the superscript δ from the \hat{u}^δ , $\hat{\psi}^\delta$, v_i^δ , \hat{v}_i^δ , h_i^δ , \hat{h}_i^δ , N^δ , and R_i^δ .

Remark 2. The expected convergence rate for our a posteriori error estimator differs depending on whether or not the initial data \bar{u}^0 contains a rapidly decreasing piece – even for first order finite volume schemes. In what follows, we will denote the mesh width used in the simulations of the v_i as h and the time step as Δt . We use explicit time-stepping such that the CFL condition implies $\Delta t \lesssim h$. In case the initial data \bar{u}^0 consists only of nearly non-decreasing pieces separated by shocks (with a size independent of h), our error estimator is $\mathcal{O}(h)$ but not $o(h)$ for stable first order schemes and we expect higher order convergence of the estimator for stable higher order schemes and sufficiently smooth (pieces of the) initial data. In contrast, if the initial data \bar{u}^0 contains at least one rapidly decreasing piece we only observe order $h^{1/4}$ scaling of our estimator. This is due to very limited control of shocks originating from the boundary of rapidly decreasing intervals. See Section 9 for more details.

Remark 3. The functions \hat{h}_i^δ are (numerical approximations of) generalized characteristics for the numerical solution \hat{u}^δ . The functions h_i^δ are the corresponding generalized characteristics for the exact solution \bar{u} . The function $\hat{\psi}^\delta$ is the ‘shifted’ version of the numerical solution. It is not necessarily a solution to the conservation law. In particular, its shocks are not necessarily travelling with the correct Rankine-Hugoniot speed.

Remark 4. While for purposes of estimating $\left\| \hat{u}^\delta(\cdot, t) - \hat{\psi}^\delta(\cdot, t) \right\|_{L^2}$ we require that \bar{u} have initial data $\bar{u}^0 \in \mathcal{S}^\epsilon$, the theory of shift techniques we employ require no regularity assumptions on \bar{u} for positive times $t > 0$ besides verifying the Strong Trace Property (Definition 2.1). This is also a general feature of the a -contraction theory for the case of systems of conservation laws: there are no regularity assumptions on the weak, entropic solution in the first slot of the relative entropy $\eta(\cdot|\cdot)$ (the \bar{u} in the context of Theorem 2.2) – see Section 3.1. It is even allowed to take vacuum states [50, 29, 40]. In fact, all of our results hold also for simply $\bar{u}^0 \in L^\infty(\mathbb{R})$. The first step is to approximate \bar{u}^0 in L^2 (on some compact interval) by an element of \mathcal{S}^ϵ (notice \mathcal{S}^ϵ is dense in L^2). However, if we do not assume any additional regularity on \bar{u}^0 besides L^∞ , and in particular $\bar{u}^0 \notin \mathcal{S}^\epsilon$, then we do not have control on the expected convergence rate of our error estimator (see Section 9).

¹See GitLab: <https://git-ce.rwth-aachen.de/jan.giesselmann/shiftsshocksaposteriori.git>

Remark 5. The Strong Trace Property (Definition 2.1) is a standard assumption in the theory of shifts and a -contraction theory. It is an open question whether the Strong Trace Property truly needs to be assumed in the theory of shifts and a -contraction well-posedness theory. Similarly, it is an open question whether solutions automatically regularize enough to attain strong traces. The topic is the focus of much recent work. For the isentropic flow of an ideal gas with $\gamma = 3$, Vasseur [49] is able to show that solutions to this system are regular in time. Further, recent work by Golding [23] shows that for this particular system, L^∞ solutions regularize, such that entropic solutions have significant regularity. However, [23] does not quite show that solutions attain the strong traces (Definition 2.1) we use in the present paper. Other recent work studies whether systems of conservation laws, with one entropy condition, can admit solutions via convex integration [28, 42, 33]. Such solutions, if they exist, will certainly not have the strong traces.

Remark 6. Estimate (2.9) follows by combining our estimates for the uncertainty in shock positions Δ_i with the difference of values of parts that might be revealed in the different solutions; plus estimates from the front tracking theory for the L^1 error in regions where we use wave front tracking.

Remark 7. Note that there are two types of discontinuities in \hat{u}^δ : those that correspond to discontinuities in \bar{u}^0 and those that come from breaking up rapidly decreasing parts of \bar{u}^0 into step functions. The former are ‘large’ in the sense that their size is independent of any discretization parameter. The size of the latter depend on the parameter $\delta > 0$ that we use for approximating the rapidly decreasing parts of the initial data \bar{u}^0 by step functions.

Remark 8. Note that we might need to compute each numerical solution \hat{v}_i^δ on all of the computational domain which makes our approach quite costly. There are two ways in which this can be mitigated: (1) all solutions \hat{v}_i^δ are independent of each other, i.e., computing them in parallel is straightforward; however, information from different solutions needs to be combined to evolve shock curves. Moreover, (2) the simulated numerical solutions result from (nearly) non-decreasing initial data so that we may use higher order schemes without the need to account for shocks. The only constraint on numerical schemes is that we need to reconstruct all numerical solutions in such a way that the global ordering condition $\hat{v}_i^\delta > \hat{v}_{i+1}^\delta$ is maintained (see (2.5) and (A.19)).

Ordering of numerical solutions and their reconstructions \hat{v}_i^δ as well as lower bounds for pointwise differences between different \hat{v}_i^δ is guaranteed *a priori* for monotone finite volume schemes and the reconstructions from [20, 14] but not for higher order schemes. Indeed, in monotone finite volume schemes, the value at time t^{n+1} in the i -th cell, denoted u_i^{n+1} can be expressed as a function

$$u_i^{n+1} = H(u_{i-1}^n, u_i^n, u_{i+1}^n)$$

where each partial derivative of H is non-negative and the sum of partial derivatives is $1 + \mathcal{O}(|u_{i-1}^n - u_i^n| + |u_i^n - u_{i+1}^n|)$. The reconstruction for piece-wise constant schemes simply uses linear interpolation which maintains ordering and gaps.

For higher order schemes and reconstructions the ordering can be verified *a posteriori* since the reconstructions are computed explicitly.

Remark 9. If we can guarantee that each of the reconstructions \hat{v}_i is non-decreasing we can drop the term $\left\| \left[\partial_x \Big|_{(x,t)} \eta'(\hat{\psi}^\delta) \right]_- \right\|_{L^\infty(K)}$, in the statement of the theorem. Otherwise, Lipschitz constants of the \hat{v}_i are a posteriori computable.

Remark 10. It should be noted that our bound on Δ_i (see (6.1), below) depends on \mathcal{R} and the bound on \mathcal{R} in (2.14) depends on the Δ_i . This interdependence can be overcome by first using a very pessimistic bound for the Δ_i and subsequent iteration. Details can be found in Section 6.

We also have the following result on the convergence of our error estimator.

Theorem 2.3 (Convergence of the estimator). *We consider the same assumptions as in Theorem 2.2 above.*

In particular, recall that we fix $\bar{u}^0 \in \mathcal{S}^\epsilon$. Further, we let \bar{u} be an exact solution to our conservation law (1.1) with initial data \bar{u}^0 .

Let $\{\delta_n\}_{n=1}^\infty \subset (0, \infty)$ be a sequence of positive numbers such that $\delta_n \rightarrow 0$ as $n \rightarrow \infty$. Then, for each $n \in \mathbb{N}$, we have, from within the context of Theorem 2.2 above, $N^{\delta_n} \in \mathbb{N}$, $v_1^{\delta_n}(x, t), \dots, v_{N^{\delta_n}+1}^{\delta_n}(x, t)$, as well as the corresponding $\hat{v}_1^{\delta_n}(x, t), \dots, \hat{v}_{N^{\delta_n}+1}^{\delta_n}(x, t)$. We also have the residuals $R_1^{\delta_n}, \dots, R_{N^{\delta_n}+1}^{\delta_n}$.

Then assume there is a constant $c_0 > 0$ (which is uniform in n) such that

$$(2.17) \quad \sup_t \text{Lip}[\hat{v}_i^{\delta_n}(\cdot, t)] \leq \frac{1}{c_0}$$

for all $i \in \mathcal{L}^{\delta_n}$, where $\mathcal{L}^{\delta_n} := \{1, \dots, N^{\delta_n} + 1\}$ is the index set for all the $\hat{v}_i^{\delta_n}$, and

$$(2.18) \quad \hat{v}_i^{\delta_n}(x, t) - \hat{v}_{i+1}^{\delta_n}(x, t) \geq c_0 \cdot \inf_y [v_i^{\delta_n}(y, 0) - v_{i+1}^{\delta_n}(y, 0)],$$

for all $(x, t) \in K$ and for all $i \in \mathcal{L}^{\delta_n}$. Recall $v_i^{\delta_n}(x, 0) - v_{i+1}^{\delta_n}(x, 0) \geq \frac{1}{2}\epsilon\delta_n > 0 \forall i$ and $\forall x$.

Furthermore, assume that

$$(2.19) \quad \frac{1}{\delta_n} \left[\int_0^T \int_{-S+sr}^{S-sr} \max_{i \in \mathcal{L}^{\delta_n}} (R_i^{\delta_n}(x, r))^2 dx dr + \sum_{i \in \mathcal{L}^{\delta_n}} \left[\left\| v_i^{\delta_n}(\cdot, 0) - \hat{v}_i^{\delta_n}(\cdot, 0) \right\|_{L^2([\hat{h}_{i-1}^{\delta_n}(0), \hat{h}_i^{\delta_n}(0)])} \right]^2 \right] \rightarrow 0 \text{ as } n \rightarrow \infty,$$

with $\hat{h}_0^{\delta_n}(0) := -S$ and $\hat{h}_{N^{\delta_n}+1}^{\delta_n}(0) := S$.

Moreover, assume that

$$\sum_{i \in \mathcal{I}^{\delta_n}} \int_0^T \left| \hat{h}_i^{\delta_n}(s) - \sigma(\hat{u}^{\delta_n}(\hat{h}_i^{\delta_n}(s)+, s), \hat{u}^{\delta_n}(\hat{h}_i^{\delta_n}(s)-, s)) \right| ds \rightarrow 0 \text{ as } n \rightarrow \infty,$$

where the quantity $\sigma(\hat{u}^{\delta n}(\hat{h}_i^{\delta n}(s)+, s), \hat{u}^{\delta n}(\hat{h}_i^{\delta n}(s)-, s))$ is the Rankine-Hugoniot speed of the shock $(\hat{u}^{\delta n}(\hat{h}_i^{\delta n}(s)+, s), \hat{u}^{\delta n}(\hat{h}_i^{\delta n}(s)-, s))$ (see (3.6)), and $\mathcal{I}^{\delta n}$ is as in Theorem 2.2.

Then, as $n \rightarrow \infty$ the right-hand sides of the estimates (2.9) and (2.13) go to zero.

For the proof of Theorem 2.3, see Section 8.

Remark 11. Compare (2.17) and (2.18) with Lemma 4.2 and Lemma 4.5 below, respectively, which concern exact solutions. In particular, remark that for the exact solutions we have

$$(2.20) \quad \sup_n \sup_{i \in \mathcal{L}^{\delta n}} \sup_t \text{Lip}[v_i^{\delta n}(\cdot, t)] < +\infty.$$

2.1. A high-level overview of the proof of Theorem 2.2 (Main Theorem).

At a high level, our method works by considering an exact solution \bar{u} to (1.1) with initial data $\bar{u}^0 \in \mathcal{S}^\epsilon$. From the initial data $\bar{u}^0 \in \mathcal{S}^\epsilon$, we find an element $\tilde{u}^0 \in \mathcal{S}_d^\epsilon$ which is L^2 -close to \bar{u}^0 . A parameter $\delta > 0$ controls the minimum size of discontinuities in the discretization of the function \bar{u}^0 to make \tilde{u}^0 . For each interval where \tilde{u}^0 is continuous, we create a Lipschitz-continuous artificial extension defined globally on all of \mathbb{R} (see Appendix A.1). Then, for each artificial extension we create a numerical solution \hat{v}_i which has this artificial extension as initial data (although for the small shocks of size proportional to δ , we do not in practice have to numerically simulate the extensions – see Section 5.1.1). Then, by gluing together the artificial solutions \hat{v}_i using the Rankine-Hugoniot condition (with a numerical ODE solver), we construct the numerical solution \hat{u} . On the other hand, we also define a function $\hat{\psi}$ which is also formed by gluing together the numerical solutions \hat{v}_i . However, the points where the \hat{v}_i are glued together are not determined by Rankine-Hugoniot, but instead by (unknown) generalized characteristics from the exact solution \bar{u} . For the construction of \hat{u} and $\hat{\psi}$, see Section 5.

At each time t , we will discern three different types of shocks in $\hat{\psi}(\cdot, t)$ and $\hat{u}(\cdot, t)$ (see Figure 1):

- *front tracking shocks* – shocks which are of size proportional to δ at time $t = 0$ and at $t = 0$ are in the interior of one of the intervals where \bar{u}^0 is rapidly decreasing. To be a ‘front tracking’ shock at time $t > 0$, the shock must have collided with only other ‘front tracking’ shocks up until (and including) time t . These shocks in \hat{u} will move according to a simple scalar front tracking scheme;
- *large shocks* – shocks which at time t are not ‘front tracking’ shocks and are not adjacent to a ‘front tracking’ shock. At time $t = 0$, they have a size independent of δ ;
- *boundary shocks* – the shocks which are neither ‘front tracking’ nor ‘large’. They are adjacent to ‘front tracking’ shocks. Remark that at later times $t > 0$, a ‘boundary’ shock might be adjacent to, both on the left and right, a ‘front tracking’ shock – such as when two ‘boundary’ shocks, separated by an interval corresponding to a nearly non-decreasing piece of \bar{u}^0 (at $t = 0$), collide (see Figure 5 and Section 6.5.1).

Due to using generalized characteristics from the exact solution \bar{u} , $\hat{\psi}$ and \bar{u} will be L^2 -stable relative to each other (see Section 7). Then, control on $\bar{u} - \hat{u}$ will come from control

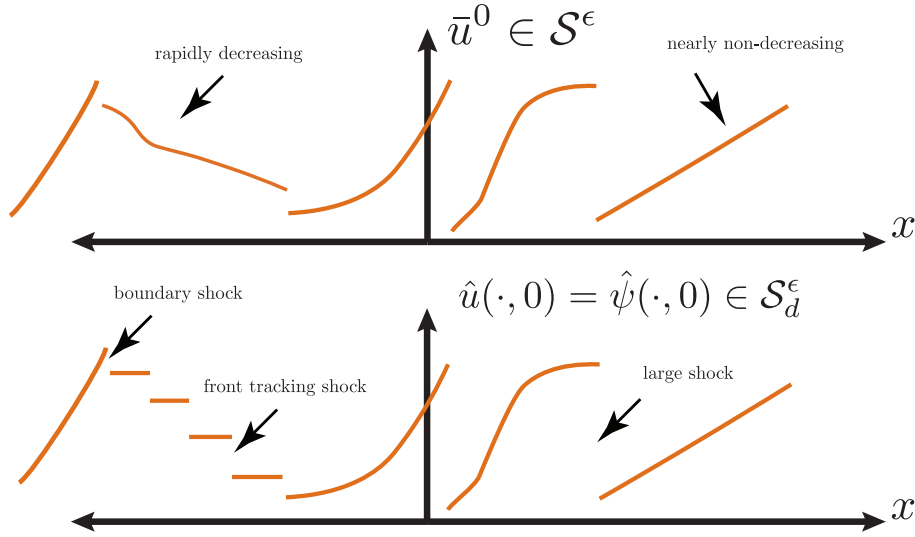


FIGURE 1. The function \bar{u}^0 is divided into *rapidly decreasing* parts and *nearly non-decreasing* parts. In $\hat{u}(\cdot, 0) = \hat{\psi}(\cdot, 0)$, we differentiate between three different types of shocks: *large shocks*, *front tracking shocks*, and *boundary shocks*.

on $\hat{u} - \hat{\psi}$. To control $\hat{u} - \hat{\psi}$, we need to determine how much the speed of the shocks in $\hat{\psi}$ differs from the Rankine-Hugoniot speed of these shocks (recall the shocks in \hat{u} move with numerically approximated Rankine-Hugoniot speed). The error intervals Δ_i which measure the difference between shock positions in \hat{u} and $\hat{\psi}$ will depend on the type of shock: large shock, front tracking shock, or boundary shock? See Section 6.

A key part of estimating the error in shock positions between $\hat{\psi}$ and \hat{u} will be determining when collisions which have occurred in \hat{u} have also occurred in $\hat{\psi}$ (Section 6.3). The general principle here will be: when two shocks (neither of which is ‘front tracking’) collide in \hat{u} , continue the two shocks forward in time as if the collision did not occur (so no change in left- or right-hand states of either shock). While continuing both shocks forward in time, calculate error intervals between the positions of these shocks and the positions of the corresponding shocks in $\hat{\psi}$ (again, under the assumption the corresponding shocks in $\hat{\psi}$ have not collided). At such a time when these two error intervals (one for each shock) no longer intersect, we can conclude by contradiction that the shocks must have collided in $\hat{\psi}$.

For the ‘front tracking’ shocks, we will control them using Bressan’s L^1 -theory [1] (see Section 6.4).

3. A BRIEF INTRODUCTION TO THE THEORY OF SHIFTS, a -CONTRACTION, AND AN OVERVIEW OF OUR PROOF

Let us motivate one of the major techniques utilized in this paper: the *theory of shifts* (and the closely related technique of *a-contraction*). The theory of shifts was devised by Vasseur to show L^2 stability for shock solutions to conservation laws [50]. The technique has reached a certain level of maturity and, recently, it has been used to show uniqueness of solutions to scalar conservation laws with convex flux in one space dimension follows from having one convex entropy, see [34]. This result is not obvious, and in fact has been proven two other times before [12, 45], albeit using entirely different techniques. In [5], the method of *a-contraction* was used to show that the small- BV solutions considered by Bressan-Crasta-Piccoli [3] are in fact stable (and unique) among the large class of entropic, weak solutions with possibly very large data. Again, a single convex entropy is used.

Remark that for the scalar conservation laws, the solutions to the Riemann problem are non-unique if the flux function has even a single inflection point. This includes for example concave-convex flux functions e.g, $f(u) = u^3 + au$ for any $a \in \mathbb{R}$. The non-uniqueness persists even if solutions are required to verify the entropy inequality for at least one strictly convex entropy (see e.g. [39]).

3.1. Shifts and a -contraction. For the system (1.1), we fix an entropy and entropy-flux $\eta: \mathbb{R} \rightarrow \mathbb{R}$ and $q: \mathbb{R} \rightarrow \mathbb{R}$, respectively. They verify the compatibility condition $q' = \eta' A'$, where A is the flux for our system (1.1).

We assume that η is strictly convex. Furthermore, for $a, b \in \mathbb{R}$, we define the relative entropy,

$$(3.1) \quad \eta(a|b) := \eta(a) - \eta(b) - \eta'(b)(a - b).$$

We define the relative entropy-flux associated with the relative entropy (3.1):

$$(3.2) \quad q(a; b) := q(a) - q(b) - \eta'(b)(A(a) - A(b)).$$

We also define the relative flux: For $a, b \in \mathbb{R}$,

$$(3.3) \quad A(a|b) := A(a) - A(b) - A'(b)(a - b).$$

Note that due to the strict convexity of the entropy η , for all a and b in a fixed compact set, there exist constants $c^*, c^{**} > 0$ such that

$$(3.4) \quad c^*(a - b)^2 \leq \eta(a|b) \leq c^{**}(a - b)^2.$$

Thus, the method of relative entropy is an L^2 -type theory.

Now, consider a weak solution u to the scalar conservation law (1.1), entropic for the entropy η . Moreover, consider an entropic pure shock solution \bar{u} ,

$$(3.5) \quad \bar{u}(x, t) := \begin{cases} u_L, & \text{if } x < \sigma(u_L, u_R)t \\ u_R, & \text{if } x > \sigma(u_L, u_R)t, \end{cases}$$

where $u_L, u_R \in \mathbb{R}$ and $\sigma(u_L, u_R)$ is the Rankine-Hugoniot speed naturally associated to the shock (u_L, u_R) , i.e.

$$(3.6) \quad \sigma(v, w) := \begin{cases} \frac{A(v)-A(w)}{v-w} & \text{if } v \neq w, \\ A'(w) & \text{if } v = w. \end{cases}$$

The focus of interest of [50] and subsequent research was in stability of the shock \bar{u} in a large class of weak solutions u with minimal regularity assumptions, asking only for a trace condition which is weaker than BV_{loc} (see Definition 2.1). More precisely, given a particular Lipschitz-continuous function of time $h(t)$, how does the quantity

$$(3.7) \quad \int_{-\infty}^{h(t)} \eta(u(x, t)|u_L) dx + \int_{h(t)}^{\infty} \eta(u(x, t)|u_R) dx$$

grow in time?

Notice that as in weak-strong stability theory, in (3.7) the solution u with low regularity is put in the first slot of the relative entropy and the solutions with more regularity, and on which there is more control, in the second slot (in this case, constant states u_L and u_R). Remark that throughout this paper, we will put exact solutions in the first slot of the relative entropy, and numerical solutions in the second slot of the relative entropy. Since we perform a posteriori analysis, we have large amounts of control over the numerical solutions.

The theory of shifts was devised to overcome the following difficulty: when $h(t) = \sigma(u_L, u_R)t$, the quantity (3.7) grows in time. More problematically, estimates in the form of Dafermos and DiPerna’s weak-strong stability theory do not hold. Simple examples show that this is true even in the case of scalar conservation laws.

However, if a particular Lipschitz function $h(t)$ is chosen, control over the quantity (3.7) can be gained. This is equivalent to studying the stability between u and the function

$$(3.8) \quad \bar{u}_{\text{shifted}}(x, t) := \begin{cases} u_L, & \text{if } x < h(t) \\ u_R, & \text{if } x > h(t). \end{cases}$$

In other words, the shock in the solution \bar{u} will no longer be moving with its natural Rankine-Hugoniot speed, but instead will be moving with an artificial velocity dictated by the special choice of h . Due to $h(t) \neq \sigma(u_L, u_R)t$, the shock in \bar{u}_{shifted} will not be traveling with Rankine-Hugoniot speed and thus \bar{u}_{shifted} is no longer an exact solution to the conservation law. We note that when u_L and u_R are truly constants, as in this example, (3.7) is a *decreasing function of time*. The artificial ‘shift’ in position of the shock forces a contraction in L^2 as measured by the relative entropy functional $(a, b) \mapsto \eta(a|b)$. This is the theory of shifts. In the context of the relative entropy method, this idea was devised by Vasseur [50].

The theory of shifts gives some control on the difference $\sigma - \dot{h}$ (a measure of how artificial the shift is). However, up until this point, the control on the shifts has never played a significant role in the theory. In both [5, 34], the stability and uniqueness results

do not rely on controlling the shift functions. Instead, the contractive property of (3.7) (as a function of time) is key.

A similar procedure works for systems, but the situation is more involved: Indeed, in the case of systems of conservation laws with multiple conserved quantities, there are examples where no function h exists such that (3.7) is decreasing in time [47]. However, by introducing a spatially inhomogeneous pseudo-distance we can regain contractivity [29]. In particular, we introduce a parameter $a > 0$ and consider the quantity

$$(3.9) \quad \int_{-\infty}^{h(t)} \eta(u(x, t)|u_L) dx + a \int_{h(t)}^{\infty} \eta(u(x, t)|u_R) dx,$$

where a is chosen sufficiently large or sufficiently small (depending on the wave family of the shock we are considering). Then, for particular values of a , there again exists a Lipschitz function of time h such that (3.9) is decreasing in time. This is the technique of *a-contraction*.

3.2. Uniqueness via shifts. While [5, 34] provide uniqueness results neither gives quantitative stability results. We will outline in this section why this is the case.

Both [5, 34] use the following framework in their proofs: given a weak solution u , entropic for a convex entropy, approximate the initial data $u(\cdot, 0)$ by piecewise-smooth initial data \hat{u}^0 . Then the initial data \hat{u}^0 are evolved forward in time according to the theory of shifts. This gives ψ , a function of time and space. One key achievement in [5, 34] is to ensure L^2 stability between ψ and u , i.e., control on $\|\psi(\cdot, t) - u(\cdot, t)\|_{L^2}$, by letting the discontinuities in ψ not travel with Rankine-Hugoniot speed but instead move according to artificial shift functions as described above. In the systems case with multiple conserved quantities, \hat{u}^0 is piecewise-constant and ψ is constructed using the front tracking algorithm, but with wave speeds dictated by shifts. Thus, ψ is in general not a solution to the conservation law under consideration. The analysis in [5, 34] proceeds by combining the facts that ψ will stay L^2 close to the weak solution u , and, by construction, ψ will have some regularity property which is uniform in the choice of initial data $\psi(\cdot, 0)$. Due to ψ staying L^2 -close to the weak solution u , and $\|\psi(\cdot, 0) - u(\cdot, 0)\|_{L^2}$ being arbitrarily small, the regularity property of ψ is transferred to the weak solution u . In the scalar case, the function ψ , even though it is not a solution to the conservation law, will always obey the decay estimate given by Oleĭnik's *condition E* [44]. We briefly recall that a solution u to (1.1) verifies condition E if

$$(3.10) \quad \left\{ \begin{array}{l} \text{There exists a constant } C > 0 \text{ such that} \\ u(x+z, t) - u(x, t) \leq \frac{C}{t} z \\ \text{for all } t > 0, \text{ almost every } z > 0, \text{ and almost every } x \in \mathbb{R}. \end{array} \right.$$

Condition E is a uniqueness criterion, so transferring this property to u implies uniqueness. In the systems case, the trace of ψ along space-like curves will have bounded variation. This is the *Bounded Variation Condition*, which is known to be a condition for uniqueness [4]. The function ψ verifies this condition in a uniform way, and this completes the proof.

3.3. More details on shifts in the scalar case. Because they will play an important role in the present paper, let us present a few more of the ideas behind how the framework for uniqueness is applied in the scalar case [34].

Firstly, the initial data $\bar{u}(\cdot, 0)$ are approximated by piecewise-smooth initial data $\hat{u}^0(\cdot) = \psi(\cdot, 0)$. In particular, $\psi(\cdot, 0)$ is piecewise-Lipschitz such that the Lipschitz pieces are monotonically increasing (cf. the space \mathcal{S}_d^ϵ). Initial data in this form is dense in L^2 (see [34]). Then, for each interval (x_i, x_{i+1}) where $\psi(\cdot, 0)$ is smooth, $\psi(\cdot, 0)|_{(x_i, x_{i+1})}$ is extended to a global-in-space non-decreasing function v_i^0 such that the extensions satisfy the pointwise ordering condition $v_i^0 \geq v_{i+1}^0$ (cf. (A.19)). Then, for each i a global-in-time smooth solution v_i to the conservation law with initial data v_i^0 is constructed.

Secondly, the quantity

$$(3.11) \quad \sum_{i=0}^N \int_{h_i(t)}^{h_{i+1}(t)} \eta(u(x, t)|v_{i+1}(x, t)) dx,$$

is considered, where $h_0 := -\infty$ and $h_{N+1} := +\infty$, and at the initial time $h_i(0) = x_i$ for $i = 1, \dots, N$. For $i = 1, \dots, N$, the h_i are shift functions constructed according to the theory of shifts.

Compare (3.7) and (3.11): A weak solution u was put in the first slot of the relative entropy, and smooth solutions go in the second slot of the relative entropy. When the h_i are appropriately chosen shift functions, (3.11) will again be a decreasing function of time. This gives a function $\psi: \mathbb{R} \times [0, \infty) \rightarrow \mathbb{R}$,

$$(3.12) \quad \psi(x, t) := \begin{cases} v_1(x, t) & \text{if } x < h_1(t) \\ v_2(x, t) & \text{if } h_1(t) < x < h_2(t) \\ \vdots & \\ v_{N+1}(x, t) & \text{if } h_N(t) < x. \end{cases}$$

When two shift functions h_i and h_j collide with each other, the v_i that was between them is simply deleted, and the two shifts are glued together (i.e., $h_i \equiv h_j$ for all future times), and then we continue running the clock forward in time. Due to there being only finitely many curves of discontinuity h_i , this process will only have to be repeated at most finitely many times. This defines the function ψ globally in time.

Then, this gives a function ψ which is L^2 -close to u for all time, due to (3.4) and (3.11) being decreasing in time. Further, $\|\psi(\cdot, 0) - u(\cdot, 0)\|_{L^2}$ can be chosen arbitrarily small. To complete the framework, it needs to be shown that ψ verifies condition E (see (3.10)). This follows because in between the h_i , ψ is a classical solution to our conservation law, and thus is well-known to verify condition E in a uniform way (independent of the v_i we chose). Furthermore, due to the choices of the extensions v_i , the function ψ will verify condition E also along the h_i . This implies u verifies condition E, and thus u is the unique solution to verify condition E. This completes the argument.

3.4. Difficulties in deriving quantitative stability results. In our program to use the theory of shifts to come up with a posteriori error estimates for numerical approximations we replace ψ by a quantity $\hat{\psi}$ where the exact solutions v_i are replaced by numerical solutions \hat{v}_i (or more precisely, by Lipschitz-continuous reconstructions of numerical solutions in the spirit of [20, 14]). The problem with this approach is that in order to keep $\hat{\psi}$ L^2 -close to u the discontinuities in $\hat{\psi}$ need to move with shifts. The speeds of the shifts are dictated by u , i.e. they are unknown and not accessible numerically. The natural choice of speeds that are accessible are Rankine-Hugoniot speeds computed using the \hat{v}_i but if the \hat{v}_i are glued together using curves with these speeds the result is not $\hat{\psi}$ but some new computable (!) quantity \hat{u} .

The natural way to obtain quantitative control on $\|\hat{u}(\cdot, t) - u(\cdot, t)\|_{L^2}$ is to combine the control on $\|\hat{\psi}(\cdot, t) - u(\cdot, t)\|_{L^2}$, that follows from including residuals in the theory of shifts, with estimates on $\|\hat{\psi}(\cdot, t) - \hat{u}(\cdot, t)\|_{L^2}$ which, in principle, can be obtained by controlling the size of the artificial shift. However, there are two difficulties with this which are essentially the same in the scalar and the system case:

For one, consider the following. Let $t^* > 0$ be such that for all $t \in [0, t^*]$, there are no interactions between waves in either \hat{u} or $\hat{\psi}$. Then, for $t \in [0, t^*]$, we can relate \hat{u} and $\hat{\psi}$ by a simple change of variables. However, if for example after time t^* two waves collide in $\hat{\psi}$ but not in \hat{u} , it is no longer possible to relate \hat{u} and $\hat{\psi}$ by a simple change of variables. This is what we refer to as the *change of variables problem*. This problem is even more involved in the systems case [5]. Indeed, in the systems case, when the waves collide in $\hat{\psi}$, the front tracking algorithm stops the clock, solves the new Riemann problem which arises, and then restarts the clock, thus fundamentally altering the relationship between $\hat{\psi}$ and \hat{u} .

The second difficulty is that in both the scalar and systems case, the control on the shift gets worse and worse as the size of the shock (being controlled by shift) decreases. This is highly problematic, as one is interested in letting $\hat{\psi}(\cdot, 0) \rightarrow u(\cdot, 0)$ in L^2 and thus the shocks in $\hat{\psi}$ will become smaller when simulations on finer meshes are considered.

This is what we call the *problem of loss of control on small shocks*.

3.5. A strategy for obtaining quantitative stability estimates. In this paper we derive *quantitative* error estimates of numerical approximations to scalar conservation laws. This requires quantitative stability estimates. We will consider weak solutions which are entropic for at least one strictly convex entropy.

In order to obtain quantitative stability estimates, we need to restrict the class of initial data, i.e. we require initial data in \mathcal{S}^ϵ which is a restriction compared to [34]. However, from a numerical point of view, this does not seem to be a severe restriction since it is not clear how to construct good approximations of less regular initial data in practice. Due to restricting ourselves to initial data in \mathcal{S}^ϵ , from here on we will call the exact solution we are considering \bar{u} instead of u .

The notation used above will be suggestive, but some slight variations are needed. In particular, we want all discontinuities to have some minimal size and this is tricky if we

approximate \bar{u}^0 by step functions in areas where it is decreasing with a slope very close to zero. Thus, we will pick a threshold $\epsilon > 0$ and treat points x with $\partial_x \bar{u}^0(x) > -\epsilon$ as points where \bar{u}^0 is non-decreasing. This gives rise to the space $\mathcal{S}_\delta^\epsilon$

We shall pick $\epsilon > 0$ such that smooth solutions to (1.1) with slope greater than $-\epsilon$ do not experience shock formation before or at time T . In fact, we choose ϵ such that no slopes less than -1 form.

Our first step is to approximate the initial data $\bar{u}(\cdot, 0)$ by some $\hat{u}^0 \in \mathcal{S}_\delta^\epsilon$. Since we wish to use the quantitative estimates in an a posteriori setting, \hat{u}^0 should also live in some finite dimensional space that can be represented numerically, e.g. some space of piecewise polynomials of a certain degree. On the intervals where $\partial_x \bar{u}(\cdot, 0) > -\epsilon$ this can be achieved by first using a standard discretization of \bar{u}^0 , i.e. projection or interpolation into a piecewise polynomial space and subsequent reconstruction as in [20]. On intervals (x_i, x_{i+1}) where $\bar{u}(\cdot, 0)$ is a monotonically decreasing Lipschitz function with slope magnitude larger than ϵ , we use step functions of width δ such that (at $t = 0$) we obtain discontinuities with sizes s_i between $\delta \cdot \epsilon$ and $\delta \cdot (\text{Lip}[\bar{u}^0|_{(x_i, x_{i+1})}])$. Note that $\delta > 0$ is a parameter that we can choose and that does not have to coincide with the mesh width h in the intervals where we use piecewise polynomials. For these ‘front tracking’ shocks (see Figure 1), the solution is evolving in time according to a simple scalar front tracking process. In this paper, our front tracking solutions will only involve shocks and are thus simple to construct. Compare this to the scalar front tracking algorithm presented in [11, Section 14.1] which is capable of handling more general initial data, but which involves some complexity due to eliminating rarefaction waves and instead using composite waves consisting of constant states, admissible shocks, and small inadmissible ‘rarefaction’ shocks. Our work compares directly to the result [5], where stability of small- BV solutions, among the class of large data L^2 solutions, is shown by utilizing a -contraction and the front tracking algorithm for systems of conservation laws. See Section 5.1 for more details on the construction of \hat{u} .

Although shocks are very well-behaved within the context of the theory of shifts, neither the relative entropy method nor the theory of shifts can cope with the *formation* of a shock as the slopes of a solution become increasingly steep. For a scalar conservation law with convex flux, a solution which is strictly decreasing in space will eventually suffer from the catastrophe of the overturning waves. This is why it is necessary to break the rapidly decreasing parts of $\bar{u}(\cdot, 0)$ into step functions to allow for analysis within the theory of shifts.

Based on \hat{u}^0 , we construct global numerical solutions \hat{v}_i , which are based on the artificial extensions similar to [34] as discussed above (but specialized to the present situation, see Appendix A.1).

As suggested by the notation above and (3.12), in this paper $\hat{\psi}$ will be constructed using shift functions such as to keep $\hat{\psi}$ L^2 -close to \bar{u} . However, instead of gluing together exact solutions v_i as in (3.12), we will glue together the \hat{v}_i constructed numerically. Nonetheless, the shifts will follow precisely the same theoretic construction. In the scalar case, the shift functions are simply generalized characteristics of the exact solution \bar{u} (for more on

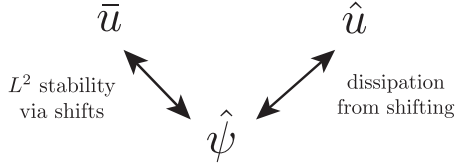


FIGURE 2. The philosophy of the present paper is to control $\hat{\psi} - \bar{u}$ via the L^2 stability we gain via shifting, while on the other hand measuring $\hat{\psi} - \hat{u}$ via the control on the shifts we get due to dissipation.

generalized characteristics, see [11, Chapter 10]). Thus, the $\hat{\psi}$ becomes an interesting mix between the exact solution \bar{u} and the numerical solution \hat{u} . See Section 5.2 for details.

We are aiming for a quantitative estimate on $\bar{u} - \hat{u}$. To do this, we will in fact give a quantitative estimate on $\hat{u}(\cdot, t) - \hat{\psi}(\cdot, t)$. Such a quantitative estimate, combined with control on $\left\| \bar{u}(\cdot, t) - \hat{\psi}(\cdot, t) \right\|_{L^2}$ due to shifts, will give us a quantitative estimate on $\bar{u}(\cdot, t) - \hat{u}(\cdot, t)$ (see Figure 2).

As discussed above, there are two difficulties in deriving a quantitative estimate on $\hat{u}(\cdot, t) - \hat{\psi}(\cdot, t)$. The first is what to do when collisions between shocks occur in one of \hat{u} , $\hat{\psi}$ but not the other, such that the two functions can no longer be related to each other through a change of variables. This issue is handled numerically by keeping track of all the possibilities for the function $\hat{\psi}$, based on what we see in the computer during the construction of the numerical solution \hat{u} . This process involves remembering shock curves and \hat{v}_i even after they are no longer needed to construct \hat{u} due to collisions between shocks in \hat{u} . In this way, we are building an ‘unfolded’ version of \hat{u} . As a result of keeping careful track of all the possibilities for the function $\hat{\psi}$, we gain an understanding about the difference in position, measured by Δ_i (see (6.1)), for where each \hat{v}_i might be revealed in \hat{u} and $\hat{\psi}$. This allows us to derive estimates on $\left\| \hat{u}(\cdot, t) - \hat{\psi}(\cdot, t) \right\|_{L^1}$.

The second difficulty discussed above in deriving a quantitative estimate on $\hat{u}(\cdot, t) - \hat{\psi}(\cdot, t)$ is how to control shifts of small shocks. For us, this issue appears when trying to control the position of the very small ‘front tracking’ shocks of size $\mathcal{O}(\delta)$ (at least, they are this size at $t = 0$). Its resolution involves an ancillary function $\hat{\psi}_{\text{fine}}$ which allows us to gain improved control on small shocks by something of a ‘localization’ procedure which minimizes the error in position of a shock due to far away errors in $\hat{u}(\cdot, 0) - \bar{u}(\cdot, 0)$. With this, we manage to devise improved control on a front tracking algorithm with shifts: a key idea is to use the L^1 -theory for control on ‘ ϵ -approximate’ front tracking solutions which have shocks traveling with Rankine-Hugoniot speed *plus an error term* (see [1] and also Lemma 4.1, below). We believe the ideas we introduce here might be applicable to the theory of shifts and a -contraction in the well-posedness theory for hyperbolic *systems* of conservation laws.

Let us remark that a fundamental source of error in the numerical solution \hat{u} is due to numerical errors in the \hat{v}_i . To glue together the \hat{v}_i to make \hat{u} , the Rankine-Hugoniot jump condition is used. More precisely, ODEs are solved numerically (see (5.1)). The position of the shock curves thus depends on the pointwise values of the \hat{v}_i at the exact points the numerical ODE solver sees. These pointwise values are a quantity on whose error we do not have good direct control. Roughly speaking, the function $\hat{\psi}$ corrects this error by always gluing together the \hat{v}_i in the places where they *should have been glued* if it weren't for this numerical error. This is done using the generalized characteristics in the exact solution \bar{u} as the curves of discontinuity – the ‘shift’. This shift in position of the curves of discontinuity between the \hat{u} and $\hat{\psi}$ causes some dissipation (see Lemma 4.4), and this allows us to control the magnitude of the shift (see the estimate (6.1)). Note that the estimate on the shift (6.1) relies on the L^2 norm of the numerical residual, as well as $\|\hat{u}(\cdot, 0) - \bar{u}(\cdot, 0)\|_{L^2}$. It is a striking consequence of the theory of shifts that by controlling non-local integral quantities, we can control the error in solving the ODE for shock position that results from pointwise errors in the \hat{v}_i . Indeed, the control we gain here is stronger than the control we would gain by transferring L^2 estimates to L^∞ estimates on the numerical error in the \hat{v}_i by using Lipschitz continuity (cf. Section 4.6).

3.5.1. *Future work for the systems case.* In this paper, we are careful to construct a theory we hope is flexible enough to extend to the systems case. As a product of using the relative entropy method and theory of shifts, we only use one entropy during our analysis. Furthermore, our analysis is done within the context of the theory of shifts and the framework first developed in [34]. One key tool is the dissipation estimate Lemma 4.4.

There is hope our work here will generalize to systems. The framework first developed in [34] has had tremendous success when used with a -contraction techniques and applied to systems to show stability of small- BV solutions [5]. As discussed above, [5] utilizes the front tracking algorithm to construct sequences of L^2 -stable approximate solutions. In the present paper, we use the front tracking theory for the analysis of very small shocks in our numerical solution (see Section 6.4). In the systems case, we remark that the front tracking theory is well-adapted for the analysis of small shocks.

Furthermore, the dissipation estimate Lemma 4.4 has near-identical analogues in the a -contraction theory (see [32, Proposition 4.1], for example). Moreover, recently an important technical contribution to the a -contraction theory has greatly enhanced the control on small shocks [24].

4. TECHNICAL PRELIMINARY

For a function $u \in L^\infty(\mathbb{R} \times [0, T])$ that verifies the Strong Trace Property (Definition 2.1), and a Lipschitz-continuous function $h: [0, T] \rightarrow \mathbb{R}$, we use the notation $u(h(t)\pm, t)$ to denote the right- and left-hand traces $u_\pm(t)$ at a time t when u verifies the Strong Trace Property, where $u_\pm(t)$ is within the context of Definition 2.1. For a time t when u has strong traces, the values $u_\pm(t)$ are well-defined, and thus the values $u(h(t)\pm, t)$ are also well-defined.

Most of the results in this preliminary section are well-known. However, we include them here (along with proofs) to ensure that we are not using more information than we

think. The solution \bar{u} in the Main Theorem (Theorem 2.2) is only assumed to be entropic for the convex entropy η – we do not use the Kruzhkov theory.

4.1. Front tracking estimate. The following Lemma will be fundamental to our control on the ‘front tracking’ shocks (see Figure 1).

Lemma 4.1 (An estimate on approximate front tracking solutions). *Consider initial data $v^0: \mathbb{R} \rightarrow \mathbb{R}$ which is monotonically decreasing, piecewise-constant and has finitely many discontinuities. Let v be the (unique) exact solution to (1.1) with initial data v^0 and which is monotonically decreasing (in space) for each fixed time. Let w be a function which is piecewise-constant (in space) and monotonically decreasing (in space) for each fixed time. In particular, there exists $\tilde{N} \in \mathbb{N}$ and Lipschitz functions $\tilde{h}_1, \dots, \tilde{h}_{\tilde{N}}: [0, \infty) \rightarrow \mathbb{R}$ such that $\tilde{h}_1(t) \leq \dots \leq \tilde{h}_{\tilde{N}}(t)$ for all $t \in [0, \infty)$ (and if $\tilde{h}_j(t_0) = \tilde{h}_k(t_0)$ for some j, k, t_0 , then $\tilde{h}_j(t) = \tilde{h}_k(t)$ for all $t > t_0$) and $w(\cdot, t)$ is constant on each interval $[\tilde{h}_i(t), \tilde{h}_{i+1}(t)]$ for all $i \in \{0, \dots, \tilde{N}\}$ (when $\tilde{h}_i(t) \neq \tilde{h}_{i+1}(t)$ and with $\tilde{h}_0 = -\infty, \tilde{h}_{\tilde{N}+1} = +\infty$). Furthermore, assume*

$$(4.1) \quad \|v(\cdot, 0) - w(\cdot, 0)\|_{L^1(\mathbb{R})} < \infty.$$

Then, for almost every t ,

$$(4.2) \quad \frac{d}{dt} \|v(\cdot, t) - w(\cdot, t)\|_{L^1(\mathbb{R})} \leq \sum_{\alpha} \left[\left| w(\tilde{h}_{\alpha}(t)-, t) - w(\tilde{h}_{\alpha}(t)+, t) \right| \left| \dot{\tilde{h}}_{\alpha} - \sigma(w(\tilde{h}_{\alpha}(t)-, t), w(\tilde{h}_{\alpha}(t)+, t)) \right| \right].$$

At time t , the summation runs over all $\alpha \in \{1, \dots, \tilde{N}\}$ with the property that if there exists $\beta \in \{1, \dots, \tilde{N}\}$ such that $\tilde{h}_{\alpha}(t) = \tilde{h}_{\beta}(t)$, then $\alpha \leq \beta$ (this way we are not double counting the dissipation from curves \tilde{h}_{α} which are stuck together).

Remark 12. Remark that v and w are so-called ‘ ϵ -approximate’ front tracking solutions in the sense of [1]. The proof of this Lemma is an immediate calculation in the scalar case. A version also holds for ϵ -approximate front tracking solutions in the systems case – see [1, Theorem 8.2]. In particular, [1, Eqn (8.22)] can be roughly summarized as stating that the time derivative of the weighted L^1 distance between solutions grows at most like a constant times the velocity error at that time. The weighted L^1 norm, which includes a *wave interaction potential* in the systems case, can be replaced by the unweighted L^1 norm in the scalar case.

Proof. We give a quick proof, largely following [1, p. 155]. Remark we do not use the Kruzhkov entropies.

Let x_1, \dots, x_N be all the points where $v(\cdot, t)$ or $w(\cdot, t)$ have a jump.

We then have

$$(4.3) \quad \frac{d}{dt} \|v(\cdot, t) - w(\cdot, t)\|_{L^1(\mathbb{R})} = \sum_{\alpha} \left[|w(x_{\alpha}(t)-, t) - v(x_{\alpha}(t)-, t)| - |w(x_{\alpha}(t)+, t) - v(x_{\alpha}(t)+, t)| \right] \dot{x}_{\alpha},$$

where the sum is over all jumps in v or w .

Since w and v are piecewise-constant, for $x \in (x_{\alpha-1}, x_{\alpha})$, we immediately have

$$(4.4) \quad |w(x, t) - v(x, t)| \sigma(w(x, t), v(x, t)) = |w(x_{\alpha-1+}, t) - v(x_{\alpha-1+}, t)| \sigma(w(x_{\alpha-1+}, t), v(x_{\alpha-1+}, t)) = |w(x_{\alpha-}, t) - v(x_{\alpha-}, t)| \sigma(w(x_{\alpha-}, t), v(x_{\alpha-}, t)).$$

Furthermore, from (4.1) we have $|w(x, t) - v(x, t)| \equiv 0$ for x outside a large (but bounded) interval. We can thus add and subtract the terms (4.4) in (4.3) without changing the total sum.

We receive,

$$(4.5) \quad \frac{d}{dt} \|v(\cdot, t) - w(\cdot, t)\|_{L^1(\mathbb{R})} = \sum_{\alpha} \left[|w(x_{\alpha}(t)+, t) - v(x_{\alpha}(t)+, t)| (\sigma(w(x_{\alpha}(t)+, t), v(x_{\alpha}(t)+, t)) - \dot{x}_{\alpha}) - |w(x_{\alpha}(t)-, t) - v(x_{\alpha}(t)-, t)| (\sigma(w(x_{\alpha}(t)-, t), v(x_{\alpha}(t)-, t)) - \dot{x}_{\alpha}) \right].$$

Define $v^{\alpha\pm} := v(x_{\alpha}(t)\pm, t)$ and $w^{\alpha\pm} := w(x_{\alpha}(t)\pm, t)$.

Furthermore, define

$$(4.6) \quad E_{\alpha} := \left[|w^{\alpha+} - v^{\alpha+}| (\sigma(w^{\alpha+}, v^{\alpha+}) - \dot{x}_{\alpha}) - |w^{\alpha-} - v^{\alpha-}| (\sigma(w^{\alpha-}, v^{\alpha-}) - \dot{x}_{\alpha}) \right].$$

Then by adding zero, we get

$$(4.7) \quad E_{\alpha} = \left[|w^{\alpha+} - v^{\alpha+}| (\sigma(w^{\alpha+}, v^{\alpha+}) - \sigma(w^{\alpha-}, w^{\alpha+})) - |w^{\alpha-} - v^{\alpha-}| (\sigma(w^{\alpha-}, v^{\alpha-}) - \sigma(w^{\alpha-}, w^{\alpha+})) \right] + \left[(\sigma(w^{\alpha-}, w^{\alpha+}) - \dot{x}_{\alpha}) (|w^{\alpha+} - v^{\alpha+}| - |w^{\alpha-} - v^{\alpha-}|) \right] := E_{\alpha,1} + E_{\alpha,2}.$$

Assume for now that

$$(4.8) \quad v(x_\alpha(t)+, t) = v(x_\alpha(t)-, t).$$

Then, define $v^\alpha := v(x_\alpha(t)+, t) = v(x_\alpha(t)-, t)$.

Now, consider the following cases:

Case 1 $v^\alpha < w^{\alpha+} < w^{\alpha-}$

Case 2 $w^{\alpha+} < w^{\alpha-} < v^\alpha$

Case 3 $w^{\alpha+} < v^\alpha < w^{\alpha-}$

By symmetry $v \longleftrightarrow w$, the cases with a discontinuity in v , but not in w , are similar; we do not consider them here.

We now handle the cases:

Case 1 and Case 2 Case 1 and Case 2 are similar. We handle only Case 1.

We rewrite the first term ($E_{\alpha,1}$) of (4.7),

$$(4.9) \quad \begin{aligned} & \left| w^{\alpha+} - v^\alpha \right| (\sigma(w^{\alpha+}, v^\alpha) - \sigma(w^{\alpha-}, w^{\alpha+})) - \left| w^{\alpha-} - v^\alpha \right| (\sigma(w^{\alpha-}, v^\alpha) - \sigma(w^{\alpha-}, w^{\alpha+})) = \\ & \sigma(w^{\alpha-}, w^{\alpha+}) \left(\left| w^{\alpha-} - v^\alpha \right| - \left| w^{\alpha+} - v^\alpha \right| \right) + \left| w^{\alpha+} - v^\alpha \right| \sigma(w^{\alpha+}, v^\alpha) - \left| w^{\alpha-} - v^\alpha \right| \sigma(w^{\alpha-}, v^\alpha). \end{aligned}$$

Then remark that in this case, $|w^{\alpha-} - v^\alpha| - |w^{\alpha+} - v^\alpha| = |w^{\alpha-} - w^{\alpha+}|$ and then from the definition of the Rankine-Hugoniot speed (see (3.6)), we get that the first term of (4.7) is identically zero.

Thus, we conclude

$$(4.10) \quad |E_\alpha| \leq \left| w^{\alpha-} - w^{\alpha+} \right| \left| \dot{x}_\alpha - \sigma(w^{\alpha-}, w^{\alpha+}) \right|.$$

Case 3

The first term of (4.7) ($E_{\alpha,1}$) is nonpositive due to $\partial_u \sigma(u, v) = \partial_v \sigma(u, v) > 0$.

Thus, we conclude

$$(4.11) \quad |\max\{E_\alpha, 0\}| \leq \left| w^{\alpha-} - w^{\alpha+} \right| \left| \dot{x}_\alpha - \sigma(w^{\alpha-}, w^{\alpha+}) \right|.$$

Assume now that

$$(4.12) \quad v(x_\alpha(t)+, t) < v(x_\alpha(t)-, t).$$

We then consider the additional 4 cases:

Case 1 $w^{\alpha+} < v^{\alpha+} < v^{\alpha-} < w^{\alpha-}$

Case 2 $v^{\alpha+} < w^{\alpha+} < w^{\alpha-} < v^{\alpha-}$

Case 3 $w^{\alpha+} < v^{\alpha+} < w^{\alpha-} < v^{\alpha-}$

Case 4 $v^{\alpha+} < w^{\alpha+} < v^{\alpha-} < w^{\alpha-}$

Remark that for almost every t , either $(v(x_\alpha(t)+, t), v(x_\alpha(t)-, t), \dot{x}_\alpha)$ is a shock verifying Rankine-Hugoniot or $v^{\alpha+} = v^{\alpha-}$. In the case when v is in BV , this is well-known. See

e.g. [40, Lemma 6] or [35, Lemma 5.2], where this is shown to hold even under the weaker Strong Trace Property (Definition 2.1).

Then again by adding zero to (4.6), we get

$$(4.13) \quad E_\alpha = \left[\begin{aligned} & \left| w^{\alpha+} - v^{\alpha+} \right| (\sigma(w^{\alpha+}, v^{\alpha+}) - \sigma(v^{\alpha-}, v^{\alpha+})) \\ & - \left| w^{\alpha-} - v^{\alpha-} \right| (\sigma(w^{\alpha-}, v^{\alpha-}) - \sigma(v^{\alpha-}, v^{\alpha+})) \end{aligned} \right] \\ + \left[(\sigma(v^{\alpha-}, v^{\alpha+}) - \dot{x}_\alpha) \left(\left| w^{\alpha+} - v^{\alpha+} \right| - \left| w^{\alpha-} - v^{\alpha-} \right| \right) \right] \\ := \tilde{E}_{\alpha,1} + \tilde{E}_{\alpha,2}.$$

Then, in each of the Cases 1-4, we have $\tilde{E}_{\alpha,2} = 0$ due to $(v(x_\alpha(t)+, t), v(x_\alpha(t)-, t), \dot{x}_\alpha)$ being a Rankine-Hugoniot shock, and $\tilde{E}_{\alpha,1} < 0$ due to $\partial_u \sigma(u, v) = \partial_v \sigma(u, v) > 0$.

This concludes the proof. \square

4.2. Control on Lipschitz constant of a smooth solution. The following Lemma will give control of the Lipschitz constant of a smooth solution to (1.1).

Lemma 4.2 (control on the Lipschitz constant of a smooth solution). *Let $\bar{u}^0: \mathbb{R} \rightarrow \mathbb{R}$ be in L^∞ and Lipschitz-continuous. Let \bar{u} be the unique entropy weak solution to (1.1) with initial data \bar{u}^0 . As long as \bar{u} is Lipschitz-continuous it verifies*

$$(4.14) \quad \text{Lip}[\bar{u}(\cdot, t)] \leq \max \left\{ \left| \frac{1}{\frac{1}{\sup(\bar{u}^0)'} + t \inf A''} \right|, \left| \frac{1}{\frac{1}{\inf(\bar{u}^0)'} + t \inf A''} \right| \right\},$$

where A'' is the second derivative of the flux function A . Here, $1/0 = +\infty$ and $1/+\infty = 0$.

Remark 13. This result follows immediately from the proof of [11, Theorem 6.1.1].

We give a brief summary of the argument, specialized to the scalar conservation laws. We remark that we do not use the large family of Kruzhkov entropies.

Proof. As long as the solution is Lipschitz-continuous it is given by the method of characteristics.

We can express \bar{u} implicitly as

$$\bar{u}(x, t) = \bar{u}^0(x - A'(\bar{u}(x, t))t)$$

and taking x -derivatives on both sides leads to

$$\bar{u}_x(x, t) = (\bar{u}^0)'(x - A'(\bar{u}(x, t))t) \cdot [1 - A''(\bar{u}(x, t))t \bar{u}_x(x, t)]$$

which (for $(\bar{u}^0)' \neq 0$) can be rearranged as

$$(4.15) \quad \bar{u}_x(x, t) = \frac{1}{\frac{1}{(\bar{u}^0)'(x - A'(\bar{u}(x, t))t)} + A''(\bar{u}(x, t))t}.$$

□

4.3. Extending the relative entropy inequality. The results from this section will be instrumental in estimating $\|\bar{u} - \hat{\psi}\|_{L^2}$.

Lemma 4.3 (An extension of the entropy inequality). *Fix $T > 0$. For $i = 1, 2$, consider weak solutions $\hat{u}_i \in L^\infty(\mathbb{R} \times [0, T])$ to (2.16) with residuals $R_i \in L^\infty((0, T) \times \mathbb{R})$, where the residuals are defined by*

$$(4.16) \quad R_i := \partial_t \hat{u}_i + \partial_x A(\hat{u}_i).$$

Moreover, assume that \hat{u}_2 is entropic for the strictly convex entropy $\eta \in C^2(\mathbb{R})$. Further, assume that \hat{u}_1 is Lipschitz.

Then for all positive, Lipschitz-continuous test functions $\phi: \mathbb{R} \times [0, T] \rightarrow \mathbb{R}$ with compact support, we have

$$(4.17) \quad \begin{aligned} & \int_0^T \int_{-\infty}^{\infty} [\partial_t \phi \eta(\hat{u}_2(x, t) | \hat{u}_1(x, t)) + \partial_x \phi q(\hat{u}_2(x, t); \hat{u}_1(x, t))] dx dt \\ & \quad + \int_{-\infty}^{\infty} \phi(x, 0) \eta(\hat{u}_2^0(x) | \hat{u}_1^0(x)) dx \\ & \geq \\ & \int_0^T \int_{-\infty}^{\infty} \phi \left[R_2(x, t) (\eta'(\hat{u}_1(x, t)) - \eta'(\hat{u}_2(x, t))) + \partial_x \hat{u}_1(x, t) \eta''(\hat{u}_1(x, t)) A(\hat{u}_2(x, t) | \hat{u}_1(x, t)) \right. \\ & \quad \left. + R_1(x, t) \eta''(\hat{u}_1(x, t)) [\hat{u}_2(x, t) - \hat{u}_1(x, t)] \right] dx dt. \end{aligned}$$

I.e., we have the following inequality in the sense of distributions

$$(4.18) \quad \begin{aligned} & \partial_t \eta(\hat{u}_2(x, t) | \hat{u}_1(x, t)) + \partial_x q(\hat{u}_2(x, t); \hat{u}_1(x, t)) \\ & \leq -R_2(x, t) (\eta'(\hat{u}_1(x, t)) - \eta'(\hat{u}_2(x, t))) - \partial_x \hat{u}_1(x, t) \eta''(\hat{u}_1(x, t)) A(\hat{u}_2(x, t) | \hat{u}_1(x, t)) \\ & \quad - R_1(x, t) \eta''(\hat{u}_1(x, t)) [\hat{u}_2(x, t) - \hat{u}_1(x, t)]. \end{aligned}$$

The equation (4.17) bears resemblance to the pivotal inequality employed in Dafermos's demonstration of weak-strong stability, which provides a relative formulation of the entropy inequality (refer to equation (5.2.10) in [11, p. 122-5]). However, unlike the original formulation, (4.17) takes into account residuals present in either of the two solutions. The derivation of (4.17) extends the well-known weak-strong stability proof by Dafermos and DiPerna [11, p. 122-5].

For the reader's convenience, the proof of Lemma 4.3 is in the appendix (Appendix A.2).

4.4. Control on shifts. In order to control $\left\| \hat{u} - \hat{\psi} \right\|_{L^1}$ we need to control shifts. This will be established using the following lemma, which says that if a discontinuity in the second slot of the relative entropy is moving at the Rankine-Hugoniot speed of the discontinuity in the first slot of the relative entropy, then there is a creation of negative entropy dissipation proportional to the difference between the natural Rankine-Hugoniot speed of the shock in the second slot and the Rankine-Hugoniot speed of the shock in the first slot.

Lemma 4.4 (negativity of entropy dissipation [8, Proposition 2.1]). *Fix $\mathfrak{s}, B > 0$. Let $u_+, u_-, \bar{u}_+, \bar{u}_- \in [-B, B]$ verify $u_- \geq u_+, \bar{u}_- - \bar{u}_+ \geq \mathfrak{s}$.*

Then,

$$(4.19) \quad q(u_+; \bar{u}_+) - q(u_-; \bar{u}_-) - \sigma(u_+, u_-)(\eta(u_+ | \bar{u}_+) - \eta(u_- | \bar{u}_-)) \\ \leq -\frac{1}{12} \inf A'' \inf \eta'' \mathfrak{s} ((u_+ - \bar{u}_+)^2 + (u_- - \bar{u}_-)^2),$$

where σ is defined in (3.6), and the infima $\inf A''$ and $\inf \eta''$ run over the set $[-B, B]$.

The proof of Lemma 4.4 follows almost immediately from [8], where the result is given (and proved) for the particular entropy $\eta(u) = \frac{u^2}{2}$. See also [35, Lemma 4.1] and [47, p. 9-10].

Remark 14. The \mathfrak{s} in (4.19) shows that smaller shocks dissipate less relative entropy and, therefore, we will have less control on positions of small shocks than on positions of large shocks.

Remark 15. For the systems case, the analogue of the dissipation estimate Lemma 4.4 would be along the lines of [32, Proposition 4.1], for example.

4.5. Pointwise difference between two solutions. In order to obtain good control of shifts we need that the shocks being shifted do not become too small (see Lemma 4.4). In practical computations, we can monitor, at any time, the minimal size of each shock by computing $\inf(\hat{v}_i(\cdot, t) - \hat{v}_{i+1}(\cdot, t))$ where the infimum is taken over the set of points where the shock might be. In addition, we would like to argue that it is plausible that the difference $\hat{v}_i - \hat{v}_{i+1}$ does not decay quickly, since there are bounds for the speed of decay of $v_i - v_{i+1}$ for exact solutions v_i, v_{i+1} . Here $\hat{v}_i, \hat{v}_{i+1}, v_i, v_{i+1}$ are in the context of the Main Theorem (Theorem 2.2).

The pointwise difference between two solutions can be decreasing. However, we can control the rate at which the gap narrows:

Lemma 4.5 (Rate of decrease on the gap between two solutions). *Fix $t, \rho > 0$. Let $v_1^0: \mathbb{R} \rightarrow \mathbb{R}$ and $v_2^0: \mathbb{R} \rightarrow \mathbb{R}$ be Lipschitz-continuous functions such that $v_1^0(x) - v_2^0(x) \geq \rho$ for all $x \in \mathbb{R}$. Assume that on the interval $[0, t]$, unique classical solutions v_i to the system (1.1) exist with initial data v_i^0 (with $i = 1, 2$). Then the difference between these solutions satisfies*

$$(4.20) \quad v_1(x, t) - v_2(x, t) \geq \frac{\rho}{1 + \mathfrak{A} \min\{\text{Lip}[v_1^0], \text{Lip}[v_2^0]\}t}$$

for all $x \in \mathbb{R}$. Here, $\mathfrak{A} := \sup A''$ where the sup is taken over the sets of values of v_1, v_2 .

Proof. We are careful not to use the Kruzhkov entropies.

We assume that $t > 0$, otherwise the proof is immediate.

It is well known that the solutions v_1 and v_2 are given by the method of characteristics. One possible reference, which does not use the Kruzhkov theory, is [11, p. 176-177]. See also the proof of [34, Lemma 2.1].

Then fix $x \in \mathbb{R}$. Since the solutions v_1 and v_2 are given by the method of characteristics, there exists x_1^0 and x_2^0 such that

$$(4.21) \quad \begin{aligned} v_1(x, t) &= v_1^0(x_1^0) \\ v_2(x, t) &= v_2^0(x_2^0), \end{aligned}$$

and

$$(4.22) \quad x = x_1^0 + A'(v_1^0(x_1^0))t = x_2^0 + A'(v_2^0(x_2^0))t,$$

where A' is the derivative of the flux function.

Set $\tilde{\rho} = v_1(x, t) - v_2(x, t) = v_1^0(x_1^0) - v_2^0(x_2^0)$. Then,

$$|x_1^0 - x_2^0| = |A'(v_2^0(x_2^0))t - A'(v_1^0(x_1^0))t| \leq \mathfrak{A}t\tilde{\rho}$$

and thus,

$$\tilde{\rho} = v_1^0(x_1^0) - v_2^0(x_2^0) \geq v_1^0(x_1^0) - v_2^0(x_1^0) - |v_2^0(x_1^0) - v_2^0(x_2^0)| \geq \rho - \mathfrak{A}\text{Lip}[v_2^0]\tilde{\rho}t.$$

Similarly,

$$\tilde{\rho} = v_1^0(x_1^0) - v_2^0(x_2^0) \geq v_1^0(x_2^0) - v_2^0(x_2^0) - |v_1^0(x_2^0) - v_1^0(x_1^0)| \geq \rho - \mathfrak{A}\text{Lip}[v_1^0]\tilde{\rho}t,$$

so that

$$(4.23) \quad \tilde{\rho} \geq \frac{\rho}{1 + \mathfrak{A} \min\{\text{Lip}[v_1^0], \text{Lip}[v_2^0]\}t}.$$

□

4.6. L^∞ -control on numerical solutions. The following Lemma will help us reduce the computational cost of our numerical scheme in Section 5.1.1.

Lemma 4.6 (L^∞ -control on Lipschitz-continuous numerical solutions). *Fix $T, S > 0$. Let $\bar{u}^0: \mathbb{R} \rightarrow \mathbb{R}$ be in $L^\infty(\mathbb{R})$, Lipschitz-continuous and nondecreasing. Let \bar{u} be the unique entropy weak solution to (1.1) with initial data \bar{u}^0 . Let \hat{u} be a Lipschitz-continuous solution to (2.16) with initial data \hat{u}^0 and residual R , defined by $R := \partial_t \hat{u} + \partial_x A(\hat{u})$. Then, we have the following L^∞ -type estimate:*

$$(4.24) \quad \begin{aligned} & \|\hat{u}(\cdot, T) - \bar{u}(\cdot, T)\|_{L^\infty(-S, S)}^3 \\ & \leq 8(\text{Lip}[\bar{u}|_{(-S, S)}(\cdot, T)] + \text{Lip}[\hat{u}|_{(-S, S)}(\cdot, T)]) \\ & \cdot Ce^{CT} \left(\|\hat{u}(\cdot, 0) - \bar{u}(\cdot, 0)\|_{L^2(-S-sT, S+sT)}^2 + \int_0^T \int_{-S-s(T-t)}^{S+s(T-t)} R^2(x, t) dx dt \right), \end{aligned}$$

where $s, C > 0$ are constants that depends only on A , η , $\|\bar{u}\|_{L^\infty}$, and $\|\hat{u}\|_{L^\infty}$.

Remark 16. For the numerical solution \hat{u} , the Lipschitz constant can be calculated a posteriori. For the exact solution \bar{u} , we can use Lemma 4.2 to estimate the Lipschitz constant.

Proof. We basically follow the famous weak-strong stability proof of Dafermos and DiPerna (see for example [11]). We work within the cone of information. We define

$$(4.25) \quad h_{\text{left}}(t) := -S - s(T - t),$$

$$(4.26) \quad h_{\text{right}}(t) := S + s(T - t),$$

where $s > 0$ is chosen such that $|q(a; b)| \leq s\eta(a|b)$ for all a, b verifying

$$(4.27) \quad |a|, |b| \leq \max\{\|\bar{u}\|_{L^\infty}, \|\hat{u}\|_{L^\infty}\}.$$

Then, we integrate (4.18) on the region

$$(4.28) \quad S := \{(x, t) \in \mathbb{R} \times [0, T] | h_{\text{left}}(t) < x < h_{\text{right}}(t)\}.$$

Within the context of (4.18), we choose $\hat{u}_1 := \bar{u}$, $R_1 := 0$, $\hat{u}_2 := \hat{u}$, and $R_2 := R$.

This gives

$$(4.29) \quad \int_{-S}^S \eta(\hat{u}(x, T)|\bar{u}(x, T)) dx \leq \int_{-S-sT}^{S+sT} \eta(\hat{u}^0(x)|\bar{u}^0(x)) dx \\ + \int_0^T \int_{h_{\text{left}}(t)}^{h_{\text{right}}(t)} -R(x, t)(\eta'(\bar{u}(x, t)) - \eta'(\hat{u}(x, t))) - \partial_x \bar{u}(x, t) \eta''(\bar{u}(x, t)) A(\hat{u}(x, t)|\bar{u}(x, t)) dx dt.$$

Remark that we have used that $\dot{h}_{\text{left}} = s$, $\dot{h}_{\text{right}} = -s$ and s is chosen such that $|q(a; b)| \leq s\eta(a|b)$ for all a, b verifying $|a|, |b| \leq \max\{\|\bar{u}\|_{L^\infty}, \|\hat{u}\|_{L^\infty}\}$.

It is classical that due to \bar{u}^0 being non-decreasing, $\bar{u}(\cdot, t)$ will be non-decreasing for all $t > 0$ (for one source of a proof of this without using the Kruzhkov theory, see [34, Lemma 2.1]). Remark also that due to the convexity of the flux A , $A(\hat{u}(x, t)|\bar{u}(x, t)) \geq 0$. Further, recall that $\eta'' > 0$. Thus,

$$(4.30) \quad -\partial_x \bar{u}(x, t) \eta''(\bar{u}(x, t)) A(\hat{u}(x, t)|\bar{u}(x, t)) \leq 0.$$

Thus, (4.29) simplifies to

$$(4.31) \quad \int_{-S}^S \eta(\hat{u}(x, T)|\bar{u}(x, T)) dx \leq \int_{-S-sT}^{S+sT} \eta(\hat{u}^0(x)|\bar{u}^0(x)) dx \\ - \int_0^T \int_{h_{\text{left}}(t)}^{h_{\text{right}}(t)} R(x, t)(\eta'(\bar{u}(x, t)) - \eta'(\hat{u}(x, t))) dx dt.$$

From (4.31), Hölder's inequality, and Young's inequality we get

$$(4.32) \quad \int_{-S}^S \eta(\hat{u}(x, T)|\bar{u}(x, T)) dx \leq \int_{-S-sT}^{S+sT} \eta(\hat{u}^0(x)|\bar{u}^0(x)) dx + \frac{1}{2} \int_0^T \int_{h_{\text{left}}(t)}^{h_{\text{right}}(t)} R^2(x, t) dx dt \\ + \frac{1}{2} \int_0^T \int_{h_{\text{left}}(t)}^{h_{\text{right}}(t)} (\eta'(\bar{u}(x, t)) - \eta'(\hat{u}(x, t)))^2 dx dt.$$

Then, we apply the Gronwall technique to (4.32). We recall (3.4). This yields

$$(4.33) \quad \|\hat{u}(\cdot, T) - \bar{u}(\cdot, T)\|_{L^2(-S, S)}^2 \\ \leq C e^{CT} \left(\|\hat{u}(\cdot, 0) - \bar{u}(\cdot, 0)\|_{L^2(-S-sT, S+sT)}^2 + \int_0^T \int_{h_{\text{left}}(t)}^{h_{\text{right}}(t)} R^2(x, t) dx dt \right),$$

where the constant $C > 0$ depends only on η , $\|\bar{u}\|_{L^\infty}$, and $\|\hat{u}\|_{L^\infty}$.

On the other hand, we can use $\|\hat{u}(\cdot, T) - \bar{u}(\cdot, T)\|_{L^\infty}$ and the Lipschitz continuity of \hat{u} and \bar{u} to control the L^2 norm from below:

Let $D := \|\hat{u}(\cdot, T) - \bar{u}(\cdot, T)\|_{L^\infty(-S, S)}$. Then, due to Lipschitz continuity of \hat{u} and \bar{u} , we know that $|\hat{u}(x, T) - \bar{u}(x, T)| > \frac{D}{2}$ on an interval of length at least L , where

$$(4.34) \quad L := \frac{\frac{D}{2}}{\text{Lip}[\bar{u}|_{(-S, S)}(\cdot, T)] + \text{Lip}[\hat{u}|_{(-S, S)}(\cdot, T)]}.$$

Then,

$$(4.35) \quad \|\hat{u}(\cdot, T) - \bar{u}(\cdot, T)\|_{L^2}^2 \geq L \left(\frac{D}{2}\right)^2 = \frac{D^3}{8(\text{Lip}[\bar{u}|_{(-S, S)}(\cdot, T)] + \text{Lip}[\hat{u}|_{(-S, S)}(\cdot, T)])}.$$

Then, we combine (4.33) and (4.35) to yield

$$(4.36) \quad L \left(\frac{D}{2}\right)^2 = \frac{D^3}{8(\text{Lip}[\bar{u}|_{(-S, S)}(\cdot, T)] + \text{Lip}[\hat{u}|_{(-S, S)}(\cdot, T)])} \\ \leq C e^{CT} \left(\|\hat{u}(\cdot, 0) - \bar{u}(\cdot, 0)\|_{L^2(-S-sT, S+sT)}^2 + \int_0^T \int_{h_{\text{left}}(t)}^{h_{\text{right}}(t)} R^2(x, t) dx dt \right).$$

This gives (4.24). □

5. CONSTRUCTION OF \hat{u} AND $\hat{\psi}$

In this section, we detail how the function \hat{u} is constructed in our numerical experiments. We also give the (theoretic) construction of the ancillary function $\hat{\psi}$.

We approximate initial data $\bar{u}^0 \in \mathcal{S}^\epsilon$, by some $\tilde{u}^0 \in \mathcal{S}_d^\epsilon$ by decomposing the rapidly decreasing parts of \bar{u}^0 (i.e., intervals where $\partial_x \bar{u}^0 < -\epsilon$) into step functions with steps of length $\delta > 0$ where δ is a parameter that we can choose. Let \tilde{u}^0 have discontinuities at points x_1, \dots, x_N . Let $x_0 = -\infty$ and $x_{N+1} = +\infty$. Then, we extend each $\tilde{u}^0|_{(x_i, x_{i+1})}$ (for $i = 0, \dots, N + 1$) by the method described in Appendix A.1 to a function v_i^0 on all of \mathbb{R} . Let v_i denote the exact (smooth) solution to (1.1) emanating from the initial data v_i^0 .

From now on, we distinguish the set of intervals (x_i, x_{i+1}) that correspond to intervals in which $\partial_x \bar{u}^0$ is bounded from below by $-\epsilon$ from the set of intervals that are sub-intervals of intervals on which $\partial_x \bar{u}^0$ is bounded from above by $-\epsilon$. We denote these sets of intervals by \mathcal{I}_{nnd} (nnd=nearly non-decreasing) and \mathcal{I}_{rd} (rd=rapidly decreasing), respectively.

For intervals $(x_i, x_{i+1}) \in \mathcal{I}_{nnd}$, we project v_i^0 onto a space of piece-wise polynomials with mesh width $h > 0$, which leads to functions $u_{h,i}^0$ that can be evolved by a numerical scheme. Reconstructing them according to the strategy given in [20], gives us Lipschitz functions \hat{v}_i^0 on all of \mathbb{R} . Afterwards, we evolve the functions $u_{h,i}^0$ using Runge-Kutta discontinuous Galerkin schemes, and reconstruct them based on the techniques described in [14] – giving rise to functions \hat{v}_i . It was demonstrated in [14] that these functions have residuals R_i (see (2.16)) of size h^{q+1} in the L^2 -norm if polynomials of degree q and upwind fluxes are used in the dG scheme, *provided the problems with the extended initial data v_i^0 have smooth solutions*.

If the v_i have kinks, i.e. points with different left- and right-sided derivatives in x , this reduces the convergence order of the L^2 norm of residuals for meshes that are not aligned with the kinks.

To mitigate this issue, in Appendix A.1, we construct the global extensions of the initial data in such a way that the v_i are C^1 in the regions where they are expected to be revealed² in either \hat{u} or $\hat{\psi}$.

For the v_i^0 (based on the constructions from Appendix A.1) corresponding to intervals $(x_{i-1}, x_i) \in \mathcal{I}_{rd}$ (rapidly decreasing intervals), we do not actually numerically simulate these v_i^0 in the computer and instead assume (in the numerical scheme we implement in the computer) the \hat{v}_i are globally constant. We postpone the discussion of these v_i^0 to Section 5.1 below.

Remark 17. It is noticeable that we do not have many requirements on which numerical solver and reconstruction procedure we use to create numerical solutions and reconstructions for our analysis to be applicable. The solver needs to be such that we can compute reconstructions of the numerical solution that preserve the pointwise ordering of the different \hat{v}_i (see (A.19)). Remark that for the exact solution, the ordering follows from the ordering of the initial data (see Lemma 4.5). See also Remark 8 after the Main Theorem (Theorem 2.2).

5.1. Construction of \hat{u} . The numerical solution \hat{u} is constructed from the \hat{v}_i as follows. For those discontinuities in \hat{u}^0 that correspond to ‘large’ shocks and ‘boundary’ shocks (see Figure 1) the following ODEs are solved numerically starting at time $t = 0$, e.g. by some

²Remark that by [11, Theorem 6.1.1], if v_i^0 is C^1 , then so is v_i for as long as v_i is Lipschitz.

Runge-Kutta method:

$$(5.1) \quad \begin{cases} \dot{\hat{h}}_i(t) = \sigma(\hat{v}_i(\hat{h}_i(t), t), \hat{v}_{i+1}(\hat{h}_i(t), t)) & \text{for } t > 0, \\ \hat{h}_i(0) = x_i, \end{cases}$$

where the x_i are as in the definition of the space \mathcal{S}_d^ϵ (see (2.2)). Since σ and the \hat{v}_i are at least Lipschitz this problem is well-posed. If the numerical scheme for computing the \hat{v}_i is higher order we should use a Runge-Kutta scheme of sufficient order so that its contribution to the position error in \hat{h}_i is smaller than other sources of position errors. Remark that for the ‘front tracking’ shocks in \hat{u} , due to the \hat{v}_ℓ and \hat{v}_r , for the left- and right-hand states of such shocks, respectively, being globally constant (see Section 5.1) we do not need Runge-Kutta and instead can employ a simple scalar front tracking scheme.

Consider the first time \hat{t}_1 such that $\hat{h}_i(\hat{t}_1) = \hat{h}_{i+1}(\hat{t}_1)$ for some i . Then we define for $0 \leq t \leq \hat{t}_1$,

$$(5.2) \quad \hat{u}(x, t) := \begin{cases} \hat{v}_1(x, t) & \text{if } x < \hat{h}_1(t), \\ \hat{v}_2(x, t) & \text{if } \hat{h}_1(t) < x < \hat{h}_2(t), \\ \vdots & \\ \hat{v}_{N+1}(x, t) & \text{if } \hat{h}_N(t) < x. \end{cases}$$

Note that the \hat{h}_i are generalized characteristics for \hat{u} .

At time \hat{t}_1 , at least two of the curves \hat{h}_i have touched. In particular, $\hat{h}_i(\hat{t}_1) = \hat{h}_{i+1}(\hat{t}_1)$ for some i . For these two curves that touch, we forget about the \hat{v}_{i+1} that was between them. For time $t > \hat{t}_1$, we redefine \hat{h}_i to solve the ODE

$$(5.3) \quad \dot{\hat{h}}_i(t) = \sigma(\hat{v}_i(\hat{h}_i(t), t), \hat{v}_{i+2}(\hat{h}_i(t), t)) \text{ for } t > \hat{t}_1,$$

keeping the value of \hat{h}_i at $t = \hat{t}_1$ unchanged. Further, we define

$$(5.4) \quad \hat{h}_i(t) = \hat{h}_{i+1}(t)$$

for all $t > \hat{t}_1$. In effect, we are gluing the two curves together as soon as they touch, forgetting about the \hat{v}_{i+1} that was between them and redefining the ODE accordingly. We do a similar thing if $\hat{h}_i(t)$, $\hat{h}_{i+1}(t)$ and $\hat{h}_{i+2}(t)$ touch simultaneously at time \hat{t}_1 : for time $t > \hat{t}_1$, we redefine \hat{h}_i to solve the ODE

$$(5.5) \quad \dot{\hat{h}}_i(t) = \sigma(\hat{v}_i(\hat{h}_i(t), t), \hat{v}_{i+3}(\hat{h}_i(t), t)) \text{ for } t > \hat{t}_1,$$

keeping the value of \hat{h}_i at $t = \hat{t}_1$ unchanged. Further, we define

$$(5.6) \quad \hat{h}_i(t) = \hat{h}_{i+1}(t) = \hat{h}_{i+2}(t)$$

for all $t > \hat{t}_1$. Similarly if four curves touch simultaneously, etc.

We do this for each set of curves of discontinuity in \hat{u} that touch at time \hat{t}_1 . This inductive process defines the \hat{u} . Remark how the labeling given by (5.4) allows to refer

to the same curve by the same index, even after collisions (and similarly for $\hat{\psi}$, which we construct below).

5.1.1. *The \hat{v}_i from rapidly decreasing intervals.* For the v_i^0 (based on the constructions from Appendix A.1) corresponding to intervals $(x_{i-1}, x_i) \in \mathcal{I}_{rd}$ (rapidly decreasing intervals), we do not actually numerically simulate these v_i^0 . Simulating these v_i^0 would require simulating $\mathcal{O}(\delta^{-1})$ numerical solutions, i.e. the number of numerical solutions would increase with mesh refinement, tremendously increasing the computational costs.

However, we cannot simply take $\hat{v}_i := v_i$, where v_i is the exact entropic solution with initial data v_i^0 , because then we do not know (even a posteriori) if the ordering condition $\hat{v}_j(x, t) > \hat{v}_{j+1}(x, t)$ (for all j and for all (x, t)) is verified³.

Instead, we do the following. Consider a global extension v_i^0 (see Appendix A.1) for an interval $(x_{i-1}, x_i) \in \mathcal{I}_{rd}$. The v_i^0 is given by (A.8), where the slope M is given by (A.3). Then we numerically simulate a solution to (1.1) with initial data

$$(5.7) \quad v^0(x_{i-1}+) + (x - x_J^i)M$$

globally on \mathbb{R} , where the value x_J^i is defined in (A.9). Call the numerical solution $\hat{\Lambda}$. For reference, we will call the exact solution with initial data (5.7) Λ . Remark that in the context of Appendix A.1, \hat{u}^0 is playing the role of v^0 .

Then, by simply translating the solution $\hat{\Lambda}$ in space, we can obtain also a numerical solution with initial data

$$(5.8) \quad v^0(x_i-) + (x - x_I^i)M$$

globally on \mathbb{R} , where the value x_I^i is defined in (A.10). Call this solution \hat{P} .

³For the scalar conservation laws it is possible to use the Lax-Oleřnik formula (see [17]) for the exact solution v_i to check a posteriori the ordering condition $\hat{v}_j(x, t) > \hat{v}_{j+1}(x, t)$ for all j (with $\hat{v}_i := v_i$), but this is extremely computationally expensive and has no analogue for the general systems case.

Further, based on (A.8), we can define a numerical version of v_i as follows

$$\begin{aligned}
(5.9) \quad \hat{v}_i(x, t) := \min & \left\{ \max \left\{ v^0(x_i-) + (x_I^i - x_i) \frac{d^-}{dx} v^0(x_i), \right. \right. \\
& \sup_{x \in (x_i, \infty)} v^0(x) + \sum_{k=i}^N (v^0(x_k-) - v^0(x_k+)) \\
& \left. + \sum_{k=i+1}^N \left((x_I^k - x_k) \left| \frac{d^-}{dx} v^0(x_k) \right| \right) \right\}, \\
& \max \left\{ \hat{P}, \min \left\{ v^0\left(\frac{x_{i-1} + x_i}{2}\right), \hat{\Lambda} \right\}, \right. \\
& \min \left\{ v^0(x_{i-1}+) + (x_J^i - x_{i-1}) \frac{d^+}{dx} v^0(x_{i-1}), \right. \\
& \inf_{x \in (-\infty, x_i)} v^0(x) - \sum_{k=1}^{i-1} (v^0(x_k-) - v^0(x_k+)) \\
& \left. \left. - \sum_{k=3}^i \left((x_J^{k-1} - x_{k-2}) \left| \frac{d^+}{dx} v^0(x_{k-2}) \right| \right) \right\} \right\},
\end{aligned}$$

where $\frac{d^\pm}{dx} v^0$ are defined in (A.1). Remark the term $(x_J^i - x_{i-1}) \frac{d^+}{dx} v^0(x_{i-1})$ from (A.8) drops out because $\frac{d^+}{dx} v^0(x_{i-1}) = 0$. Similarly, remark that the term $(x_I^i - x_i) \frac{d^-}{dx} v^0(x_i)$ from (A.8) drops out because $\frac{d^-}{dx} v^0(x_i) = 0$.

Notice that if there is no numerical error in \hat{P} and $\hat{\Lambda}$, then $\hat{v}_i \equiv v_i$ (for a schematic diagram of the v_i , see Figure 14 below).

To construct the other \hat{v}_j corresponding to rapidly decreasing pieces of \bar{u}^0 , without doing any more numerical simulations, simply remark that we can translate \hat{P} and $\hat{\Lambda}$ in space (to match the corresponding v_j of interest) and again get numerical solutions to (2.16) by applying a construction similar to (5.9).

Remark that if \hat{v}_i and \hat{v}_{i+1} are both constructed using \hat{P} and $\hat{\Lambda}$ (following (5.9) for \hat{v}_i and the analogous construction for \hat{v}_{i+1}), then as long as \hat{P} and $\hat{\Lambda}$ are strictly increasing, we automatically have $\hat{v}_i(x, t) > \hat{v}_{i+1}(x, t)$ for all (x, t) . Remark that the strict monotonicity of \hat{P} and $\hat{\Lambda}$ can be checked a posteriori. Note also that smooth exact solutions with strictly increasing initial data will be strictly increasing (in x) for all time – this follows from (the proof) of Lemma 4.2 (in particular, see (4.15)).

On the other hand, if \hat{v}_i is constructed following (5.9) while \hat{v}_{i+1} (or \hat{v}_{i-1}) corresponds to a nearly non-decreasing piece of \bar{u}^0 , then the ordering condition $\hat{v}_i(x, t) > \hat{v}_{i+1}(x, t)$ (or $\hat{v}_{i-1}(x, t) > \hat{v}_i(x, t)$) for all (x, t) can be checked a posteriori. See also Remark 8.

In the numerical construction of the \hat{u} in the computer, we simply take \hat{v}_i to be globally constant with value $v^0\left(\frac{x_{i-1} + x_i}{2}\right)$ (recall, for intervals $(x_{i-1}, x_i) \in \mathcal{I}_{rd}$, we have that

$\hat{u}^0|_{(x_{i-1}, x_i)}$ is constant). However, we continue to use \hat{v}_i as defined in (5.9) for the construction of $\hat{\psi}$ below in Section 5.2. This is justified by the following consideration.

If the Rankine-Hugoniot ODEs, used to glue the various \hat{v}_i together to make \hat{u} , are solved with decent accuracy, then the construction of \hat{u} is oblivious to whether \hat{v}_i is a numerically simulated version of the globally-defined extensions from Appendix A.1 or we simply take \hat{v}_i to be globally constant. One way to see this is to remark that in the case when there is no numerical error in the \hat{v}_i (so $\hat{v}_i = v_i$ for all i) and no numerical error in \hat{u} , and they are thus exact solutions to (1.1), then any part of the functions \hat{v}_i not revealed in \hat{u} at $t = 0$ will never be revealed for all $t > 0$. This itself can be seen in the following way. At time t , consider a shock at position \hat{h}_i with v_ℓ as the left-hand state and v_r as the right-hand state. Note that the speed of the characteristic of the function v_ℓ going through the point $(\hat{h}_i(t), t)$ is travelling faster than the Rankine-Hugoniot speed of the shock $(v_\ell(\hat{h}_i(t), t), v_r(\hat{h}_i(t), t))$, while the speed of the characteristic of the function v_r going through the point $(\hat{h}_i(t), t)$ is travelling slower. Thus, artificial extensions are never revealed. Remark here that $v_\ell > v_r$ pointwise.

If numerical errors are present in solving the Rankine-Hugoniot ODEs, these errors will be of the order $(\Delta t)^q$ where q is the convergence rate of the numerical ODE solver (see Section 5.1 for more details). Note that the (absolute) differences between the velocities of the characteristics through the point $(\hat{h}_i(t), t)$ and the shock speed $\sigma(v_\ell(\hat{h}_i(t), t), v_r(\hat{h}_i(t), t))$ are bounded from above (for all $t \in [0, T]$) by

$$\frac{\delta \varepsilon \inf A''}{4(1+\mathfrak{A}MT)},$$

which follows from (A.19) and Lemma 4.5, with $\mathfrak{A} := \sup A''$. Moreover, we choose δ to be approximately $h^{1/2}$, so that any reasonable ODE solver will preserve the ordering of velocities if Δt is chosen small enough – note that the CFL condition implies $\Delta t \lesssim h$. Whether this is the case can be verified in an a posteriori fashion if a posteriori error control for the ODE solver is implemented. The cost for using a high order Runge-Kutta scheme for solving the Rankine-Hugoniot ODEs is negligible compared to the other costs of our numerical scheme for \hat{u} .

We remark that these arguments about when the artificial extensions of the v_i^0 are actually revealed will be used again in Section 6.4.2.

Finally, to ensure that in the construction of the \hat{u} in the computer, we can simply take \hat{v}_i to be globally constant with value $v^0(\frac{x_{i-1}+x_i}{2})$, we need to ensure that at each time t the construction given in (5.9) will never give values for $\hat{v}_i(\cdot, t)$ different from $v^0(\frac{x_{i-1}+x_i}{2})$ on an open set containing the interval $[\hat{h}_{i-1}(t), \hat{h}_i(t)]$. This follows if the level set (in space-time) $\{\hat{\Lambda} = v^0(\frac{x_{i-1}+x_i}{2})\}$ is close to the characteristic of the function v_i emanating from the point x_j^i . Note that the position error of the level set can be bounded by the L^∞ error $\|\Lambda - \hat{\Lambda}\|_{L^\infty}$ (which can be controlled by Lemma 4.6) divided by the minimal slope of $\hat{\Lambda}$. For a first order finite volume scheme this L^∞ error estimator is expected to be $\mathcal{O}(h^{2/3})$.

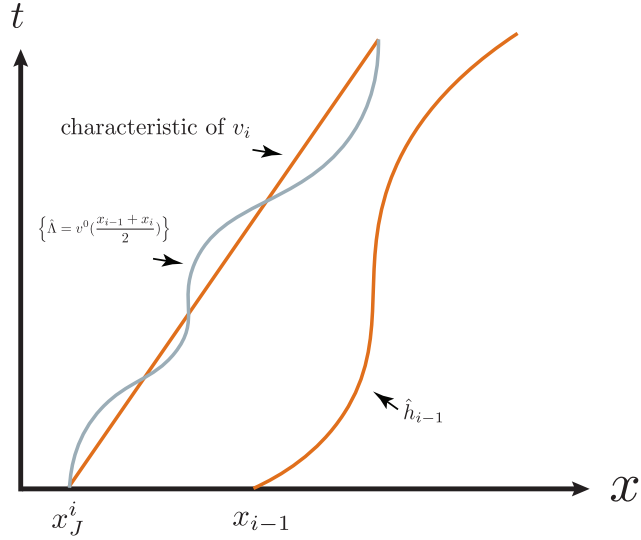


FIGURE 3. To ensure that our analysis is applicable to a function \hat{u} that is defined using \hat{v}_i globally constant (as opposed to the global extensions from Appendix A.1), we need to ensure the level set of $\hat{\Lambda}$ is not too far away from the corresponding characteristic of v_i (and similarly with \hat{P}).

Remark also that (in the context of (A.8)),

$$(5.10) \quad x_{i-1} - x_J^i > \frac{\varepsilon\delta}{2M} \quad \text{and} \quad x_I^i - x_i > \frac{\varepsilon\delta}{2M},$$

and this gap between the characteristic of v_i and the shock \hat{h}_{i-1} cannot shrink in time (as discussed above, if the ODE solver error is small enough, this gap is even growing linearly in time). Thus, by using a fine enough mesh width, we conclude by considering the numerical residual $\partial_t \hat{\Lambda} + \partial_x A(\hat{\Lambda})$ a posteriori and invoking Lemma 4.6. See Figure 3.

5.2. Construction of $\hat{\psi}$. The function $\hat{\psi}$ is defined similarly. The only difference between $\hat{\psi}$ and \hat{u} is that the curves \hat{h}_i (generalized characteristics for \hat{u}) are replaced by curves h_i which are generalized characteristics for the exact solution \bar{u} . More precisely, until the first time t_1 that two of the h_i collide, they are defined as the solution to (in the sense of Filippov)

$$(5.11) \quad \begin{cases} \dot{h}_i(t) = \sigma(\bar{u}(h_i(t)+, t), \bar{u}(h_i(t)-, t)) \text{ for } t > 0, \\ h_i(0) = x_i. \end{cases}$$

Then we define for $0 \leq t \leq t_1$,

$$(5.12) \quad \hat{\psi}(x, t) := \begin{cases} \hat{v}_1(x, t) & \text{if } x < h_1(t), \\ \hat{v}_2(x, t) & \text{if } h_1(t) < x < h_2(t), \\ \vdots & \\ \hat{v}_{N+1}(x, t) & \text{if } h_N(t) < x. \end{cases}$$

Remark that in the definition of $\hat{\psi}$ we still use the numerical solutions \hat{v}_i . Further, $\hat{h}_i(0) = h_i(0)$ for all i , and thus $\hat{u}(\cdot, 0) = \hat{\psi}(\cdot, 0)$.

Furthermore, remark that instead of defining the various h_i using (5.11), we could instead define each h_i as the solution to

$$(5.13) \quad \begin{cases} \dot{h}_i(t) = \sigma(v_i(h_i(t), t), v_{i+1}(h_i(t), t)) \text{ for } t > 0, \\ h_i(0) = x_i, \end{cases}$$

and use a restarting procedure (as above for \hat{u}) when two of the h_i curves collide. This follows immediately from the proof of the main result in [34] (as discussed above in Section 3.2 and Section 3.3).

Both of these ways ((5.11) and (5.13)) of defining the h_i are equivalent. Note that (5.11) is the definition of a generalized characteristic for the solution \bar{u} . The existence of generalized characteristics is well-known when the solution is BV . However, when the solution is only known to verify the Strong Trace Property (Definition 2.1), one possible reference for the existence of generalized characteristics is [35, Lemma 5.2].

Thus, the function $\hat{\psi}$ has discontinuities which follow generalized characteristics for the exact solution \bar{u} , but with the functions in between the discontinuities being the functions from the numerical solver, and not the exact solution itself.

6. ALGORITHM FOR CONTROLLING SHIFTS

We use different arguments to control shifts of different shocks (and derive estimates on Δ_i). In particular, those ‘large’ shocks in \hat{u} (with size independent of δ) that correspond to discontinuities in \bar{u}^0 will be treated differently from those shocks of size proportional to δ (at time $t = 0$) that arise from discretizing rapidly decreasing parts of \bar{u}^0 .

6.1. Controlling Δ_i of ‘large’ shocks. To compute the $\Delta_i(t)$, the estimate on

$$\left| \hat{h}_i(t) - h_i(t) \right|,$$

alluded to in the Main Theorem (Theorem 2.2), we use the following procedure.

Let $\hat{L}_i(t) \in \mathbb{N}$ and $\hat{R}_i(t) \in \mathbb{N}$ denote the integers corresponding to the \hat{v}_k which are to the left and right, respectively, of the discontinuity \hat{h}_i in \hat{u} at time t . Thus, $\hat{v}_{\hat{L}_i(t)}$ is to the left of \hat{h}_i and $\hat{v}_{\hat{R}_i(t)}$ is to the right of \hat{h}_i . Likewise, let $L_i(t) \in \mathbb{N}$ and $R_i(t) \in \mathbb{N}$ denote the integers corresponding to the v_k which are to the left and right, respectively, of the

discontinuity h_i in $\hat{\psi}$ at time t . Thus, $\hat{v}_{L_i(t)}$ is to the left of h_i and $\hat{v}_{R_i(t)}$ is to the right of h_i .

An upper bound on $\left| \hat{h}_i(t) - h_i(t) \right|$ is then given by,

$$(6.1) \quad \Delta_i(t) \leq A_i + B_i + C_i,$$

where A_i, B_i, C_i are defined in (6.2), (6.3), and (6.4):

$$(6.2) \quad A_i := \int_0^t \zeta(t, s) \left| \dot{\hat{h}}_i(s) - \sigma(\hat{v}_{\hat{L}_i(s)}(\hat{h}_i(s), s), \hat{v}_{\hat{R}_i(s)}(\hat{h}_i(s), s)) \right| ds$$

$$(6.3)$$

$$B_i := \int_0^t \zeta(t, s) \left| \sigma(\hat{v}_{\hat{L}_i(s)}(\hat{h}_i(s), s), \hat{v}_{\hat{R}_i(s)}(\hat{h}_i(s), s)) - \sigma(\hat{v}_{L_i(s)}(\hat{h}_i(s), s), \hat{v}_{R_i(s)}(\hat{h}_i(s), s)) \right| ds$$

and

$$(6.4) \quad C_i := \left\| \frac{\zeta(t, \cdot)}{\sqrt{\mathfrak{s}_i(\cdot)}} \right\|_{L^2(0,t)} \cdot \left[C e^{Ct} \left(\int_{-S}^S \eta(\bar{u}(x, 0) | \hat{\psi}(x, 0)) dx + \mathcal{R}(t) \right) \right]^{\frac{1}{2}},$$

where \mathcal{R} is from (2.14), $\mathfrak{s}_i: [0, T] \rightarrow \mathbb{R}$ is any lower bound on $\left| \hat{\psi}(h_i(t)-, t) - \hat{\psi}(h_i(t)+, t) \right|$ and with

$$(6.5) \quad \zeta(t, s) := \exp \left(\int_s^t \mathfrak{A} \max_{i \in \{1, \dots, N+1\}} \text{Lip}[\hat{v}_i(r, \cdot)] dr \right).$$

The proof of (6.1) is postponed to Section 7 (in particular, see Section 7.3).

Let us briefly comment on the sources of errors represented by A_i, B_i, C_i . The term A_i results from not solving the ODE for the position of the discontinuity in \hat{u} , i.e. (5.1), exactly. It can be made small by using a high order Runge-Kutta scheme for solving (5.1) independent of other sources of error. The term B_i reflects errors due to uncertainty which solutions \hat{v}_i furnish the right and left-hand states of the discontinuity in $\hat{\psi}$ (and the right and left-hand states of the corresponding shock in \hat{u} may very well be different). For ‘large’ shocks, the term B_i is expected to be zero most of the time but of order one in those (short) periods of time in which there is uncertainty about which collisions have or have not taken place in $\hat{\psi}$ and thus about which \hat{v}_i provide left and right states. It is expected that under mesh refinement in the numerical scheme the lengths of time intervals of uncertainty go to zero and as a consequence B_i will go to zero. The term C_i results from the shocks in $\hat{\psi}$ not moving with any Rankine-Hugoniot speed according to the \hat{v}_i but following generalized characteristics of \bar{u} . It is this term where the dissipation estimate Lemma 4.4 is used.

To use the formula (6.1), we need to calculate an upper bound of B_i where the upper bound will depend on all the possible $L_i(t)$ and $R_i(t)$ (based on possible collisions between

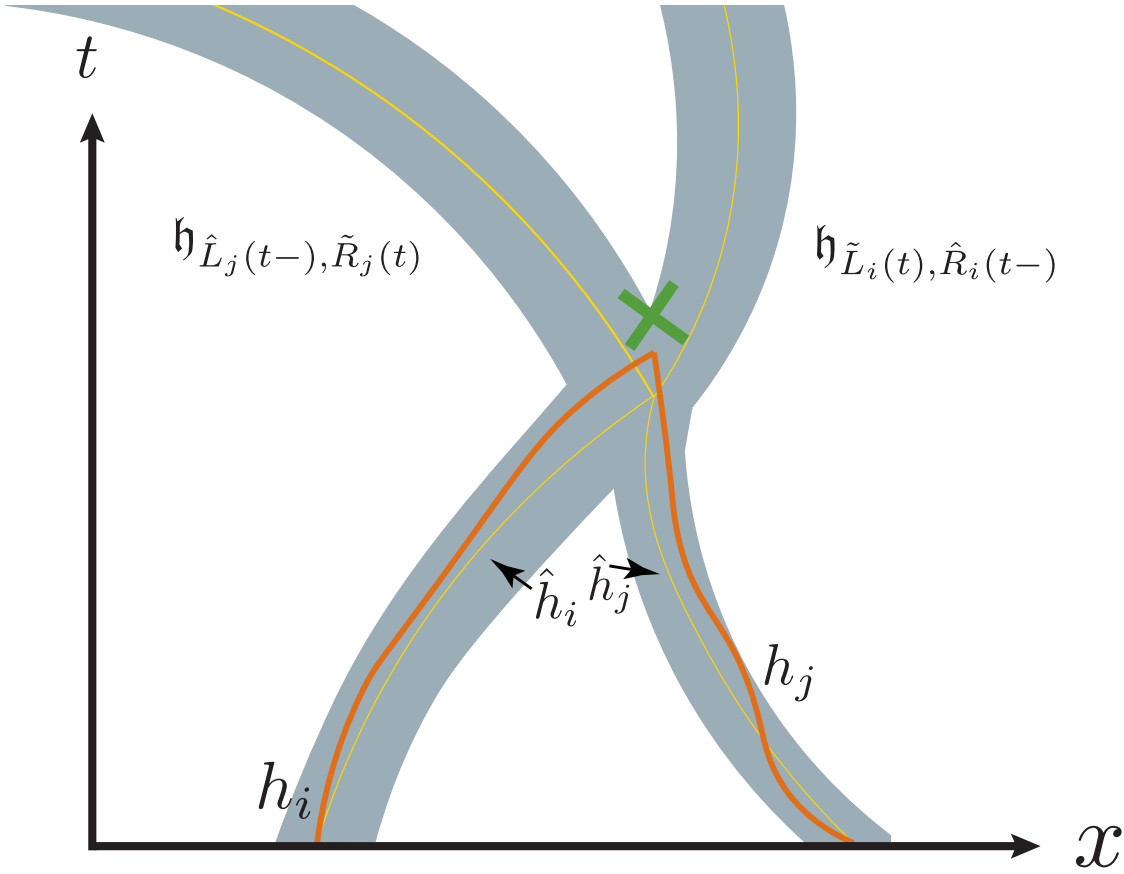


FIGURE 4. An illustration showing $h_i, h_j, \hat{h}_i, \hat{h}_j, \mathfrak{h}_{\tilde{L}_i(t), \hat{R}_i(t-)}$, and $\mathfrak{h}_{\hat{L}_j(t-), \tilde{R}_j(t)}$. Note the green X marks where the two error intervals stop overlapping, and thus the first time we can conclude that the h_i and h_j must have merged.

the h_i we determine from the algorithm given in this section). This means this quantity, as well as C_i , depend on the various Δ_j . Thus, the upper bound on Δ_i depends on Δ_i . To overcome this, we employ the following algorithm.

Recall first that if two characteristics touch, then they are glued together, such that there is some time t^* such that for some i and j , $\hat{h}_i(t^*) = \hat{h}_j(t^*)$ (or $h_i(t^*) = h_j(t^*)$), then for all $t > t^*$, $\hat{h}_i(t) = \hat{h}_j(t)$ (respectively, $h_i(t) = h_j(t)$). See Section 5 for more details on this.

Then, control on the $\Delta_i(t)$ comes from employing the following algorithm:

6.2. Algorithm for bounding (6.3) and (6.4).

- (1) At each time step, for each i , use the fact that there is a uniform upper bound on the \dot{h}_i (and $\dot{\hat{h}}_i$) to estimate in a very rough way the largest possible interval where h_i might be. Let us call this interval I .

We work inductively, and based on our knowledge of previous collisions which must have occurred, let $\tilde{L}_i(t) \in \mathbb{N}$ denote an upper bound on the integer k such that \hat{v}_k is on the left of h_i in the function $\hat{\psi}$ at time t .

Similarly, let $\tilde{R}_i(t) \in \mathbb{N}$ denote a lower bound on the integer k such that \hat{v}_k is on the right of h_i in the function $\hat{\psi}$ at the time t . Remark that $\tilde{L}_i(t) \leq i$ and $\tilde{R}_i(t) \geq i + 1$.

Then, within the rough interval I where h_i might live, calculate a minimal shock size

$$(6.6) \quad \mathfrak{s}_i := \inf_{x \in I} [\hat{v}_{\tilde{L}_i(t)}(x, t) - \hat{v}_{\tilde{R}_i(t)}(x, t)].$$

This then gives a preliminary function \mathfrak{s}_i for use in $\Delta_i(t)$. Then, $\Delta_i(t)$ will give an interval (around \hat{h}_i) of possible positions of h_i which might be narrower than the roughly calculated interval I . Using this improved interval, the infimum in (6.6) can be recalculated over this smaller interval, and thus the \mathfrak{s}_i will increase, which in turn provides for a narrower possible interval for h_i . Inductively repeating this process gives a pointwise non-decreasing sequence of \mathfrak{s}_i 's bounded below by zero. Thus, the sequence of \mathfrak{s}_i 's will have a limit. One can in practice iteratively calculate \mathfrak{s}_i until major increases in \mathfrak{s}_i stop. Remark that if, due to shock interaction, $\hat{v}_{\tilde{L}_i(t)}$ and $\hat{v}_{\tilde{R}_i(t)}$ are not to the left and right, respectively, of h_i in the function $\hat{\psi}$ at time t , then due to the ordering of the \hat{v}_i (see (A.19)), the gap $\hat{\psi}(h_i(t)-, t) - \hat{\psi}(h_i(t)+, t)$ might be larger but not smaller than the \mathfrak{s}_i calculated using the above iteration, i.e. we compute an upper bound C_i that is larger than it would need to be.

- (2) With the \mathfrak{s}_i from step (1), at each fixed time t , use the current location of $\hat{h}_i(t)$ and the formula for $\Delta_i(t)$ to calculate the interval of possible positions of h_i .

After each time step, the formula for $\Delta_i(t)$ will give a larger interval of possible positions of h_i (due to \mathcal{R} growing). Use the error intervals around each \hat{h}_i to determine which curves of discontinuity h_i in $\hat{\psi}$ might have touched (and hence, merged). For each i , let $\hat{L}_i(t) \in \mathbb{N}$ and $\hat{R}_i(t) \in \mathbb{N}$ denote the integers such that $\hat{v}_{\hat{L}_i(t)}$ and $\hat{v}_{\hat{R}_i(t)}$ are to the left and right, respectively, of the discontinuity \hat{h}_i in \hat{u} at time t . Likewise, let $L_i(t) \in \mathbb{N}$ and $R_i(t) \in \mathbb{N}$ denote the integers such that $\hat{v}_{L_i(t)}$ and $\hat{v}_{R_i(t)}$ are to the left and right, respectively, of the discontinuity h_i in $\hat{\psi}$ at time t . Note that there are situations where due to ambiguity about which shifts h_i have merged the numbers L_i, R_i are not known but usually the set of possible pairs (L_i, R_i) is small (the set of possible pairs can be reduced using the analysis in Section 6.3 below).

Then, at each time t , calculate

$$(6.7) \quad \max_{\{(L_i, R_i)\}} \left[\sigma(\hat{v}_{\hat{L}_i(t)}(\hat{h}_i(t)+, t), \hat{v}_{\hat{R}_i(t)}(\hat{h}_i(t)-, t)) \right. \\ \left. - \sigma(\hat{v}_{L_i(t)}(\hat{h}_i(t)+, t), \hat{v}_{R_i(t)}(\hat{h}_i(t)-, t)) \right],$$

where the maximum is taken over the set of possible pairs $L_i(t), R_i(t)$ (based on possible collisions between the h_i). Remark that a worst-case bound for the $|\sigma(\dots) - \sigma(\dots)|$ term in (6.3) is simply two times the supersonic speed, $2 \sup A'$.

6.3. Determining when shocks have collided in $\hat{\psi}$. When two curves of discontinuity, corresponding to either ‘large’ shocks or ‘boundary’ shocks (see Figure 1) in the numerical solution, \hat{h}_i and \hat{h}_j (for $i < j$) collide (and merge) at a time t , we would like to assert whether the corresponding h_i and h_j have collided (and merged) in the function $\hat{\psi}$.

6.3.1. Collisions involving at least one ‘large’ shock. Assume that at least one of the shocks \hat{h}_i or \hat{h}_j are ‘large.’ There are certain scenarios where we can be sure that h_i and h_j have collided. This can be seen as follows:

We work inductively, and based on our knowledge of previous collisions which must have occurred, let $\tilde{L}_i(t) \in \mathbb{N}$ denote an upper bound on the integer k such that \hat{v}_k is on the left of h_i in the function $\hat{\psi}$ at time t . The lower our estimate on $\tilde{L}_i(t)$, the better.

Similarly, let $\tilde{R}_j(t) \in \mathbb{N}$ denote a lower bound on the integer k such that \hat{v}_k is on the right of h_j in the function $\hat{\psi}$ at the time t . The higher our estimate on $\tilde{R}_j(t)$, the better.

Let $\hat{R}_i(t-) \in \mathbb{N}$ denote the integer such that the $\hat{v}_{\hat{R}_i(t-)}$ is to the right of the discontinuity \hat{h}_i in \hat{u} just before the collision at time t . Similarly, let $\hat{L}_j(t-) \in \mathbb{N}$ denote the integer such that the $\hat{v}_{\hat{L}_j(t-)}$ is to the left of the discontinuity \hat{h}_j in \hat{u} just before the collision at time t . Remark that $\hat{R}_i(t-) = \hat{L}_j(t-)$. Then, we consider the solutions to the following initial value problem

$$(6.8) \quad \begin{cases} \mathfrak{h}_{\tilde{L}_i(t), \hat{R}_i(t-)}(t) = \hat{h}_i(t) = \hat{h}_j(t) \\ \mathfrak{h}_{\tilde{L}_i(t), \hat{R}_i(t-)}(s) = \sigma(\hat{v}_{\tilde{L}_i(t)}(\mathfrak{h}_{\tilde{L}_i(t), \hat{R}_i(t-)}(s), s), \hat{v}_{\hat{R}_i(t-)}(\mathfrak{h}_{\tilde{L}_i(t), \hat{R}_i(t-)}(s), s)) \text{ for } s > t, \end{cases}$$

and similarly for $\mathfrak{h}_{\hat{L}_j(t-), \tilde{R}_j(t)}$.

Roughly speaking, we are continuing the curves in \hat{u} as if they did not collide at time t .

We argue by contradiction: we assume the two curves h_i and h_j have not merged in $\hat{\psi}$.

More precisely, we assume that for all $s > t$:

$$(6.9) \quad \begin{aligned} L_j(s) &= \hat{L}_j(t-), \\ R_j(s) &= \tilde{R}_j(t), \\ L_i(s) &= \tilde{L}_i(t), \\ R_i(s) &= \hat{R}_i(t-). \end{aligned}$$

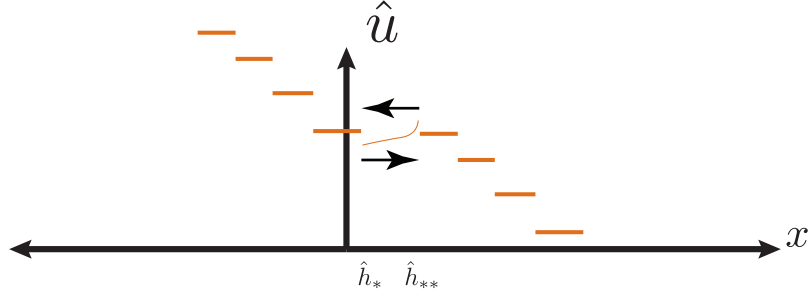


FIGURE 5. The two ‘boundary’ shocks, here denoted by \hat{h}_* and \hat{h}_{**} , are separated by a Lipschitz-continuous piece (originating from a nearly non-decreasing part of \bar{u}^0), and are about to collide in \hat{u} .

We then use the control on the shifts (see (6.1) for ‘large’ shocks and Section 6.5 for ‘boundary’ shocks) to estimate $|\mathfrak{h}_{\tilde{L}_i(t), \hat{R}_i(t-)} - h_i|$ and $|\mathfrak{h}_{\hat{L}_j(t-), \tilde{R}_j(t)} - h_j|$. Under the assumptions (6.9), we know that the quantity (6.3) is zero when we apply the estimate (6.1).

If the two curves $\mathfrak{h}_{\tilde{L}_i(t), \hat{R}_i(t-)}$ and $\mathfrak{h}_{\hat{L}_j(t-), \tilde{R}_j(t)}$ have a distance large enough, i.e. if there is a time when the two error intervals around h_i and h_j no longer intersect (and $\mathfrak{h}_{\tilde{L}_i(t), \hat{R}_i(t-)} > \mathfrak{h}_{\hat{L}_j(t-), \tilde{R}_j(t)}$), then we can conclude that h_i and h_j must have merged in the function $\hat{\psi}$ before this time, see Figure 4.

If $\tilde{L}_i(t) > L_i(t)$ and/or $\tilde{R}_j(t) < R_j(t)$, this simply means we are underestimating the speed at which the two curves $\mathfrak{h}_{\tilde{L}_i(t), \hat{R}_i(t-)}$ and $\mathfrak{h}_{\hat{L}_j(t-), \tilde{R}_j(t)}$ are pulling apart, and due to this underestimate we determine at a later time that h_i and h_j have merged. This is due to the definition of the \tilde{L}_i , \hat{R}_i , \hat{L}_j , \tilde{R}_j , and (A.19). Remark also that $\partial_u \sigma(u, v) = \partial_v \sigma(u, v) > 0$.

Similarly, due to running this algorithm on other pairs of shock curves, at some later time $s > t$ we might be able to deduce a collision has occurred between shock curves in $\hat{\psi}$, leading to an improved estimate on either $\tilde{L}_i(s)$ and/or $\tilde{R}_j(s)$. If at this point in time s we have not yet determined if the h_i and h_j have merged, we can use these improved estimate(s) to increase the speed at which the two curves pull apart. The increase in speed shall start at time s .

6.3.2. Collisions between two ‘boundary’ shocks separated by a nearly non-decreasing piece. Consider two ‘boundary’ shocks $\hat{h}_*(t) < \hat{h}_{**}(t)$ which are separated by a Lipschitz-continuous piece between them (corresponding to a nearly non-decreasing piece in \bar{u}^0 at time $t = 0$). Assume that \hat{h}_* and \hat{h}_{**} collide in \hat{u} at time t_1 . Then we want to know when the two corresponding ‘boundary’ shocks h_* and h_{**} have also collided in $\hat{\psi}$ (see Figure 5). Let (x_i, x_{i+1}) be the nearly non-decreasing interval in \bar{u}^0 at time $t = 0$ corresponding to the Lipschitz-continuous piece which is between the two ‘boundary’ shocks. The idea is the same as in Section 6.3.1 above: in the computer, after the time of the collision, continue both of the two ‘boundary’ shocks forward in time *as if they did not collide* (so, with the Lipschitz-continuous piece to the left for one of the ‘boundary’ shocks, and to the right for

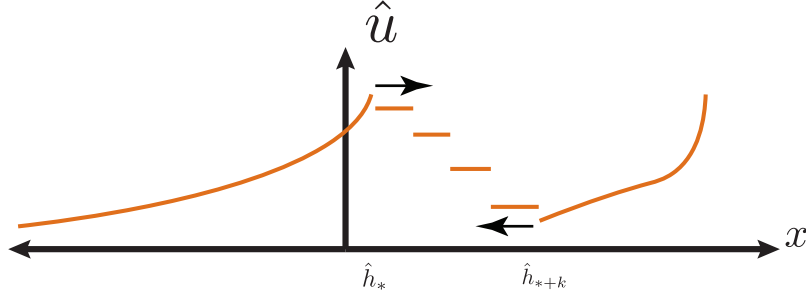


FIGURE 6. The two ‘boundary’ shocks, here denoted by \hat{h}_* and \hat{h}_{*+k} , are the left and right boundary of a region with ‘front tracking’ shocks and they are about to collide in \hat{u} .

the other). Then, under the assumption that the two ‘boundary’ shocks also did not collide in $\hat{\psi}$, use the error intervals from Section 6.5. At the time when the two error intervals have pulled apart and no longer overlap (as in Figure 4), we can conclude by contradiction that the two boundary curves must have collided in $\hat{\psi}$. Remark that there must be a time $t_0 \in [0, t_1]$ such that $\hat{h}_*(t_0) - \hat{h}_{**}(t_0) \geq \frac{x_{i+1} - x_i}{T}$ (otherwise, the two ‘boundary’ shocks \hat{h}_* and \hat{h}_{**} would never touch). Thus, from the moment the two error intervals around \hat{h}_* and \hat{h}_{**} intersect, the length of time until we can determine that h_* and h_{**} have collided in $\hat{\psi}$ will be proportional to the sum of the length of the two error intervals.

6.3.3. *Collision between the left and right ‘boundary’ shocks of a rapidly decreasing piece.*

The procedure explained above in Section 6.3.1 for determining whether a collision has to have taken place in $\hat{\psi}$ works well when at least one ‘large’ shock is involved.

If, however, we consider a possible collision between two curves h_* and h_{*+k} that are the left and right boundary of a region with ‘front tracking’ shocks (corresponding to a rapidly decreasing piece of \bar{u}^0 , see Figure 6), then, if we look at the possible speeds of h_* and h_{*+k} , separately, the lowest possible speed of h_* and the largest possible speed of h_{*+k} may be very close to each other. However, these largest and smallest values cannot be obtained simultaneously in practice. If h_* and h_{*+k} have not collided then h_* can only have collided with ‘front tracking’ shocks that h_{*+k} has not collided with – indeed the right trace of h_* is larger or equal than the left trace of h_{*+k} . Thus, the minimal Rankine-Hugoniot speed difference is

$$(6.10) \quad m := \inf_{(w,v,u)} \sigma(w, v) - \sigma(v, u),$$

where the infimum is over the set

$$(6.11) \quad \left\{ (w, v, u) \in \mathbb{R}^3 : |w|, |v|, |u| \leq \max\{\|v_*\|_{L^\infty(K)}, \|v_{*+k+1}\|_{L^\infty(K)}\}, w - u > \rho, v \in [w, u] \right\},$$

and where $\rho > 0$ is chosen such that $v_*(x, t) - v_{*+k+1}(x, t) > \rho$ on the set K . Recall (from Theorem 2.2), $K := \{(x, t) : -S + st < x < S - st\}$. Note that we have $m = \rho/2$ for Burgers equation

Let t_{tch} be the time when \hat{h}_* and \hat{h}_{*+k} touch in the computer. Then, once $t > t_{tch}$ is so large that

$$(6.12) \quad m(t - t_{tch}) > \Delta_*(t_{tch}) + \Delta_{*+k}(t_{tch}) + \Upsilon_*(t) + \Upsilon_{*+k}(t)$$

holds (where m is from (6.10)), we can be sure that the shocks h_* and h_{*+k} have collided. Note that the Υ -terms in (6.12) come from the fact that the shocks in $\hat{\psi}$ are not actually traveling with Rankine-Hugoniot speed but have an error controlled by (6.15) below.

Remark here that, as above in Section 6.2, we are assuming that after the \hat{h}_* and \hat{h}_{*+k} touch in the computer, the h_* and h_{*+k} have not yet touched in $\hat{\psi}$. The formulas for $\Delta_*(t_{tch})$ and $\Delta_{*+k}(t_{tch})$ come from Section 6.5 and the assumption that the h_* and h_{*+k} have not yet touched in $\hat{\psi}$.

Then, we argue by contradiction: when the error intervals around \hat{h}_* and \hat{h}_{*+k} have pulled apart (as dictated by (6.12) and as shown in Figure 4), we can by contradiction conclude that h_* and h_{*+k} must have touched. Equation (6.12) gives us an upper bound on the time when the error intervals must pull apart. After we can be sure that h_* and h_{*+k} must have touched, we can treat the combined shock as a ‘large’ shock using the techniques from Section 6.1 and Section 6.3.1, but we start the Gronwall calculation (see (7.27)) at the time when we are sure h_* and h_{*+k} have combined, and replace the $|h_i(0) - \hat{h}_i(0)|$ term in (7.27) with the position uncertainty at the time when we are sure h_* and h_{*+k} have combined.

6.4. Improved control on ‘front tracking’ shocks. Let us begin by giving some scaling arguments, that suppose that the L^2 norm of the initial data approximation error is $\mathcal{O}(\sqrt{\delta^2 + h^2})$ but not $o(\sqrt{\delta^2 + h^2})$ and the L^2 norm of the residuals (see (2.16)) is $\mathcal{O}(h)$ but not $o(h)$. This is the case in our numerical experiments for first order schemes. The estimates on uncertainty of shock positions made above (see (6.1)) at best provide $\mathcal{O}(\frac{1}{\sqrt{\delta}}\sqrt{\delta^2 + h^2}) \geq \mathcal{O}(\sqrt{\delta})$ upper bounds on position errors of shocks of size proportional to δ (originating from areas where \bar{u}^0 is rapidly decreasing). Since these shocks are initially only δ apart there is essentially no control of the order in which their collisions happen and of the consequences of these collisions. Thus, a different methodology is needed in order to control the difference $\hat{u} - \hat{\psi}$ in these areas. This will be based on a combination of Bressan’s results on wave front tracking solutions [1, Eqn (8.22)] and an improved estimate for velocity errors.

6.4.1. Improved velocity control. To obtain better control on the velocity of any one of the small ‘front tracking’ shocks we fix this shock, denote its position by h_* , and create another version of $\hat{\psi}$, called $\hat{\psi}_{\text{fine}}$. At time $t = 0$, $\hat{\psi}_{\text{fine}}$ is also in the form of (2.2), and

$\hat{\psi}_{\text{fine}}(\cdot, 0)$ is related to $\hat{\psi}(\cdot, 0)$ in the following way: $\hat{\psi}_{\text{fine}}$ chooses a much finer piecewise-constant approximation (made up of extremely tiny shocks) in areas where $\bar{u}(\cdot, 0)$ is rapidly decreasing. This is done in all rapidly decreasing parts *except at the shock \hat{h}_\star* (the size of this shock is the same in both $\hat{\psi}$ and $\hat{\psi}_{\text{fine}}$ – let us call this shock the \star -th shock in both $\hat{\psi}$ and $\hat{\psi}_{\text{fine}}$). See Figure 7. On the domains of the nearly non-decreasing parts of $\bar{u}(\cdot, 0)$, i.e., those with $\partial_x \bar{u}(\cdot, 0) > -\epsilon$ we let $\hat{\psi}_{\text{fine}}(\cdot, 0)$ and $\hat{\psi}(\cdot, 0)$ agree.

For both $\hat{\psi}(\cdot, 0)$ and $\hat{\psi}_{\text{fine}}(\cdot, 0)$, on each interval where these functions are Lipschitz-continuous, we need to extend the Lipschitz-continuous pieces to be functions on the whole real line. We extend each of these pieces following Appendix A.1, giving extensions v_i^0 . We evolve the v_i^0 corresponding to the nearly non-decreasing parts of \bar{u}^0 numerically (giving numerical solutions \hat{v}_i) whereas we evolve the extended initial data v_i corresponding to rapidly decreasing pieces following Section 5.1.1.

By doing this, we get that

$$(6.13) \quad \int_{\mathbb{R}} \eta(\bar{u}(\cdot, 0)|\hat{\psi}_{\text{fine}}(\cdot, 0)) dx \\ \leq 2\delta\mathfrak{H} \left(\sum_{*\in\{k: h_k(0) \text{ 'boundary' shock, } \bar{u}^0(h_k(0)+)=\bar{u}^0(h_k(0)-)\}} [\mathfrak{s}_*(0)^2] + \mathfrak{s}_*(0)^2 \right) \\ + \sum_{(x_i, x_{i+1}) \in \mathcal{I}_{\text{nd}}} \int_{x_i}^{x_{i+1}} \eta(v_i^0(x)|\hat{v}_i(x, 0)) dx,$$

where $\mathfrak{H} := \sup \eta''$, $\mathfrak{s}_*(0)$ is the height of the shock at \hat{h}_\star (at time $t = 0$) and \mathcal{I}_{nd} is the set of nearly non-decreasing intervals. For the function $\hat{\psi}$, we have the ordering (2.5). In order to make sure the analogous ordering holds also with the function $\hat{\psi}_{\text{fine}}$, we may also need to keep the sizes of the ‘front tracking’ shocks adjacent to ‘boundary’ shocks in $\hat{\psi}(\cdot, 0)$ the same size in $\hat{\psi}_{\text{fine}}(\cdot, 0)$ as they are in $\hat{\psi}(\cdot, 0)$ (see Figure 7). This is where the term $\sum_{*\in\{k: h_k(0) \text{ 'boundary' shock, } \bar{u}^0(h_k(0)+)=\bar{u}^0(h_k(0)-)\}} [\mathfrak{s}_*(0)^2]$ in (6.13) comes from.

The function $\mathfrak{s}_*(t) > 0$, which verifies the bound $\hat{\psi}(h_\star(t)-, t) - \hat{\psi}(h_\star(t)+, t) \geq \mathfrak{s}_*(t)$, can be chosen proportional to δ for all $t \in [0, T]$ (in the case of exact solutions, this follows from Lemma 4.5, and we can check it a posteriori for the numerical solutions \hat{v}_i).

Then, applying the dissipation estimate (7.18) to the \star -th shock in $\hat{\psi}_{\text{fine}}$ implies an (average) velocity error, i.e. the difference of the speed of the shock from its Rankine-Hugoniot speed, measured in the L^2 -in-time norm, of

$$(6.14) \quad \int_0^t \left[c\mathfrak{s}_*(r) (\sigma(\bar{u}(h_\star(r)+, r), \bar{u}(h_\star(r)-, r)) - \sigma(\hat{\psi}(h_\star(r)+, r), \hat{\psi}(h_\star(r)-, r)))^2 \right] dr \\ \leq C \left(\int_{-S}^S \eta(\bar{u}(x, 0)|\hat{\psi}_{\text{fine}}(x, 0)) dx + \int_0^t \int_{-S+sr}^{S-sr} (R_{\hat{\psi}_{\text{fine}}}(x, r))^2 dx dr \right) e^{Ct},$$

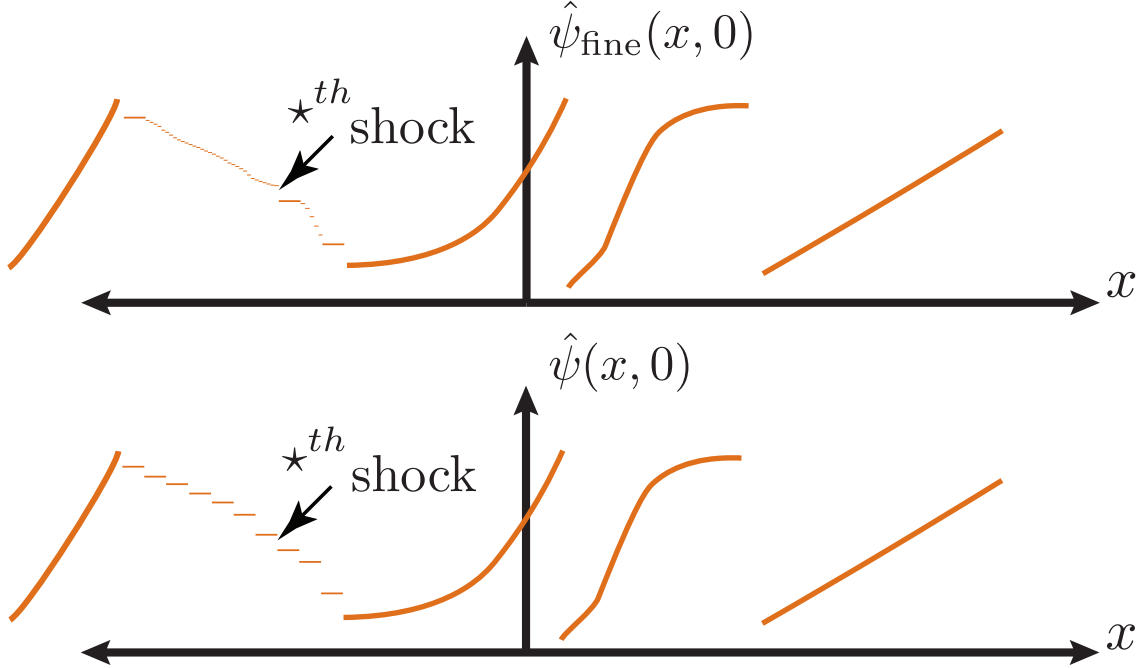


FIGURE 7. For each ‘front tracking’ shock in $\hat{\psi}$ (and correspondingly in \hat{u}), we introduce a function $\hat{\psi}_{\text{fine}}$ which helps us study that particular shock.

where $c > 0$ is defined in (7.17). The function $R_{\hat{\psi}_{\text{fine}}}$ is defined analogously to $R_{\hat{\psi}}$ (see (7.6)). The relative entropy $\int \eta(\bar{u}(x, 0)|\hat{\psi}(x, 0)) dx$ is expected to be $\mathcal{O}(\delta^3 + h^2)$ but not $o(\delta^3 + h^2)$ and the squared L^2 norm of the residual is expected to be $\mathcal{O}(h^{\frac{3}{2}})$ caused by the kinks in the extensions. Thus the optimal scaling is $\delta \sim h^{1/2}$ and the right-hand side of (6.14) is $\mathcal{O}(\delta^3) = \mathcal{O}(h^{3/2})$.

The point is that because the shift functions for both $\hat{\psi}$ and $\hat{\psi}_{\text{fine}}$ are simply generalized characteristics of \bar{u} , the position of the \star -th shock will be *the exact same* in both $\hat{\psi}$ and $\hat{\psi}_{\text{fine}}$ for all time.

However, due to the many tiny shocks in $\hat{\psi}_{\text{fine}}$ that are not in $\hat{\psi}$, some of these tiny shocks will hit and combine with the \star -th shock we are concerned with, changing its left or right state and thus its natural Rankine-Hugoniot speed. This means that the Rankine-Hugoniot speed of this shock in $\hat{\psi}_{\text{fine}}$ might be slightly different than the Rankine-Hugoniot speed of the same shock in $\hat{\psi}$. This will be problematic in Section 6.4.2 since in Bressan’s theory we need to control the error of the velocity compared to the natural Rankine-Hugoniot speed. However, this difference in Rankine-Hugoniot speeds between $\hat{\psi}_{\text{fine}}$ and $\hat{\psi}$ is moderated by the fact that the shocks in $\hat{\psi}$ and $\hat{\psi}_{\text{fine}}$ are both travelling with velocities given by generalized characteristics of \bar{u} , i.e. only the tiny shocks in $\hat{\psi}_{\text{fine}}$ that start between the $\star - 1$ -th and \star -th shocks in $\hat{\psi}$ can combine with the \star -th shock (in $\hat{\psi}_{\text{fine}}$) before the $\star - 1$ -th

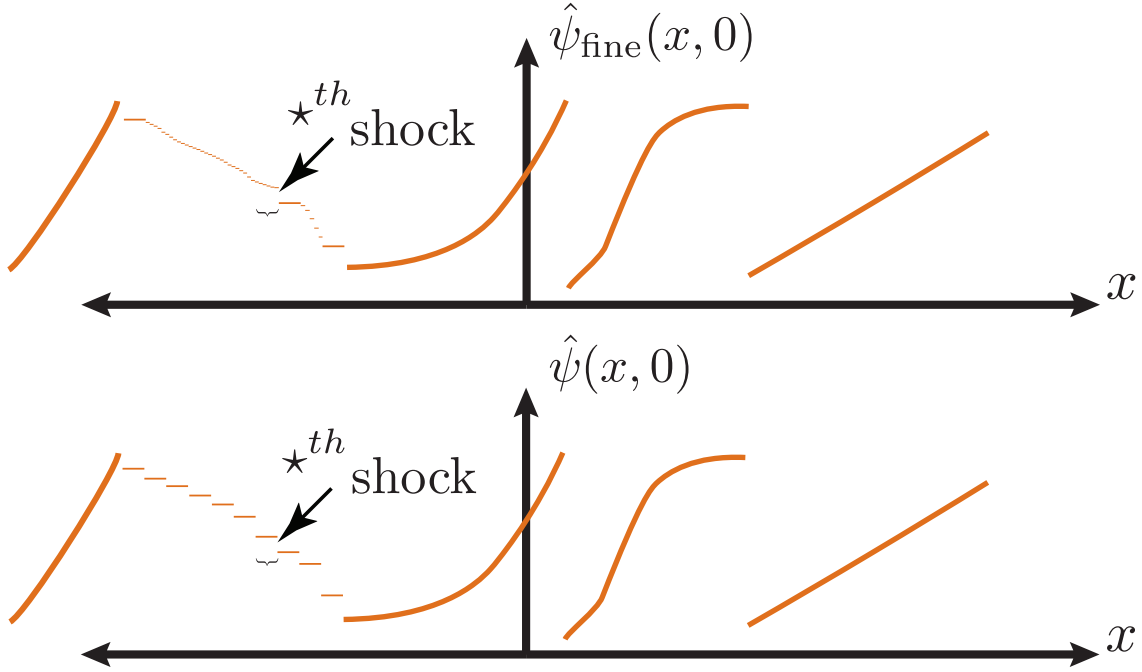


FIGURE 8. Multiple of the tiny shocks in $\hat{\psi}_{\text{fine}}$ (moving with velocity dictated by shift functions), such as indicated here by the bracket to the left of the \star -th shock, might interact before any interaction has occurred in $\hat{\psi}$. However, if enough of the tiny shocks interact with the \star -th shock in $\hat{\psi}_{\text{fine}}$, then necessarily one of the shocks to the left of the \star -th shock in $\hat{\psi}$ (indicated again by a bracket) must interact with the \star -th shock, bringing the Rankine-Hugoniot speeds of the \star -th shocks in $\hat{\psi}_{\text{fine}}$ and $\hat{\psi}$ close to parity.

shock in $\hat{\psi}$ combines with it as well. See Figure 8. The same holds for shocks to the right and future collisions.

All in all, we get that, the velocity error of the \star -th shock in $\hat{\psi}$ (in the $L^1(0, t)$ norm) is bounded by,

$$\begin{aligned}
(6.15) \quad & \int_0^t |\dot{h}_*(s) - \sigma(v_{L_*(s)}(h_*(s), s), v_{R_*(s)}(h_*(s), s))| ds \\
& \leq \frac{\sqrt{t}}{\min_t \sqrt{\mathfrak{s}_*(t)}} \left(2\mathfrak{H} \delta \left(\mathfrak{s}_*(0)^2 + \sum_{* \in \{k: h_k(0) \text{ 'boundary' shock, } \bar{u}^0(h_k(0)+)=\bar{u}^0(h_k(0)-)\}} [\mathfrak{s}_*(0)^2] \right) \right. \\
& \quad + \sum_{(x_i, x_{i+1}) \in \mathcal{I}_{nd}} \int_{x_i}^{x_{i+1}} \eta(v_i^0(x) | \hat{v}_i(x, 0)) dx + \int_0^t \int_{-S+sr}^{S-sr} (R_{\hat{\psi}_{fine}}(x, r))^2 dx dr \left. \right)^{\frac{1}{2}} e^{Ct} \\
& \quad + t\bar{s} \cdot \mathfrak{A} =: \Upsilon_*(t),
\end{aligned}$$

where \mathfrak{H} is an upper bound for η'' , we recall that \mathfrak{A} is an upper bound for the Lipschitz constant of Rankine-Hugoniot speeds (see (3.6)), and

$$(6.16) \quad \bar{s} := \sup_t \max_j \sup_{x \in \mathbb{R}} [\hat{v}_j(x, t) - \hat{v}_{j+1}(x, t)],$$

where the maximum over j is taken over *all* ‘front tracking’ shocks h_j in $\hat{\psi}(\cdot, 0)$ (corresponding to all of the rapidly decreasing parts of \bar{u}^0).

In the situation that we observe, i.e. with kinks in the extensions, the L^2 norms of $R_{\hat{\psi}_{fine}}$ (and $R_{\hat{\psi}}$) are $\mathcal{O}(h^{3/4})$ but not $o(h^{3/4})$ (and δ is chosen as $h^{\frac{1}{2}}$) then (6.15) provides an estimate for the uncertainty of shock position of order $\mathcal{O}(\delta)$.

Compare this with the discussion at the beginning of this section (Section 6.4) on uncertainty of shock positions via using (6.1) directly – this only provides uncertainty of $\mathcal{O}(\sqrt{\delta})$.

6.4.2. *Control on the regions of \hat{u} coming from rapidly decreasing parts.* Let us focus on one interval

$$(6.17) \quad [h_k(0), h_{k+\ell}(0)]$$

where \bar{u}^0 is rapidly decreasing. We wish to use estimates from the front tracking technique but $\hat{\psi}$ is not a front tracking solution (due to its increasing parts). Thus, we define a function $\hat{\psi}_{ft}$ that can be understood as an approximate front tracking solution. We construct the piecewise-constant (in space) function $\hat{\psi}_{ft}$ from the same piece-wise constant approximation of $\bar{u}^0|_{[h_k(0), h_{k+\ell}(0)]}$ as $\hat{\psi}$ but using globally constant extensions for each piece (instead of the extensions in Appendix A.1). Furthermore, at time $t = 0$, we define $\hat{\psi}_{ft}$ to be constant outside of $[h_k(0), h_{k+\ell}(0)]$ with $\hat{\psi}_{ft}(x, 0) = \hat{\psi}_{ft}(h_k(0)+, 0)$ for $x < h_k(0)$ and $\hat{\psi}_{ft}(x, 0) = \hat{\psi}_{ft}(h_{k+\ell}(0)-, 0)$ for $x > h_{k+\ell}(0)$. See Figure 9.

Thus, for all time t , $\hat{\psi}_{ft}(\cdot, t)$ is piecewise-constant on \mathbb{R} . For each discontinuity in $\hat{\psi}_{ft}$, the space-time curves of discontinuity in $\hat{\psi}_{ft}$ are the same as for the corresponding shock in $\hat{\psi}$ (the movement of the shocks is dictated by the same function).

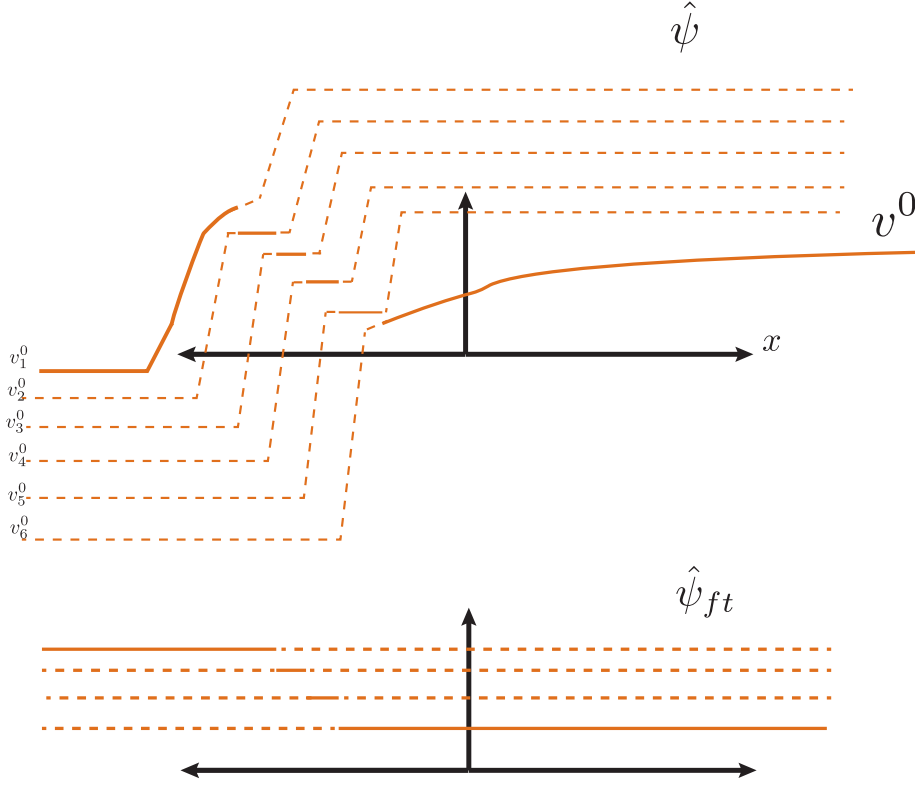


FIGURE 9. We define the function $\hat{\psi}_{ft}$, which, in contrast with $\hat{\psi}$, uses constant extensions. Here the extensions are shown as dotted lines.

For each interval (6.17), we will also compute a numerical solution \hat{u}_{ft} with initial data $\hat{\psi}_{ft}(\cdot, 0)$ and with shocks moving with exact Rankine-Hugoniot speed. The curves of discontinuity in \hat{u}_{ft} will be indexed as $\hat{h}_{ft,i}$. At time $t = 0$, $\hat{h}_{ft,i}(0) = \hat{h}_i(0)$ for all i such that $\hat{h}_i(0) \in [h_k(0), h_{k+\ell}(0)]$. Recall that at $t = 0$, $\hat{h}_i = h_i$ for all i .

Similarly, for each $p, q \in \mathbb{N}$, $k \leq p < q \leq k + \ell$, we construct the piecewise-constant (in space) function $\hat{\psi}_{ft}^{p,q}$ from the same piece-wise constant approximation of $\bar{u}^0|_{[h_k(0), h_{k+\ell}(0)]}$ as $\hat{\psi}$ but only on the interval $[h_p(0), h_q(0)]$. At time $t = 0$, we define $\hat{\psi}_{ft}^{p,q}$ to be constant outside of $[h_p(0), h_q(0)]$ with $\hat{\psi}_{ft}^{p,q}(x, 0) = \hat{\psi}_{ft}(h_p(0)-, 0)$ for $x < h_p(0)$ and $\hat{\psi}_{ft}^{p,q}(x, 0) = \hat{\psi}_{ft}(h_q(0)+, 0)$ for $x > h_q(0)$.

As with $\hat{\psi}_{ft}$, we use globally constant extensions for each constant piece of $\hat{\psi}_{ft}^{p,q}$ (instead of the extensions in Appendix A.1). For each discontinuity in $\hat{\psi}_{ft}^{p,q}$, the shock curves in $\hat{\psi}_{ft}^{p,q}$ are the same as for the corresponding shock in $\hat{\psi}$ (the movement of the shocks is dictated by the same function). In analogy with \hat{u}_{ft} , we also define in a similar way $\hat{u}_{ft}^{p,q}$.

For our numerical scheme to construct the \hat{u} , we will numerically simulate the various \hat{u}_{ft} associated with \hat{u} .

We would like to infer bounds on velocity errors in $\hat{\psi}_{ft}$ from (6.15) but we need to account for the fact that the natural Rankine-Hugoniot speeds in $\hat{\psi}$ and $\hat{\psi}_{ft}$ are different due to potentially different left- and right-hand states at each shock (due to nonconstant extensions in $\hat{\psi}$ – see Appendix A.1). To understand how this can be done let us focus on one discontinuity h_i in $\hat{\psi}$, with adjacent solutions v_ℓ, v_r and hence left-hand state (at time t) $v_\ell(h_i(t), t)$ and right-hand state $v_r(h_i(t), t)$. Remark that if for some time $t_0 > 0$, for all $t > t_0$ this discontinuity happens to be traveling with the natural Rankine-Hugoniot speed, then any part of the functions v_ℓ, v_r not revealed in $\hat{\psi}$ at $t = t_0$ will then never be revealed for all $t > t_0$. This can be seen in two ways. One way is to note that the speed of the characteristic of the function v_ℓ going through the point $(h_i(t), t)$ is travelling faster than the Rankine-Hugoniot speed of the shock $(v_\ell(h_i(t), t), v_r(h_i(t), t))$, while the speed of the characteristic of the function v_r going through the point $(h_i(t), t)$ is travelling slower. Remark here that $v_\ell > v_r$ pointwise.

A second way to see this is the following. Consider the case when there is no numerical error, i.e. $\mathcal{R}_j \equiv 0$ for all j . Furthermore, assume that there exists some $t_0 > 0$ such that for all $t > t_0$, all the discontinuities in $\hat{\psi}$ suddenly begin to travel with natural Rankine-Hugoniot speed. Then, for $t > t_0$ the function $\hat{\psi}$ is an exact solution to (1.1). In particular, it verifies Oleĭnik's *condition E* (see (3.10)) – which is a uniqueness criterion. Thus, the artificial extensions of the v_ℓ, v_r can never be revealed after time t_0 . If they could be revealed, this would violate uniqueness because at time t_0 the hidden parts of the extensions can be arbitrarily perturbed (as long as smoothness is preserved).

Thus, the artificial extensions of the v_ℓ, v_r will only be revealed when h_i is traveling not at Rankine-Hugoniot speed. We are interested in the height difference between the constant values of the v_ℓ and v_r which are exposed at $t = 0$ and the values of the extensions which are revealed at later time. Thus, from (6.15) we see that there is a maximum height difference (relative to the constant state at time $t = 0$) of

$$(6.18) \quad \hat{M}\Upsilon_i(t)$$

where

$$(6.19) \quad \hat{M} := \sup_t \text{Lip}[\hat{\Lambda}(\cdot, t)],$$

cf. (A.3) and where we have used the formulas for the extensions (see Section 5.1.1).

From (6.18), we get an estimate on difference in Rankine-Hugoniot speeds (and thus in velocity errors) that result from the fact that $\hat{\psi}$ has non-constant extensions, while $\hat{\psi}_{ft}$ uses constant extensions.

Similarly, we can use (6.18) in order to bound the difference between $\hat{\psi}$ and $\hat{\psi}_{ft}$. In particular,

$$(6.20) \quad \|\hat{\psi}(\cdot, t) - \hat{\psi}_{ft}(\cdot, t)\|_{L^\infty} \leq \hat{M} \max_{\alpha} \Upsilon_{\alpha}(t) := \Upsilon,$$

where the max is taken over the set of all shocks in $\hat{\psi}_{ft}$.

Fix a time $t > 0$. Inside the cone $\{(x, t) : x \in [h_k(t), h_{k+\ell}(t)]\}$ we can interpret $\hat{\psi}_{ft}$ as an approximate front tracking solution whose shocks move with a velocity error (relative to the natural Rankine-Hugoniot speed of the shocks in $\hat{\psi}_{ft}$). The velocity error is controlled by (6.15) and (6.18). Then, let $\bar{p} \in \mathbb{N}$ be the lowest integer such that $h_{\bar{p}}(t) \in (h_k(t), h_{k+\ell}(t))$ (so in particular $h_{\bar{p}}$ has not collided with h_k) and similarly let $\bar{q} \in \mathbb{N}$ be the largest integer such that $h_{\bar{q}}(t) \in (h_k(t), h_{k+\ell}(t))$ (so in particular, $h_{\bar{q}}$ has not collided with $h_{k+\ell}$). Then we receive from Lemma 4.1,

Claim.

$$(6.21) \quad \begin{aligned} & \|\hat{\psi}_{ft}(\cdot, t) - \hat{u}_{ft}^{\bar{p}, \bar{q}}(\cdot, t)\|_{L^1([h_k(t), h_{k+\ell}(t)])} \\ & \leq \left((\max \hat{\psi}_{ft} - \min \hat{\psi}_{ft}) + \frac{h_{k+\ell}(0) - h_k(0)}{\delta} \hat{M} \max_{\alpha} \Upsilon_{\alpha}(t) \right)^{\frac{1}{2}} \times \\ & \sqrt{t} \left[C \left(\int_{-S}^S \eta(\bar{u}(x, 0)) |\hat{\psi}(x, 0)| dx + \int_0^t \int_{-S+sr}^{S-sr} (R_{\hat{\psi}}(x, r))^2 dx dr \right) e^{Ct} \right]^{\frac{1}{2}} \\ & \quad + 2 \frac{h_{k+\ell}(0) - h_k(0)}{\delta} \hat{M} (\max_{\alpha} \Upsilon_{\alpha}(t))^2 \\ & + \left((\max \hat{\psi}_{ft} - \min \hat{\psi}_{ft}) + \frac{h_{k+\ell}(0) - h_k(0)}{\delta} \hat{M} \max_{\alpha} \Upsilon_{\alpha}(t) \right) 2\mathfrak{A} \hat{M} t \max_{\alpha} \Upsilon_{\alpha}(t) \\ & \qquad \qquad \qquad =: \Gamma(t), \end{aligned}$$

where the max (in $\max_{\alpha} \Upsilon_{\alpha}$) is over the set of all shocks in $\hat{\psi}_{ft}^{\bar{p}, \bar{q}}$. See (6.15) for the definition of Υ_{α} .

In particular, (6.21) comes from comparing $\hat{\psi}_{ft}^{\bar{p}, \bar{q}}$ to $\hat{u}_{ft}^{\bar{p}, \bar{q}}$ using Lemma 4.1. Remark that on the interval $[h_{\bar{p}}(t), h_{\bar{q}}(t)]$ we have $\hat{\psi}_{ft}^{\bar{p}, \bar{q}} = \hat{\psi}_{ft}$.

We now prove the claim.

Proof of Claim. From Lemma 4.1, we have

$$(6.22) \quad \begin{aligned} & \|\hat{\psi}_{ft}(\cdot, t) - \hat{u}_{ft}^{\bar{p}, \bar{q}}(\cdot, t)\|_{L^1([h_k(t), h_{k+\ell}(t)])} \\ & \leq \int_0^t \sum_{\alpha} \left[\left| \hat{\psi}_{ft}(h_{\alpha}(s)-, s) - \hat{\psi}_{ft}(h_{\alpha}(s)+, s) \right| \left| \dot{h}_{\alpha} - \sigma(\psi_{ft}(h_{\alpha}(s)-, s), \psi_{ft}(h_{\alpha}(s)+, s)) \right| \right] ds, \end{aligned}$$

where at each time s , the sum is over all distinct curves of discontinuity h_{α} of the function $\hat{\psi}_{ft}^{\bar{p}, \bar{q}}$. Then, from (6.18), we get

$$\begin{aligned}
(6.23) \quad &\leq \int_0^t \sum_{\alpha} \left[\left| \hat{\psi}(h_{\alpha}(s)-, s) - \hat{\psi}(h_{\alpha}(s)+, s) \right| \left| \dot{h}_{\alpha} - \sigma(\hat{\psi}(h_{\alpha}(s)-, s), \hat{\psi}(h_{\alpha}(s)+, s)) \right| \right] ds \\
&+ \int_0^t 2\hat{M} \max_{\alpha} \Upsilon_{\alpha}(s) \sum_{\alpha} \left| \dot{h}_{\alpha} - \sigma(\hat{\psi}(h_{\alpha}(s)-, s), \hat{\psi}(h_{\alpha}(s)+, s)) \right| ds \\
&+ \left((\max \hat{\psi}_{ft} - \min \hat{\psi}_{ft}) + \frac{h_{k+\ell}(0) - h_k(0)}{\delta} \hat{M} \max_{\alpha} \Upsilon_{\alpha}(t) \right) 2\mathfrak{A}t \|\hat{\psi} - \hat{\psi}_{ft}\|_{L^{\infty}}
\end{aligned}$$

where we have used that $\sum_{\alpha} \left| \hat{\psi}_{ft}(h_{\alpha}(s)-, s) - \hat{\psi}_{ft}(h_{\alpha}(s)+, s) \right| \leq \max \psi_{ft} - \min \psi_{ft}$. Also recall, at $t = 0$ the rapidly decreasing pieces of \bar{u}^0 are broken up into steps of width δ to make $\hat{\psi}(\cdot, 0)$, and thus there are at most $\frac{h_{k+\ell}(0) - h_k(0)}{\delta}$ of these steps. Then, using Cauchy-Schwartz' inequality, we get the estimate,

$$\begin{aligned}
(6.24) \quad &\leq \left[\int_0^t \sum_{\alpha} \left| \hat{\psi}(h_{\alpha}(s)-, s) - \hat{\psi}(h_{\alpha}(s)+, s) \right| ds \right]^{\frac{1}{2}} \times \\
&\left[\int_0^t \sum_{\alpha} \left| \hat{\psi}(h_{\alpha}(s)-, s) - \hat{\psi}(h_{\alpha}(s)+, s) \right| \left| \dot{h}_{\alpha} - \sigma(\hat{\psi}(h_{\alpha}(s)-, s), \hat{\psi}(h_{\alpha}(s)+, s)) \right|^2 ds \right]^{\frac{1}{2}} \\
&\quad + 2 \frac{h_{k+\ell}(0) - h_k(0)}{\delta} \hat{M} (\max_{\alpha} \Upsilon_{\alpha}(t))^2 \\
&+ \left((\max \hat{\psi}_{ft} - \min \hat{\psi}_{ft}) + \frac{h_{k+\ell}(0) - h_k(0)}{\delta} \hat{M} \max_{\alpha} \Upsilon_{\alpha}(t) \right) 2\mathfrak{A} \hat{M} t \max_{\alpha} \Upsilon_{\alpha}(t)
\end{aligned}$$

Then, note again that $\sum_{\alpha} \left| \hat{\psi}_{ft}(h_{\alpha}(s)-, s) - \hat{\psi}_{ft}(h_{\alpha}(s)+, s) \right| \leq \max \psi_{ft} - \min \psi_{ft}$. Also recall, at $t = 0$ the rapidly decreasing pieces of \bar{u}^0 are broken up into steps of width δ to make $\hat{\psi}(\cdot, 0)$, and thus there are at most $\frac{h_{k+\ell}(0) - h_k(0)}{\delta}$ of these steps. Recall also (6.18). Thus, from the dissipation estimate (7.16),

$$\begin{aligned}
 (6.25) \quad &\leq \left((\max \hat{\psi}_{ft} - \min \hat{\psi}_{ft}) + \frac{h_{k+\ell}(0) - h_k(0)}{\delta} \hat{M} \max_{\alpha} \Upsilon_{\alpha}(t) \right)^{\frac{1}{2}} \times \\
 &\sqrt{t} \left[C \left(\int_{-S}^S \eta(\bar{u}(x,0)|\hat{\psi}(x,0)) dx + \int_0^t \int_{-S+sr}^{S-sr} (R_{\hat{\psi}}(x,r))^2 dx dr \right) e^{Ct} \right]^{\frac{1}{2}} \\
 &\quad + 2 \frac{h_{k+\ell}(0) - h_k(0)}{\delta} \hat{M} (\max_{\beta} \Upsilon_{\beta}(t))^2 \\
 &\quad + \left((\max \hat{\psi}_{ft} - \min \hat{\psi}_{ft}) + \frac{h_{k+\ell}(0) - h_k(0)}{\delta} \hat{M} \max_{\alpha} \Upsilon_{\alpha}(t) \right) 2\mathfrak{A} \hat{M} t \max_{\alpha} \Upsilon_{\alpha}(t)
 \end{aligned}$$

■

We can bound the $L^1(h_k(t), h_{k+\ell}(t))$ distance between $\hat{\psi}(\cdot, t)$ and $\hat{u}(\cdot, t)$ by combining (6.21) and (6.20).

6.4.3. *From $\hat{\psi}_{ft}$, we construct $\hat{\Psi}_{ft}$.* For the next Section 6.4.4 we want estimates on $\|\hat{u}_{ft} - \hat{\psi}_{ft}\|_{L^1(\mathbb{R})}$ (globally on \mathbb{R} !). However, (6.21) only gives us error estimates on the interval $[h_k(t), h_{k+\ell}(t)]$ and for the function $\hat{u}_{ft}^{\tilde{p}, \tilde{q}}$ instead of \hat{u}_{ft} . To circumvent this issue we construct an intimately connected function $\hat{\Psi}_{ft}$ on which we have the desired global L^1 estimates relative to \hat{u}_{ft}

Indeed, we cannot measure $\|\hat{u}_{ft} - \hat{\psi}_{ft}\|_{L^1(\mathbb{R})}$ using the L^1 estimates from front tracking (i.e., Lemma 4.1) because the shocks at position $h_k(t)$ or $h_{k+\ell}(t)$ in $\hat{\psi}_{ft}$ will not necessarily be moving with Rankine-Hugoniot speed plus a controllable error. This is because the shocks in $\hat{\psi}_{ft}$ might start being influenced by pieces of $\hat{\psi}$ coming from nearly non-decreasing pieces of \bar{u}^0 – the ‘boundary’ shocks in particular (see Figure 1).

Thus, we are led to the construction of the function $\hat{\Psi}_{ft}: \mathbb{R} \times [0, T] \rightarrow \mathbb{R}$. The construction of $\hat{\Psi}_{ft}$ follows precisely the construction of $\hat{\psi}_{ft}$, except we will make modifications outside of the interval $[h_k(t), h_{k+\ell}(t)]$, such that

$$(6.26) \quad \left\| \hat{u}_{ft}(\cdot, t) - \hat{\Psi}_{ft}(\cdot, t) \right\|_{L^1(\mathbb{R})} \leq \Gamma(t),$$

where Γ was defined in (6.21), holds for all t .

Note (6.26) is possible by simply slowing down (or speeding up) the shocks in $\hat{\psi}_{ft}$ when they start moving too fast (or too slow) due to the corresponding ‘front tracking’ shock in $\hat{\psi}$ colliding with a ‘boundary’ shock in $\hat{\psi}$ coming from the left (or the right). This slowing or speeding up process yields the $\hat{\Psi}_{ft}$. Remark that by slowing down shocks on the left of the function $\hat{\psi}_{ft}$, which have collided with h_k , we are preventing some collisions from occurring, further slowing down some shocks in $\hat{\Psi}_{ft}$. Similarly, by speeding up shocks on the right of the function $\hat{\psi}_{ft}$, which have collided with $h_{k+\ell}$, we are preventing some

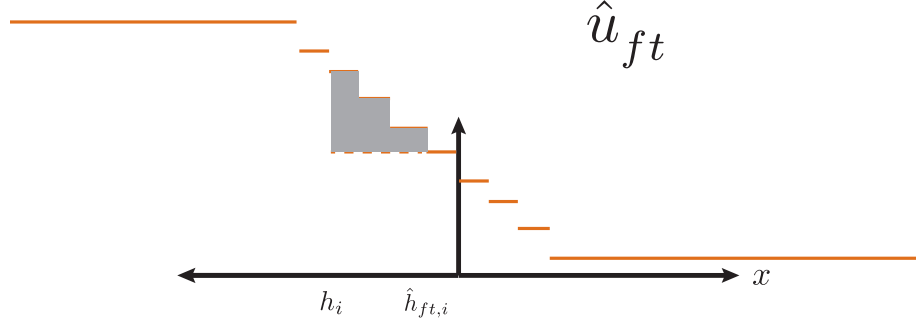


FIGURE 10. If the distance between $\hat{h}_{ft,i}$ and h_i is too large, the L^1 distance between $\hat{\Psi}_{ft}$ and \hat{u}_{ft} (represented by the gray ‘triangle’ in this diagram) is too large, violating (6.26).

collisions from occurring, further speeding up some shocks in $\hat{\Psi}_{ft}$. This will ensure

$$(6.27) \quad \hat{\Psi}_{ft}(\cdot, t) = \hat{\psi}_{ft}(\cdot, t)$$

on the interval $[h_k(t), h_{k+\ell}(t)]$ (for all t).

Recall also that $\hat{v}_i(x, t) > \hat{v}_{i+1}(x, t)$ for all i and for all (x, t) and $\partial_u \sigma(u, v) = \partial_v \sigma(u, v) > 0$. Remark also that the argument in Section 6.4.1 (and in particular, (6.15)) actually holds for every shock in $\hat{\psi}$. Recall also (6.20). Finally, recall (the proof of) (6.21). This will ensure (6.26).

6.4.4. *Position estimates on ‘front tracking’ shocks.* By construction \bar{u}^0 is strictly decreasing with slope magnitude at least ϵ on $[\hat{h}_k(0), \hat{h}_{k+\ell}(0)]$ otherwise we would not have treated this part of the solution as rapidly decreasing. This property is preserved in the exact solution \hat{u}_{ft} which, actually, gets steeper in time. In order to obtain estimates for the positions of discontinuities in \hat{u} we would like to argue that \hat{u}_{ft} has a minimal slope which is obviously not true, strictly speaking, since it consists of constant pieces. We make the following observation instead. By construction, \hat{u}_{ft} can be chosen such that

$$(6.28) \quad \inf \frac{\hat{u}_{ft}(x, t) - \hat{u}_{ft}(y, t)}{y - x} > \frac{\epsilon}{2},$$

where at time t the infimum runs over all x, y in the interval between the first and last shocks in \hat{u}_{ft} and verifying $y > x + \delta$. This ‘discrete slope’ of $\hat{u}_{ft}(\cdot, t)$ is computable and we denote it by $\mathcal{S}(\hat{u}_{ft}(\cdot, t))$.

Thus, for shocks h_i which are inside the interval $(h_k(t), h_{k+\ell}(t))$ at time t , from (6.26), and (6.27) we obtain a maximal position error of each such shock of

$$(6.29) \quad \left| h_i(t) - \hat{h}_{ft,i}(t) \right| \leq \frac{\sqrt{2}}{\sqrt{\max\{\epsilon/2, \mathcal{S}(\hat{u}_{ft}(\cdot, t))\}}} \left(\Gamma(t) \right)^{1/2} =: \Delta_{inner}.$$

Remark that if $\hat{h}_i(t)$ is in the interval $(\hat{h}_k(t), \hat{h}_{k+\ell}(t))$, then $\hat{h}_{ft,i}(t) = \hat{h}_i(t)$ and thus (6.29) gives us control on Δ_i , (recall Δ_i simply denotes our best upper bound on $|h_i(t) - \hat{h}_i(t)|$). See Figure 10.

Local versions of $\mathcal{S}(\hat{u}_{ft}(\cdot, t))$ can be computed to improve the estimate (6.29). In general, the formula (6.29) is only valid when the interval $(\hat{h}_{ft,i} - \Delta_{inner}, \hat{h}_{ft,i} + \Delta_{inner})$ it gives for the position of the shock h_i verifies

$$(6.30) \quad (\hat{h}_{ft,i} - \Delta_{inner}, \hat{h}_{ft,i} + \Delta_{inner}) \subset [\hat{h}_{ft,k+1}(t), \hat{h}_{ft,k+\ell-1}(t)].$$

This is because outside the interval between the first and last shocks, \hat{u}_{ft} is constant and thus the estimate (6.28) on the discrete slope is not valid.

Let us then consider the case when both (6.30) and (6.29) are not verified. We first consider the left-most shocks in \hat{u}_{ft} and $\hat{\Psi}_{ft}$.

Our goal is to bound from above the difference $\hat{h}_{ft,k+1}(t) - h_{ft,k+1}^{\hat{\Psi}}(t)$, where $h_{ft,k+1}^{\hat{\Psi}}(t)$ is the position of the left-most shock in $\hat{\Psi}_{ft}$. Then, if

$$(6.31) \quad \hat{\Psi}_{ft}(h_{ft,k+1}^{\hat{\Psi}}(t)-, t) - \hat{\Psi}_{ft}(h_{ft,k+1}^{\hat{\Psi}}(t)+, t) \leq \left(\Gamma(t)\right)^{1/2},$$

then $h_{ft,k+1}^{\hat{\Psi}}(t)$ and $\hat{h}_{ft,k+1}(t)$ verify

$$(6.32) \quad \hat{h}_{ft,k+1}(t) - h_{ft,k+1}^{\hat{\Psi}}(t) \leq (\mathfrak{A}\hat{M}T + 1) \max_{\alpha} \Upsilon_{\alpha}(t) + \mathfrak{A}T \left(\Gamma(t)\right)^{1/2},$$

where we have used (6.20) and (6.15) and we recall that \mathfrak{A} is an upper bound for the Lipschitz constant of Rankine-Hugoniot speeds (see (3.6)). As above, the max is taken over the set of all shocks in $\hat{\psi}_{ft}$.

If (6.31) does not hold, then from (6.26) we can deduce

$$(6.33) \quad \hat{h}_{ft,k+1}(t) - h_{ft,k+1}^{\hat{\Psi}}(t) \leq \left(\Gamma(t)\right)^{1/2}.$$

We have similar estimates on the right-most shocks in \hat{u}_{ft} and $\hat{\Psi}_{ft}$.

We conclude that if (6.29) is not verified, then

$$(6.34) \quad \left| h_i(t) - \hat{h}_{ft,i}(t) \right| \leq \Delta_{inner} + (\mathfrak{A}\hat{M}T + 1) \max_{\alpha} \Upsilon_{\alpha}(t) + (\mathfrak{A}T + 1) \left(\Gamma(t)\right)^{1/2},$$

because we know that $h_i(t)$ must be between either the left-most shock in $\hat{\Psi}_{ft}$ and the left-most shock in \hat{u}_{ft} , or the between the right-most shock in $\hat{\Psi}_{ft}$ and the right-most shock in \hat{u}_{ft} . Remark that the right-hand side of (6.34) is always greater than or equal to the right-hand side of (6.29), so (6.34) gives a worst-case bound.

As above with (6.29), the formula (6.34) clearly only holds for shocks i such that $h_i \in (h_k(t), h_{k+\ell}(t))$. Further, remark that if $\hat{h}_i(t)$ is in the interval $(\hat{h}_k(t), \hat{h}_{k+\ell}(t))$, then $\hat{h}_{ft,i}(t) = \hat{h}_i(t)$ and thus (6.34) gives us control on Δ_i .

If $h_i \notin (h_k(t), h_{k+\ell}(t))$ or $\hat{h}_i \notin (\hat{h}_k(t), \hat{h}_{k+\ell}(t))$, then there are three cases (assuming $\hat{h}_k(t), \hat{h}_{k+\ell}(t)$ are sufficiently far apart, otherwise the estimates are trivial):

- Case 1 Both h_i and \hat{h}_i have collided with a ‘boundary’ shock. In this case, control on $|h_i(t) - \hat{h}_i(t)|$ comes from Section 6.5.
- Case 2 If only h_i collided with a ‘boundary’ shock h_* (here, $h_* = h_k$ or $h_* = h_{k+\ell}$), then use $|h_i(t) - \hat{h}_i(t)| \leq |h_i(t) - \hat{h}_*(t)| + |\hat{h}_*(t) - h_*(t)|$ and see again Section 6.5.
- Case 3 If only \hat{h}_i collided with a ‘boundary’ shock \hat{h}_k (or $\hat{h}_{k+\ell}$), then use that \hat{h}_{i+j} (or \hat{h}_{i-j}) has not collided with a ‘boundary’ shock (for some $j \in \mathbb{N}$, choose the smallest possible) and neither has h_{i+j} (or h_{i-j}). Then, we have control on $|\hat{h}_{i+j} - h_{i+j}|$ ($|\hat{h}_{i-j} - h_{i-j}|$) from (6.34). Moreover, $|\hat{h}_{i+j} - \hat{h}_i|$ ($|\hat{h}_{i-j} - \hat{h}_i|$) is expected to be small ($\mathcal{O}(\delta)$), but this can be checked a posteriori). Finally, remark that h_i is between h_{i+j} (or h_{i-j}) and h_k (or $h_{k+\ell}$).

6.5. Control on the ‘boundary’ shocks. Section 6.1 has provided control of position uncertainty for ‘large’ shocks and Section 6.4.2 has provided control on position uncertainty for ‘front tracking’ shocks (coming from the rapidly decreasing regions of \bar{u}^0) as long as they do not interact with other parts of the solution. It remains to control position uncertainty of left and right-most shocks in the ‘front tracking’ parts of $\hat{u}, \hat{\psi}$ (corresponding to rapidly decreasing regions) – the *boundary shocks*. We are going to discuss the ‘left-most shock’ case in detail where to the left of the shock is a \hat{v}_i corresponding to a nearly non-decreasing region of \bar{u}^0 (see Figure 11); the ‘right-most shock’ case (with a nearly non-decreasing region to the right) is analogous. The case of a ‘front tracking’ (corresponding to rapidly decreasing) region to both the left *and* right of the shock is also analogous and we omit the details (see Section 6.5.1).

Note that the estimates from Section 6.1 apply to these shocks but are not particularly useful (in particular, see (6.1)). One issue is that dissipation estimate (4.4) only provides rather weak velocity control due to the small size of the shock but the key issue that needs to be sorted out is how many of the ‘front tracking’ shocks might collide with the shock in question, and to show that this cannot be a process feeding on itself. Let us denote the shock in question as the $*$ -th shock (see Figure 11) and notice that, due to the position uncertainty of the small shocks to its right (6.29), there is an immediate contribution to Δ_* due to the uncertainty about its right-hand state. The main idea is to transfer the control we have on ‘front tracking’ shocks (see Section 6.4.4) to in turn control the ‘boundary’ shocks.

The contributions A_*, C_* to Δ_* are as above (see (6.1)); it is the size of B_* we wish to discuss. Let us stress that velocity errors only add to position errors if both have the same sign. Thus, we distinguish four cases (see Figure 12):

- Case 1 $\hat{h}_* > h_*$, \hat{h}_* **has collided with more small shocks than** h_* :

In this case, the erroneous collisions actually reduce the position error, B_* does not contribute to the growth of Δ_* .

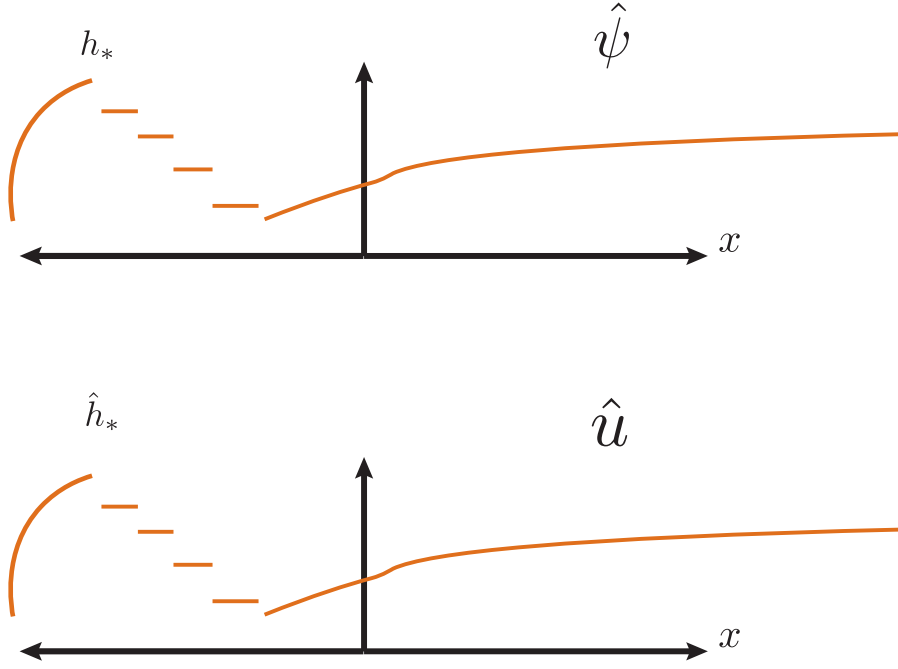


FIGURE 11. The definition of the $*$ -th shock.

Case 2: $\hat{h}_* > h_*$, \hat{h}_* has collided with less small shocks than h_* :

Consider the last of the ‘front tracking’ shocks to collide with h_* , and whose collision with h_* was not reproduced in \hat{h}_* : let’s call it h_j . Before h_j collides with h_* , h_j has a position error (from (6.34)) of

$$(6.35) \quad |h_j - \hat{h}_j| < \Delta_{inner} + (\mathfrak{A}\hat{M}T + 1) \max_{\alpha} \Upsilon_{\alpha}(t) + (\mathfrak{A}T + 1) \left(\Gamma(t) \right)^{1/2}.$$

The important remark here is that the formula (6.34) continues to hold for the shock h_j even after the ‘boundary’ shock h_* has collided with the shock h_j : this will only push h_j and \hat{h}_j closer together, due to the collision with the ‘boundary’ shock h_* increasing the value of the left-hand state $\hat{\psi}(h_j(t)-, t)$. Remark here that we are using that h_j is the last of the ‘front tracking’ shocks to collide with h_* , and whose collision with h_* was not reproduced in \hat{h}_* .

To conclude, due to $\hat{h}_* < \hat{h}_j$, we have

$$(6.36) \quad |h_* - \hat{h}_*| < \Delta_{inner} + (\mathfrak{A}\hat{M}T + 1) \max_{\alpha} \Upsilon_{\alpha}(t) + (\mathfrak{A}T + 1) \left(\Gamma(t) \right)^{1/2}.$$

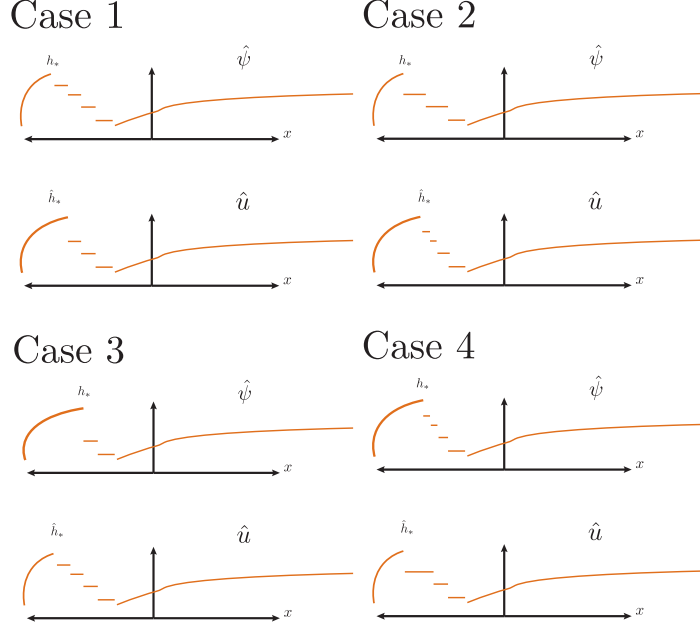


FIGURE 12. The four cases used to control $|\hat{h}_* - h_*|$.

Case 3: $\hat{h}_* < h_*$, \hat{h}_* has collided with fewer small shocks than h_* :

Here the erroneous collisions actually reduce the position error, B_* does not contribute to the growth of Δ_* .

Case 4: $\hat{h}_* < h_*$, \hat{h}_* has collided with more small shocks than h_* :

This case is exactly analogous to Case 2 above.

Consider the last of the ‘front tracking’ shocks to collide with \hat{h}_* , and whose collision with \hat{h}_* was not reproduced in h_* : let’s call it \hat{h}_j . Before \hat{h}_j collides with \hat{h}_* , \hat{h}_j has a position error (from (6.34)) of

$$(6.37) \quad \left| h_j - \hat{h}_j \right| < \Delta_{inner} + (\mathfrak{A}\hat{M}T + 1) \max_{\alpha} \Upsilon_{\alpha}(t) + (\mathfrak{A}T + 1) \left(\Gamma(t) \right)^{1/2}.$$

Thus, due to $h_* < h_j$,

$$(6.38) \quad \left| h_* - \hat{h}_* \right| < \Delta_{inner} + (\mathfrak{A}\hat{M}T + 1) \max_{\alpha} \Upsilon_{\alpha}(t) + (\mathfrak{A}T + 1) \left(\Gamma(t) \right)^{1/2}.$$

All in all, in Case 1 and Case 3 above, this means that the impact of B_* on Δ_* is bounded by a term that contributes to the exponential growth factor in a Gronwall-type argument analogous to (7.25). We write,

$$(6.39) \quad \Delta_* \leq \tilde{A}_* + \tilde{B}_* + \tilde{C}_* + \tilde{D}_*$$

with

$$(6.40) \quad \tilde{A}_* := \int_0^t \tilde{\zeta}(t, s) \left| \dot{\hat{h}}_*(s) - \sigma(\hat{v}_{\hat{L}_*(s)}(\hat{h}_*(s), s), \hat{v}_{\hat{R}_*(s)}(\hat{h}_*(s), s)) \right| ds$$

and

$$(6.41) \quad \tilde{B}_* := \int_0^t \tilde{\zeta}(t, s) \left(\mathfrak{A} \left| \hat{v}_{\hat{L}_*/\hat{R}_*(s)}(\hat{h}_*(s), s) - \hat{v}_{L_*/R_*(s)}(\hat{h}_*(s), s) \right| \right) ds$$

where the subscript is L, R depending on whether h_* is on the left or the right of the wave front tracking area. The integrand in \tilde{B}_* accounts for uncertainty of trace values resulting from shocks coming from outside the wave front tracking area.

Lastly,

$$(6.42) \quad \tilde{C}_* := \left\| \frac{\tilde{\zeta}(t, \cdot)}{\sqrt{\mathfrak{s}_*(\cdot)}} \right\|_{L^2(0, t)} \cdot \left[C e^{Ct} \left(\int_{-S}^S \eta(\bar{u}(x, 0)) |\hat{\psi}(x, 0)| dx + \mathcal{R}(t) \right) \right]^{\frac{1}{2}},$$

and

$$(6.43) \quad \tilde{D}_* := \zeta(t, 0) \cdot [\text{maximum error from Case 2 or Case 4 above}],$$

with ζ as in (6.5). The ‘maximum error from Case 2 or Case 4 above’ in \tilde{D}_* means the largest possible value of $|\hat{h}_* - h_*|$ assuming we are in Case 2 or Case 4 for the entire time interval $[0, T]$ – this is necessary due to potentially switching into Case 1 or Case 3 after having been in Case 2 or Case 4 for a while. Thus, we get

$$(6.44) \quad \tilde{D}_* \leq \zeta(t, 0) \cdot \left[\Delta_{inner} + (\mathfrak{A}MT + 1) \max_{\alpha} \Upsilon_{\alpha}(t) + (\mathfrak{A}T + 1) \left(\Gamma(t) \right)^{1/2} \right].$$

6.5.1. ‘*Front tracking*’ shock on both sides. As mentioned above, we now consider the case when the ‘boundary’ shock \hat{h}_*, h_* might be adjacent to, both on the left and right, a ‘front tracking’ shock. In other words, there is an interval corresponding to a rapidly decreasing region in \bar{u}^0 at $(t = 0)$ to both the left *and* right of the shock \hat{h}_*, h_* (for example, this can occur as in Figure 5). This situation is analogous to the above and we omit the details. In particular, two major cases occur here. First, note there are two perspectives: the ‘left-most shock’ or ‘right-most shock’, depending on which rapidly decreasing region we consider. The first case: in both the ‘left-most shock’ or ‘right-most shock’ perspective, Case 1 or Case 3 above applies. The second case: from at least one of the ‘left-most shock’ or ‘right-most shock’ perspective, Case 2 or Case 4 applies, and this gives us control on $|\hat{h}_* - h_*|$.

7. THE L^2 ESTIMATE AND DISSIPATION CALCULATIONS

To prove Theorem 2.2, we need to show (2.13) holds. Furthermore, we need to show that (6.1) is a suitable upper bound for the quantity $|\hat{h}_i(t) - h_i(t)|$.

7.1. Step 1: proof of (2.13). We now show how to control the growth in time of $\|\bar{u}(\cdot, t) - \hat{\psi}(\cdot, t)\|_{L^2}$. We follow an argument from [5, Section 7] (see also [34])⁴.

We work on the cone of information. First, choose some $S > 0$ such that

$$(7.1) \quad S > \max\{|x_1|, |x_N|\} + sT + T \sup |A'|,$$

and where $s > 0$ is chosen such that $|q(a; b)| \leq s\eta(a|b)$ for all a, b verifying $|a|, |b| \leq \max\{\|\bar{u}\|_{L^\infty}, \|\hat{u}\|_{L^\infty}\}$. Then define $h_0(t) := -S + st$ and $h_{N+1}(t) := S - st$. Note that the speeds of the generalized characteristics h_i are bounded by $\sup |A'|$ and thus S is chosen such that the curves h_0 and h_{N+1} do not intersect the generalized characteristic curves h_i on the time interval $[0, T]$.

Consider two successive times $\hat{t}_j < \hat{t}_{j+1}$ such that there is no interaction between the h_i on the interval $[\hat{t}_j, \hat{t}_{j+1}]$.

We denote by \mathfrak{l}_j the set of all i such that $h_i(t) \neq h_{i+1}(t)$ for all $t \in [t_j, t_{j+1}]$. Then, we fix $i \in \mathfrak{l}_j$ and for $t \in [t_j, t_{j+1}]$, integrate (4.18) over the region

$$(7.2) \quad \{(x, r) | t_j < r < t, h_i(r) < x < h_{i+1}(r)\}.$$

Remark that on this set $\hat{\psi} = \hat{v}_{i+1}$. In the context of (4.18), pick \bar{u} to be playing the role of \hat{u}_2 and pick \hat{v}_{i+1} to be playing the role of \hat{u}_1 . This gives,

$$(7.3) \quad \int_{h_i(t)}^{h_{i+1}(t)} \eta(\bar{u}(x, t)) |\hat{\psi}(x, t)| dx - \int_{h_i(t_j)}^{h_{i+1}(t_j)} \eta(\bar{u}(x, t_j)) |\hat{\psi}(x, t_j)| dx \\ \leq \int_{t_j}^t F_i^+(r) - F_{i+1}^-(r) dr - \int_{t_j}^t \int_{h_i(r)}^{h_{i+1}(r)} \left[\left(\partial_x \Big|_{(x,r)} \eta'(\hat{\psi}) \right) A(\bar{u}(x, r) | \hat{\psi}(x, r)) \right. \\ \left. + R_i(x, t) \eta''(\hat{\psi}(x, r)) [\bar{u}(x, r) - \hat{\psi}(x, r)] \right] dx dr,$$

⁴Our arguments in this section will involve stopping and restarting the clock every time there is a collision between generalized characteristics h_i . Weak solutions u to (1.1) will automatically have $C^0([0, \infty); W^{-1, \infty}(\mathbb{R}))$ regularity. The integral formulation of the entropy inequality (1.5) includes the $t = 0$ boundary term, and from this we get u is continuous at $t = 0$ with values in $L^1_{\text{loc}}(\mathbb{R})$. Because $L^1_{\text{loc}}(\mathbb{R})$ is a strong topology, we get the same regularity for the function $t \mapsto \eta(u(\cdot, t))$. For positive times $t > 0$, we do not enjoy this regularity and $\eta(u)$ is only defined at almost every time. However, this difficulty with stopping and restarting the clock at positive times is not a real roadblock and can be handled with the use of approximate limits. We omit these technical details here. For a reference, see [5, Section 7 and Lemma 7.1].

where R_i is the residual for the numerical solution \hat{v}_i (see (2.16)), and

$$(7.4) \quad F_i^\pm(r) := q(\bar{u}(h_i(r)\pm, r); \hat{\psi}(h_i(r)\pm, r)) - \dot{h}_i(r)\eta(\bar{u}(h_i(r)\pm, t)|\hat{\psi}(h_i(r)\pm, r)).$$

We sum (7.3) over all $i \in \mathfrak{I}_j$. We group the terms corresponding to F_i^\pm together, and the F_{i+1}^\pm together. This yields,

$$(7.5) \quad \int_{-S+st}^{S-st} \eta(\bar{u}(x, t)|\hat{\psi}(x, t)) dx - \int_{-S+st_j}^{S-st_j} \eta(\bar{u}(x, \hat{t}_j)|\hat{\psi}(x, t_j)) dx \\ \leq \int_{\hat{t}_j}^t \sum_i F_i^+(r) - F_i^-(r) dr - \int_{\hat{t}_j}^t \int_{-S+sr}^{S-sr} \left[\left(\partial_x \Big|_{(x,r)} \eta'(\hat{\psi}) \right) A(\bar{u}(x, r)|\hat{\psi}(x, r)) \right. \\ \left. + R_{\hat{\psi}}(x, t)\eta''(\hat{\psi}(x, r))[\bar{u}(x, r) - \hat{\psi}(x, r)] \right] dx dr,$$

where we have used that $F_{N+1}^-, F_0^+ \leq 0$ due to the definition of s and $\dot{h}_0 = s, \dot{h}_{N+1} = -s$. Furthermore, we define

$$(7.6) \quad R_{\hat{\psi}}(x, t) := \begin{cases} R_1(x, t) & \text{if } x < h_1(t), \\ R_2(x, t) & \text{if } h_1(t) < x < h_2(t), \\ \vdots & \\ R_{N+1}(x, t) & \text{if } h_N(t) < x, \end{cases}$$

where R_i is the residual for the numerical solution \hat{v}_i (see (2.16)). Compare (7.6) with (2.14). In practice, we cannot compute $\|R_{\hat{\psi}}\|_{L^2}$ due to the h_i being unknown, so we must use (2.14).

Then, due to Lemma 4.4, we have that

$$(7.7) \quad \sum_i F_i^+(r) - F_i^-(r) \leq 0.$$

Observe that we can apply Lemma 4.4 because for all i and almost every r , $\bar{u}(h_i(r)-, r) \geq \bar{u}(h_i(r)+, r)$. This is in fact true for any Lipschitz function h_i . In the case when \bar{u} is in BV , this is well-known. When \bar{u} is only known to verify the Strong Trace Property (Definition 2.1), then this follows from Lemma 6 in [40] (see also [35, Lemma 5.2]). Further, by assumption on the reconstruction process⁵ we will also have $\hat{v}_i(x, t) > \hat{v}_{i+1}(x, t)$ for all i and for all $(x, t) \in \mathbb{R} \times [0, T]$.

Consider now any $0 < t < T$ and let $0 < t_1 < \dots < t_J$ denote the times at which there is interaction between the h_i , with $t_0 := 0$ and $t_{J+1} := t$. Then, we can write a telescoping

⁵For the v_i corresponding to the ‘front tracking’ shocks, see Section 5.1.1.

sum

$$(7.8) \quad \int_{-S+st}^{S-st} \eta(\bar{u}(x,t)|\hat{\psi}(x,t)) dx - \int_{-S}^S \eta(\bar{u}(x,0)|\hat{\psi}(x,0)) dx$$

$$= \sum_{j=1}^{J+1} \left[\int_{-S+st_j}^{S-st_j} \eta(\bar{u}(x,t_j)|\hat{\psi}(x,t_j)) dx - \int_{-S+st_{j-1}}^{S-st_{j-1}} \eta(\bar{u}(x,t_{j-1})|\hat{\psi}(x,t_{j-1})) dx \right]$$

Then, from (7.5)

$$(7.9) \quad \int_{-S+st}^{S-st} \eta(\bar{u}(x,t)|\hat{\psi}(x,t)) dx - \int_{-S}^S \eta(\bar{u}(x,0)|\hat{\psi}(x,0)) dx$$

$$\leq \int_0^t \sum_i F_i^+(r) - F_i^-(r) dr - \int_0^t \int_{-S+sr}^{S-sr} \left[\left(\partial_x \Big|_{(x,r)} \eta'(\hat{\psi}) \right) A(\bar{u}(x,r)|\hat{\psi}(x,r)) \right.$$

$$\left. + R_{\hat{\psi}}(x,t)\eta''(\hat{\psi}(x,r))[\bar{u}(x,r) - \hat{\psi}(x,r)] \right] dx dr,$$

for all $t \in [0, T]$. Remark that we are only evaluating $\partial_x \eta'(\hat{\psi})$ away from the points $x = h_i(t)$ ($i = 1, \dots, N$), so we do not pick up any Dirac masses in the derivative.

We move the first term on the right-hand side of (7.9) to the left-hand side and also use (7.7), to get

$$(7.10) \quad \int_0^t \sum_i F_i^-(r) - F_i^+(r) dr$$

$$+ \int_{-S+st}^{S-st} \eta(\bar{u}(x,t)|\hat{\psi}(x,t)) dx - \int_{-S}^S \eta(\bar{u}(x,0)|\hat{\psi}(x,0)) dx$$

$$\leq - \int_0^t \left[\int_0^r \sum_i F_i^+(r) - F_i^-(r) dr + \int_{-S+sr}^{S-sr} \left[\left(\partial_x \Big|_{(x,r)} \eta'(\hat{\psi}) \right) A(\bar{u}(x,r)|\hat{\psi}(x,r)) \right. \right.$$

$$\left. \left. + R_{\hat{\psi}}(x,r)\eta''(\hat{\psi}(x,r))[\bar{u}(x,r) - \hat{\psi}(x,r)] \right] dx \right] dr,$$

for all $t \in [0, T]$.

We now apply the Gronwall inequality to (7.10).

Recall that the relative flux $A(a|b)$ is locally quadratic in $a - b$. Recall also (3.4) and that $A(a|b) \geq 0$ due to the convexity of A . Thus, we only have to consider

$$(7.11) \quad \left(\partial_x \Big|_{(x,t)} \eta'(\hat{\psi}) \right) A(\bar{u}(x,t)|\hat{\psi}(x,t))$$

when $\partial_x \Big|_{(x,t)} \eta'(\hat{\psi}) < 0$.

The Gronwall and Young's inequality then give

$$(7.12) \quad \int_0^t \sum_i F_i^-(r) - F_i^+(r) dr + \int_{-S+st}^{S-st} \eta(\bar{u}(x,t)|\hat{\psi}(x,t)) dx \\ \leq C \left(\int_{-S}^S \eta(\bar{u}(x,0)|\hat{\psi}(x,0)) dx + \int_0^t \int_{-S+sr}^{S-sr} (R_{\hat{\psi}}(x,r))^2 dx dr \right) e^{Ct},$$

where the constant $C > 0$ depends on $\max \left\{ \|\bar{u}\|_{L^\infty}, \|\hat{\psi}\|_{L^\infty} \right\}$, the flux A , entropy η and their derivatives. Furthermore, C depends⁶ on $\left\| \left[\partial_x \Big|_{(x,t)} \eta'(\hat{\psi}) \right]_- \right\|_{L^\infty}$, where $[\cdot]_- := \min(0, \cdot)$. Note that by construction, we choose⁷ that $h_i(0) = \hat{h}_i(0)$ (see Section 5) and thus $\hat{\psi}(\cdot, 0) = \hat{u}(\cdot, 0)$.

7.2. Step 2A: calculation of dissipation due to shifting. We now give control on $|\hat{h}_i - h_i|$, but first we need to derive a key dissipation estimate.

From (4.19), and the fact that the h_i are generalized characteristics for \bar{u} , we have for $i = 1, \dots, N$,

$$(7.13) \quad F_i^+(t) - F_i^-(t) = q(\bar{u}(h_i(t)+, t); \hat{\psi}(h_i(t)+, t)) - q(\bar{u}(h_i(t)-, t); \hat{\psi}(h_i(t)-, t)) \\ - \dot{h}_i(t) (\eta(\bar{u}(h_i(t)+, t)|\hat{\psi}(h_i(t)+, t)) - \eta(\bar{u}(h_i(t)-, t)|\hat{\psi}(h_i(t)-, t))) \\ \leq -\frac{1}{12} \inf A'' \inf \eta'' \mathfrak{s}_i ((\bar{u}(h_i(t)+, t) - \hat{\psi}(h_i(t)+, t))^2 + (\bar{u}(h_i(t)-, t) - \hat{\psi}(h_i(t)-, t))^2),$$

where $\mathfrak{s}_i(t) > 0$ is any lower bound for the shock size, i.e. any function of t that verifies $\hat{\psi}(h_i(t)-, t) - \hat{\psi}(h_i(t)+, t) \geq \mathfrak{s}_i(t)$ for all t .

⁶Remark that if $\partial_x \Big|_{(x,r)} \eta'(\hat{\psi}) \geq 0$, then we can drop the term $\left(\partial_x \Big|_{(x,r)} \eta'(\hat{\psi}) \right) A(\bar{u}(x,r)|\hat{\psi}(x,r))$ from (7.8).

⁷Although, we remark that this choice is not strictly necessary for our arguments, and if $h_i(0) \neq \hat{h}_i(0)$, it will simply add a term to the Gronwall argument in Section 7.3 – see (7.23).

Then,

$$(7.14) \quad \begin{aligned} & (\sigma(\bar{u}(h_i(t)+, t), \bar{u}(h_i(t)-, t)) - \sigma(\hat{\psi}(h_i(t)+, t), \hat{\psi}(h_i(t)-, t)))^2 \\ & \leq 2\mathfrak{A}((\bar{u}(h_i(t)+, t) - \hat{\psi}(h_i(t)+, t))^2 + (\bar{u}(h_i(t)-, t) - \hat{\psi}(h_i(t)-, t))^2), \end{aligned}$$

for a detailed proof of this, see [35, p. 2516]. Recall $\mathfrak{A} = \sup A''$.

Then, from (7.13) and (7.14), we get

$$(7.15) \quad \begin{aligned} & q(\bar{u}(h_i(t)+, t); \hat{\psi}(h_i(t)+, t)) - q(\bar{u}(h_i(t)-, t); \hat{\psi}(h_i(t)-, t)) \\ & \quad - \dot{h}_i(t)(\eta(\bar{u}(h_i(t)+, t)|\hat{\psi}(h_i(t)+, t)) - \eta(\bar{u}(h_i(t)-, t)|\hat{\psi}(h_i(t)-, t))) \\ & \leq -\frac{\inf A'' \inf \eta''}{24\mathfrak{A}} \mathfrak{s}_i(t) (\sigma(\bar{u}(h_i(t)+, t), \bar{u}(h_i(t)-, t)) - \sigma(\hat{\psi}(h_i(t)+, t), \hat{\psi}(h_i(t)-, t)))^2. \end{aligned}$$

Finally, use (7.15), (7.12) and also remark that because $\eta(\cdot, \cdot) \geq 0$, due to the convexity of η , we can drop the second term on the left-hand side of (7.12), to get

$$(7.16) \quad \begin{aligned} & \int_0^t \sum_i \left[c\mathfrak{s}_i(r) (\sigma(\bar{u}(h_i(r)+, r), \bar{u}(h_i(r)-, r)) - \sigma(\hat{\psi}(h_i(r)+, r), \hat{\psi}(h_i(r)-, r)))^2 \right] dr \\ & \leq C \left(\int_{-S}^S \eta(\bar{u}(x, 0)|\hat{\psi}(x, 0)) dx + \int_0^t \int_{-S+sr}^{S-sr} (R_{\hat{\psi}}(x, r))^2 dx dr \right) e^{Ct}, \end{aligned}$$

with

$$(7.17) \quad c := \frac{\inf A'' \inf \eta''}{24\mathfrak{A}}.$$

Remark that following the definition of the set \mathfrak{l}_j , the sum $\sum_i[\dots]$ in (7.16) is only over all those curves, at time $t = r$, that are distinct in $\hat{\psi}$ – we are not allowed to count curves that have already collided multiple times.

In particular, for $i = 1, \dots, N$, we have

$$(7.18) \quad \begin{aligned} & \int_0^t \left[c\mathfrak{s}_i(r) (\sigma(\bar{u}(h_i(r)+, r), \bar{u}(h_i(r)-, r)) - \sigma(\hat{\psi}(h_i(r)+, r), \hat{\psi}(h_i(r)-, r)))^2 \right] dr \\ & \leq C \left(\int_{-S}^S \eta(\bar{u}(x, 0)|\hat{\psi}(x, 0)) dx + \int_0^t \int_{-S+sr}^{S-sr} (R_{\hat{\psi}}(x, r))^2 dx dr \right) e^{Ct}. \end{aligned}$$

7.3. Step 2B: proof that (6.1) is upper bound. We gain control on the shock positions via a Gronwall argument.

Let \hat{u} be from the context of the Main Theorem (Theorem 2.2), with Lipschitz-continuous curves of discontinuity $\hat{h}_i(t)$. Note that \hat{h}_i is not necessarily the Rankine-Hugoniot speed

of the discontinuity

$$(7.19) \quad (\hat{u}(\hat{h}_i(t)+, t), \hat{u}(\hat{h}_i(t)-, t))$$

due to numerical error.

We now give control on $h_i - \hat{h}_i$. Let $\hat{L}_i(t) \in \mathbb{N}$ and $\hat{R}_i(t) \in \mathbb{N}$ denote the integers corresponding to the \hat{v}_i which are to the left and right, respectively, of the discontinuity \hat{h}_i in \hat{u} at time t . Likewise, let $L_i(t) \in \mathbb{N}$ and $R_i(t) \in \mathbb{N}$ denote the integers corresponding to the \hat{v}_i which are to the left and right, respectively, of the discontinuity h_i in $\hat{\psi}$ at time t . Then, we can control $h_i - \hat{h}_i$ using the following Gronwall argument:

$$(7.20) \quad \begin{aligned} \dot{\hat{h}}_i(t) - \dot{h}_i(t) &= \left(\dot{\hat{h}}_i(t) - \sigma(\hat{v}_{\hat{L}_i(t)}(\hat{h}_i(t), t), \hat{v}_{\hat{R}_i(t)}(\hat{h}_i(t), t)) \right) \\ &+ \left(\sigma(\hat{v}_{\hat{L}_i(t)}(\hat{h}_i(t), t), \hat{v}_{\hat{R}_i(t)}(\hat{h}_i(t), t)) - \sigma(\hat{v}_{L_i(t)}(\hat{h}_i(t), t), \hat{v}_{R_i(t)}(\hat{h}_i(t), t)) \right) \\ &+ \left(\sigma(\hat{v}_{L_i(t)}(\hat{h}_i(t), t), \hat{v}_{R_i(t)}(\hat{h}_i(t), t)) - \sigma(\hat{v}_{L_i(t)}(h_i(t), t), \hat{v}_{R_i(t)}(h_i(t), t)) \right) \\ &+ \left(\sigma(\hat{v}_{L_i(t)}(h_i(t), t), \hat{v}_{R_i(t)}(h_i(t), t)) - \sigma(\bar{u}(h_i(t)+, t), \bar{u}(h_i(t)-, t)) \right) \end{aligned}$$

Then, from (7.20), we get

$$(7.21) \quad \begin{aligned} \left| \dot{\hat{h}}_i(t) - \dot{h}_i(t) \right| &\leq \left| \dot{\hat{h}}_i(t) - \sigma(\hat{v}_{\hat{L}_i(t)}(\hat{h}_i(t), t), \hat{v}_{\hat{R}_i(t)}(\hat{h}_i(t), t)) \right| \\ &+ \left| \sigma(\hat{v}_{\hat{L}_i(t)}(\hat{h}_i(t), t), \hat{v}_{\hat{R}_i(t)}(\hat{h}_i(t), t)) - \sigma(\hat{v}_{L_i(t)}(\hat{h}_i(t), t), \hat{v}_{R_i(t)}(\hat{h}_i(t), t)) \right| \\ &+ \left| \sigma(\hat{v}_{L_i(t)}(\hat{h}_i(t), t), \hat{v}_{R_i(t)}(\hat{h}_i(t), t)) - \sigma(\hat{v}_{L_i(t)}(h_i(t), t), \hat{v}_{R_i(t)}(h_i(t), t)) \right| \\ &+ \left| \sigma(\hat{v}_{L_i(t)}(h_i(t), t), \hat{v}_{R_i(t)}(h_i(t), t)) - \sigma(\bar{u}(h_i(t)+, t), \bar{u}(h_i(t)-, t)) \right| \end{aligned}$$

from which we infer

$$(7.22) \quad \begin{aligned} \left| \dot{\hat{h}}_i(t) - \dot{h}_i(t) \right| &\leq \left| \dot{\hat{h}}_i(t) - \sigma(\hat{v}_{\hat{L}_i(t)}(\hat{h}_i(t), t), \hat{v}_{\hat{R}_i(t)}(\hat{h}_i(t), t)) \right| \\ &+ \left| \sigma(\hat{v}_{\hat{L}_i(t)}(\hat{h}_i(t), t), \hat{v}_{\hat{R}_i(t)}(\hat{h}_i(t), t)) - \sigma(\hat{v}_{L_i(t)}(\hat{h}_i(t), t), \hat{v}_{R_i(t)}(\hat{h}_i(t), t)) \right| \\ &\quad + \left| \hat{h}_i(t) - h_i(t) \right| \mathfrak{A} \max\{\text{Lip}[\hat{v}_{L_i(t)}], \text{Lip}[\hat{v}_{R_i(t)}]\} \\ &+ \left| \sigma(\hat{v}_{L_i(t)}(h_i(t), t), \hat{v}_{R_i(t)}(h_i(t), t)) - \sigma(\bar{u}(h_i(t)+, t), \bar{u}(h_i(t)-, t)) \right| \end{aligned}$$

We then apply Gronwall's inequality, which yields, for $0 < t < T$,

$$(7.23) \quad \left| h_i(t) - \hat{h}_i(t) \right| \leq \zeta(t, 0) \left(\left| h_i(0) - \hat{h}_i(0) \right| + \int_0^t \zeta(0, s) \left[\left| \dot{\hat{h}}_i(s) - \sigma(\hat{v}_{\hat{L}_i(s)}(\hat{h}_i(s), s), \hat{v}_{\hat{R}_i(s)}(\hat{h}_i(s), s)) \right| + \left| \sigma(\hat{v}_{\hat{L}_i(s)}(\hat{h}_i(s), s), \hat{v}_{\hat{R}_i(s)}(\hat{h}_i(s), s)) - \sigma(\hat{v}_{L_i(s)}(\hat{h}_i(s), s), \hat{v}_{R_i(s)}(\hat{h}_i(s), s)) \right| + \left| \sigma(\hat{v}_{L_i(s)}(h_i(s), s), \hat{v}_{R_i(s)}(h_i(s), s)) - \sigma(\bar{u}(h_i(s)+, s), \bar{u}(h_i(s)-, s)) \right| \right] ds \right).$$

Note that to use the Gronwall inequality, we utilize

$$(7.24) \quad \left| \hat{h}_i(t) - h_i(t) \right| \leq \left| \hat{h}_i(0) - h_i(0) \right| + \int_0^t \left| \dot{\hat{h}}_i(s) - \dot{h}_i(s) \right| dt,$$

which follows from the Fundamental Theorem of Calculus for $W_{\text{loc}}^{1,1}$ functions.

Moreover, remark that in (7.23), using the ζ function (see (6.5)) is a rough upper bound. In fact, within the ζ function, we only need to consider the Lipschitz constants of the \hat{v}_i which might possibly be to the left or right of h_i in $\hat{\psi}$ at time s .

Then (7.23) can be rewritten as

$$(7.25) \quad \left| h_i(t) - \hat{h}_i(t) \right| \leq \zeta(t, 0) \left| h_i(0) - \hat{h}_i(0) \right| + \int_0^t \zeta(0, s) \left[\left| \dot{\hat{h}}_i(s) - \sigma(\hat{v}_{\hat{L}_i(s)}(\hat{h}_i(s), s), \hat{v}_{\hat{R}_i(s)}(\hat{h}_i(s), s)) \right| + \left| \sigma(\hat{v}_{\hat{L}_i(s)}(\hat{h}_i(s), s), \hat{v}_{\hat{R}_i(s)}(\hat{h}_i(s), s)) - \sigma(\hat{v}_{L_i(s)}(\hat{h}_i(s), s), \hat{v}_{R_i(s)}(\hat{h}_i(s), s)) \right| + \left| \sigma(\hat{v}_{L_i(s)}(h_i(s), s), \hat{v}_{R_i(s)}(h_i(s), s)) - \sigma(\bar{u}(h_i(s)+, s), \bar{u}(h_i(s)-, s)) \right| \right] ds.$$

Then, remark that from L^2 - L^2 Hölder duality, we get,

$$(7.26) \quad \begin{aligned} \left| h_i(t) - \hat{h}_i(t) \right| &\leq \zeta(t, 0) \left| h_i(0) - \hat{h}_i(0) \right| \\ &\quad + \int_0^t \zeta(t, s) \left[\left| \dot{\hat{h}}_i(s) - \sigma(\hat{v}_{\hat{L}_i(s)}(\hat{h}_i(s), s), \hat{v}_{\hat{R}_i(s)}(\hat{h}_i(s), s)) \right| \right. \\ &\quad \left. + \left| \sigma(\hat{v}_{\hat{L}_i(s)}(\hat{h}_i(s), s), \hat{v}_{\hat{R}_i(s)}(\hat{h}_i(s), s)) - \sigma(\hat{v}_{L_i(s)}(\hat{h}_i(s), s), \hat{v}_{R_i(s)}(\hat{h}_i(s), s)) \right| \right] ds \\ &\quad + \left\| \frac{\zeta(t, \cdot)}{\sqrt{\mathfrak{s}_i(\cdot)}} \right\|_{L^2(0,t)} \left\| \sqrt{\mathfrak{s}_i(\cdot)} \left(\sigma(\hat{v}_{L_i(\cdot)}(h_i(\cdot), \cdot), \hat{v}_{R_i(\cdot)}(h_i(\cdot), \cdot)) - \sigma(\bar{u}(h_i(\cdot)+, \cdot), \bar{u}(h_i(\cdot)-, \cdot)) \right) \right\|_{L^2(0,t)}, \end{aligned}$$

where we recall $\mathfrak{s}_i(t) > 0$ is a lower bound for the size of the i -th shock.

Due to the definition of L_i and R_i we may use the dissipation estimate (7.18), which implies

$$(7.27) \quad \begin{aligned} \left| h_i(t) - \hat{h}_i(t) \right| &\leq \zeta(t, 0) \left| h_i(0) - \hat{h}_i(0) \right| \\ &\quad + \int_0^t \zeta(t, s) \left[\left| \dot{\hat{h}}_i(s) - \sigma(\hat{v}_{\hat{L}_i(s)}(\hat{h}_i(s), s), \hat{v}_{\hat{R}_i(s)}(\hat{h}_i(s), s)) \right| \right. \\ &\quad \left. + \left| \sigma(\hat{v}_{\hat{L}_i(s)}(\hat{h}_i(s), s), \hat{v}_{\hat{R}_i(s)}(\hat{h}_i(s), s)) - \sigma(\hat{v}_{L_i(s)}(\hat{h}_i(s), s), \hat{v}_{R_i(s)}(\hat{h}_i(s), s)) \right| \right] ds \\ &\quad + \left\| \frac{\zeta(t, \cdot)}{\sqrt{\mathfrak{s}_i(\cdot)}} \right\|_{L^2(0,t)} \left[C e^{Ct} \left(\int_{-S}^S \eta(\bar{u}(x, 0) |\hat{\psi}(x, 0)) dx + \int_0^t \int_{-S+sr}^{S-sr} (R_{\hat{\psi}}(x, r))^2 dx dr \right) \right]^{\frac{1}{2}}. \end{aligned}$$

Finally, (7.27) gives us control on the difference $\left| h_i(t) - \hat{h}_i(t) \right|$. This yields the formula (6.1).

8. PROOF OF THEOREM 2.3

Theorem 2.3 follows from the formulas for Δ_i , see (6.1), (6.39), and Section 6.4.4. This includes the logic for determining when shocks have collided in $\hat{\psi}$ (see Section 6.3). We also use the formulas for $\Gamma_d(t)$ (see (6.21)) and $\Upsilon_d(t)$ (see in(6.20)). Finally, we use that the function \bar{u}^0 is fixed, and \bar{u}^0 is broken into only a finite number $\bar{N} + 1$ of intervals such that on each interval, \bar{u}^0 is either rapidly decreasing or nearly non-decreasing (this is the \bar{N} in the context of Theorem 2.2).

9. EXPECTED CONVERGENCE OF ESTIMATOR

Let us discuss how we expect our error estimator to scale for mesh refinement, i.e. in the case $h, \delta \rightarrow 0$ and how h, δ should be related. Here, δ is from the context of the Main Theorem (Theorem 2.2) and h is the mesh width.

In order to keep the discussion concise let us discuss the case of a dG scheme with polynomials of degree 0 and an upwind type numerical flux, say Engquist-Osher, and an explicit SSP Runge-Kutta time discretization with a time step chosen according to a suitable CFL condition. In this case, (L^2 -norms of) residuals are expected to be $\mathcal{O}(h)$ provided the corresponding exact solution is C^1 . This is the case if we can build extensions where kinks are very unlikely to be revealed in $\hat{\psi}$. In particular, this is the case if we only have ‘large’ shocks. This situation is discussed in Section 9.1. Remark that by ‘kink’, we mean a point that is not differentiable (in space) because it has differing one-sided derivatives.

If the exact solution contains kinks (which are potentially revealed) then (L^2 -norms of) residuals are expected to be $\mathcal{O}(h^{3/4})$. This situation is discussed in Section 9.2.

Let us remark, that we can only expect the error estimator to converge, for $\delta, h \rightarrow 0$, if the underlying scheme (as described above) is reasonable. For a scheme that is unstable or fails to converge the error estimator cannot converge.

We stress that our error estimate is valid even if total variation and oscillation of the numerical solution is large, but, obviously, only convergent schemes can lead to convergent estimators. We will also assume that time step sizes are chosen proportional to h , which makes sense from the point of view of CFL conditions.

9.1. ‘Large’ shocks. Let us focus, in this section, on the case that \bar{u}^0 only has nearly non-decreasing parts. In this case δ does not appear and there is a number of discontinuities in \hat{u} that is independent of δ .

The analysis and the numerical experiments in [20, 14] show that we can expect the residuals R_i (see (2.16)) to have L^2 norms that are $\mathcal{O}(h)$ and the same is true for the initial data approximation error. Thus, until the first time that two shocks might have collided, we expect C_i in (6.1) to be $\mathcal{O}(h)$, whereas B_i is zero during this time and the size of A_i depends on the Runge-Kutta scheme used for solving (5.1) – it can be easily made much smaller than $\mathcal{O}(h)$.

Once there is uncertainty of whether two shocks have merged, B_i is of order one and the question is how long this time interval of uncertainty is. Since the shocks in question have a speed difference that is independent of h and the position error of each is proportional to h we expect the interval of uncertainty to be proportional to h .

Thus, for each possible collision, the uncertainty in Δ_i increases by a term proportional to h . Since the number of possible collisions is finite and independent of h we expect Δ_i to be proportional to h . Inserting this into (2.9) leads to a bound for $\|\hat{\psi} - \hat{u}\|_{L^\infty(0,T;L^1(\mathbb{R}))}$ of order h , since $\mathcal{B}(t)$ (in the context of the Main Theorem Theorem 2.2) consists of a number of intervals each of which has a size proportional to h and the function that is integrated has size independent of h . Moreover, since the initial data approximation error

and the residuals are of order h the bound for $\|\hat{\psi} - \bar{u}\|_{L^\infty(0,T;L^2(\mathbb{R}))}$ from (2.13) is of order h . Thus, since on a compact domain the L^2 norm controls the L^1 norm, the overall bound for $\|\hat{u} - \bar{u}\|_{L^\infty(0,T;L^1(\mathbb{R}))}$ (see (2.8)) is also of order h , which is optimal from an approximation theory viewpoint, although one might hope to obtain such estimates also in L^p -norms with $1 < p \leq 2$, cf. [51]. In the scenario where \bar{u}^0 has no rapidly decreasing parts, we indeed also obtain error estimates in the $L^p(-S - st, S + st)$ norm for $1 < p \leq 2$ but the position uncertainty of the shocks leads to (sub-optimal) error bounds of order $h^{\frac{1}{p}}$. Note that the a posteriori error bound for the L^∞ -in-time L^1 -in-space norm we obtain is $\mathcal{O}(h)$ which is much smaller than the $\mathcal{O}(h^{\frac{1}{2}})$ bound obtained by Kruzhkov-type error estimates or the $\mathcal{O}(h^{\frac{1}{3}})$ obtained in [2]. This comes at the price of significantly modifying the numerical scheme, though.

9.2. ‘Front tracking’ shocks. If there are rapidly decreasing parts of \bar{u}^0 we have two smallness parameters δ, h . Compared to the only ‘large’ shocks scenario discussed above we also have additional error estimator components: uncertainty of positions of ‘boundary’ shocks and estimates for the L^1 error in the front tracking regions with ‘front tracking’ shocks coming from parts where \bar{u}^0 is rapidly decreasing (see Figure 1). These L^1 estimates are based on (6.21) and (6.20).

The initial data approximation error $(\int \eta(\bar{u}(\cdot, 0))|\hat{\psi}(\cdot, 0))dx)^{\frac{1}{2}}$ is expected to be

$$\mathcal{O}(\sqrt{\delta^2 + h^2})$$

but not $o(\sqrt{\delta^2 + h^2})$. In contrast, the corresponding term in (6.15), using $\hat{\psi}_{fine}$ instead of $\hat{\psi}$, is $\mathcal{O}(\sqrt{\delta^3 + h^2})$ since all the \mathfrak{s}_* are proportional to δ and we retain h^2 for the nearly non-decreasing pieces. Since the extensions of the initial data, from Appendix A.1, contain (a finite number) of kinks (nondifferentiable points) which are likely to be revealed in $\hat{\psi}$, we expect the squared space-time L^2 norm of the residual to be $\mathcal{O}(h^{3/2})$ but not $o(h^{3/2})$ for both $\hat{\psi}$ and $\hat{\psi}_{fine}$. Thus, the right-hand side of (6.15) is

$$\mathcal{O}\left(\frac{1}{\sqrt{\delta}}(\delta^3 + h^2 + h^{3/2})^{\frac{1}{2}} + \delta\right)$$

but not smaller, in general, and we see that the optimal scaling for δ is $\delta \sim \sqrt{h}$ leading to $\Upsilon_\alpha \sim \delta \sim \sqrt{h}$ for all α . Using the facts that $\Upsilon_\alpha \sim \delta$ for all α and that the initial data approximation error is $\mathcal{O}(\sqrt{\delta^2 + h^2})$ and that the squared space-time L^2 norm of the residual is $\mathcal{O}(h^{3/2})$, we can infer the scaling of Γ from (6.21)

$$\Gamma = \mathcal{O}\left(\sqrt{C + \frac{\Upsilon}{\delta}}\sqrt{\delta^2 + h^2 + h^{3/2}} + \frac{\Upsilon^2}{\delta} + (C + \frac{\Upsilon}{\delta})\Upsilon\right) = \mathcal{O}(\delta) \sim \mathcal{O}(\sqrt{h})$$

and finally $\Delta_{inner} \sim \sqrt{\Gamma} \sim \sqrt{\delta} \sim h^{1/4}$ (see (6.29)). Here $C > 0$ is a constant and Υ denotes the maximum of the Υ_α coming from the corresponding rapidly decreasing piece.

All in all, the position uncertainty of ‘boundary’ shocks is expected to be $\mathcal{O}(h^{1/4})$. The size of C_i (see (6.4)) in position estimates of ‘large’ shocks is $\mathcal{O}(\sqrt{\delta^2 + h^2}) = \mathcal{O}(h^{1/2})$, but not smaller in general.

In contrast, A_i stays small. In cases where ‘large’ shocks might have interacted with ‘boundary’ shocks the B_i term for these shocks is expected to be of order $\mathcal{O}(h^{1/4})$ since the length of time intervals of uncertainty whether the collisions have taken place is $\mathcal{O}(h^{1/4})$ as it is dictated by the position uncertainty of the shock positions. An analogous argument holds for collision of two ‘boundary’ shocks originating from the same rapidly decreasing piece. The minimal velocity difference of these shocks is order 1 and the position uncertainty of both is $\mathcal{O}(h^{1/4})$, thus the time interval of uncertainty whether the collision has happened is $\mathcal{O}(h^{1/4})$ as is the resultant additional position uncertainty (see Section 6.3.3). The case of two ‘boundary’ shocks separated by a \hat{v}_i corresponding to a nearly non-decreasing interval of \bar{u}^0 , and then colliding, is similar, with again a resultant additional position uncertainty of $\mathcal{O}(h^{1/4})$ See Section 6.3.2.

In any case, the uncertainty of ‘boundary’ shock positions dominates all other terms in the $\sup_{t \in [0, T]} \|\bar{u}(\cdot, t) - \hat{u}(\cdot, t)\|_{L^1(-S+st, S-st)}$ error estimate such that we expect

$$\sup_{t \in [0, T]} \|\bar{u}(\cdot, t) - \hat{u}(\cdot, t)\|_{L^1(-S+st, S-st)} = \mathcal{O}(h^{1/4}).$$

Note that this is a rather low convergence rate. Indeed, it is less than what is obtained in [2] and [21] for systems; and using Kruzhkov-type estimates for scalar problems. Part of the reason for this is the suboptimal rate $h^{3/2}$ for the squared L^2 norm of the residuals, that is caused by the exact v_i having kinks. In the case with only ‘large’ shocks we could build the extensions in such a way that kinks are not seen (for h small enough). This is not possible, if there are transitions from nearly non-decreasing to rapidly decreasing pieces in \bar{u}^0 without any jump at a point x_i , e.g. \bar{u}^0 is nearly non-decreasing on (x_{i-1}, x_i) and rapidly decreasing on (x_i, x_{i+1}) and $\bar{u}^0(x_i-) = \bar{u}^0(x_i+)$. In this case, then there is only a very short area (with length proportional to δ) on which we can extend the nearly non-decreasing piece without prescribing the slope M - usually this piece is so short that it is revealed after a short simulation time. See the construction in Appendix A.1 and (A.3). Instead of having a kink in this piece, we could use a quadratic polynomial to build a C^1 extension but the C^2 norm of this extension would have to be proportional to δ^{-1} . This extension, would improve the rate of the squared L^2 norm of the residual - but not to h^2 . Thus, we have opted for the simpler extensions including kinks.

One way to improve the rate of the squared L^2 norm of the residual to h^2 would be to use numerical schemes on meshes that move such that the kink is aligned with some cell boundary for all times (using the fact that each extended initial data, following Appendix A.1, has at most one or two kinks likely to be revealed and their positions can be computed for all times). Redoing the above computations in this case would suggest to choose $\delta \sim h^{2/3}$ and lead to an $\sup_{t \in [0, T]} \|\bar{u}(\cdot, t) - \hat{u}(\cdot, t)\|_{L^1(-S+st, S-st)}$ error estimator that is $\mathcal{O}(h^{1/3})$, i.e. with the same rate as the estimates in [2] and [21]. In particular, this

coincides with the scaling of a posteriori error bounds obtained by Bressan and co-workers [2].

10. NUMERICAL EXPERIMENTS

We have implemented our error estimator in MATLAB and carried out several numerical experiments in order to experimentally assess its scaling behaviour, i.e. to check whether it scales as discussed in Section 9. Our experiments are carried out for Burgers equation and use a first-order piece-wise constant finite volume scheme, with explicit Euler time-stepping and upwind numerical flux. Our code is available at

<https://git-ce.rwth-aachen.de/jan.giesselmann/shiftsshocksaposteriori.git>

The whole purpose of the code is to provide validation of the scaling; it is not optimized in any way. In particular, the preprocessing of the initial data, i.e., its decomposition into nearly non-decreasing and rapidly decreasing parts, is not automated.

We have conducted numerical experiments for two initial data: One in which only ‘large’ shocks occur and a second one in which a rapidly decreasing piece forms a shock during the simulation time.

Before we present the experiments, let us mention one trick we used to slightly decrease the computational costs of the code: Our error estimator contains several terms in which integrals are multiplied by exponential functions, and approximating these integrals by quadrature in each time step is inconvenient. Instead, we compute these terms iteratively based on their value in the previous time step which is simplified by the fact that the integrands are constant in each time step. Indeed, for any two non-negative sequences $\{\alpha_k\}_{k \in \mathbb{N}}$, $\{\beta_k\}_{k \in \mathbb{N}}$, the following holds:

$$(10.1) \quad F_i := \sum_{j=0}^i \alpha_j \Delta t \exp \left(\sum_{k=j}^i \beta_k \Delta t \right)$$

satisfies

$$(10.2) \quad F_{i+1} = F_i \exp \left(\beta_{i+1} \Delta t \right) + \alpha_{i+1} \Delta t \exp \left(\beta_{i+1} \Delta t \right).$$

10.1. Experiment with ‘large’ shocks only. In this experiment the computational space-time domain is $[0, 1] \times [0, .3]$ and the initial data are given by

$$(10.3) \quad \bar{u}^0(x) = \begin{cases} 3 & \text{if } x < 0.25 \\ 1 + 2x & \text{if } 0.25 < x < 0.5 \\ x & \text{if } 0.5 < x < 0.625 \\ 0 & \text{if } x > 0.625 \end{cases}$$

In Table 1, we report the upper bounds for position errors, $\sup_{t \in [0, T]} \|\bar{u}(\cdot, t) - \hat{\psi}(\cdot, t)\|_{L^2}$, and $\sup_{t \in [0, T]} \|\bar{u}(\cdot, t) - \hat{u}(\cdot, t)\|_{L^1}$ provided by our error estimator as well as $\|\hat{u}_{\text{fine}}(\cdot, T) - \hat{u}(\cdot, T)\|_{L^1}$, where \hat{u}_{fine} is a finite volume solution on a much finer mesh, and we use this as an approximation of the ‘true’ value of $\|\bar{u}(\cdot, T) - \hat{u}(\cdot, T)\|_{L^1}$.

In Figure 13 we show snapshots of the numerical solution at times

$$t \in \{0.05, 0.1, 0.15, 0.2, 0.25, 0.3\}.$$

In the areas where it is unclear which \hat{v}_i is revealed in $\hat{\psi}$, we color in red the branches of the \hat{v}_i that are not revealed in \hat{u} but that might be revealed in $\hat{\psi}$. We observe that, as expected, all monitored quantities converge with order $\mathcal{O}(h)$.

For each quantity in an even column we display its *Experimental order of Convergence* (EoC) in the adjacent column to the right. For any quantity $E(h)$ that depends on the mesh width h we define the EoC for two consecutive mesh widths h_1 and h_2 as

$$\text{EoC}_{12} = \frac{\log\left(\frac{E(h_1)}{E(h_2)}\right)}{\log\left(\frac{h_1}{h_2}\right)},$$

the idea being that if $E(h) = Ch^p$ then $\text{EoC} = p$.

#cells	$\max_i \Delta_i$	EoC	$\ \bar{u} - \hat{\psi}\ _{L^2}$	EoC	$\ \bar{u} - \hat{u}\ _{L^1}$	EoC	$\ \hat{u}_{\text{fine}} - \hat{u}\ _{L^1}$	EoC
3200	$4.13 \cdot 10^{-3}$	—	$3.26 \cdot 10^{-4}$	—	$9.46 \cdot 10^{-3}$	—	$1.44 \cdot 10^{-4}$	—
6400	$2.06 \cdot 10^{-3}$	1.0	$1.63 \cdot 10^{-4}$	1.0	$4.73 \cdot 10^{-3}$	1.0	$8.21 \cdot 10^{-5}$	0.82
12800	$1.03 \cdot 10^{-3}$	1.0	$8.14 \cdot 10^{-5}$	1.0	$2.35 \cdot 10^{-3}$	1.0	$3.59 \cdot 10^{-5}$	1.19
25600	$5.14 \cdot 10^{-4}$	1.0	$4.07 \cdot 10^{-5}$	1.0	$1.18 \cdot 10^{-3}$	1.0	$2.05 \cdot 10^{-5}$	0.81

TABLE 1. Error estimator results for the example with ‘large’ shocks only: estimates on $\|\bar{u} - \hat{u}\|_{L^1}$ and $\|\bar{u} - \hat{\psi}\|_{L^2}$. We also include the values of $\|\hat{u} - \hat{u}_{\text{fine}}\|_{L^1}$.

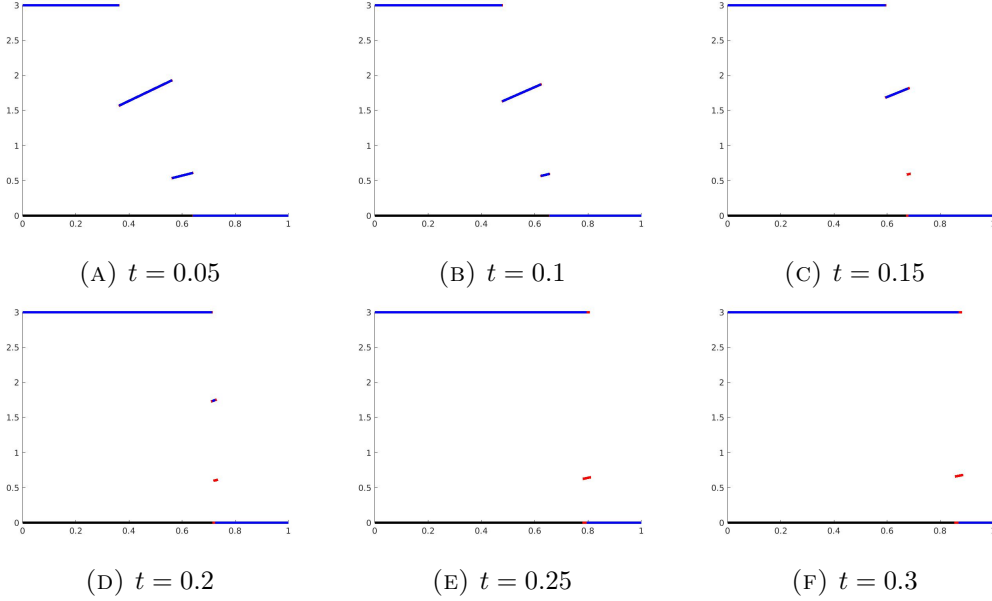
10.2. Experiment including a rapidly decreasing piece. In this experiment, the computational space-time domain is $[0, 1] \times [0, .22]$ and the initial data are given by

$$(10.4) \quad \bar{u}^0(x) = \begin{cases} 2.5 & \text{if } x < 0.2 \\ 3.5 - 5x & \text{if } 0.2 < x < 0.4 \\ 1.1 + x & \text{if } 0.4 < x < 0.625 \\ 0 & \text{if } x > 0.625 \end{cases}$$

The time interval in the example is long enough for the ‘boundary’ shocks of the rapidly decreasing piece to collide (in the exact solution and in the computer).

In Table 2, we report $\max_\alpha \Upsilon_\alpha(T)$, Γ and Δ_{inner} for the rapidly decreasing piece for a sequence of meshes. Note that these terms scale as predicted in Section 9.2. In Table 3, we also report the upper bounds on $\sup_{t \in [0, T]} \|\bar{u}(\cdot, t) - \hat{\psi}(\cdot, t)\|_{L^2}$ and $\sup_{t \in [0, T]} \|\bar{u}(\cdot, t) - \hat{u}(\cdot, t)\|_{L^1}$ provided by our analysis as well as $\|\hat{u}_{\text{fine}}(\cdot, T) - \hat{u}(\cdot, T)\|_{L^1}$, where \hat{u}_{fine} is a finite volume solution on a much finer mesh and we use this as an approximation of the ‘true’ value of $\|\bar{u}(\cdot, T) - \hat{u}(\cdot, T)\|_{L^1}$. Note that in this experiment the simulation ‘sees’ the kinks in the extensions of the increasing pieces (as discussed in Section 9, above). Thus $\sup_{t \in [0, T]} \|\bar{u}(\cdot, t) - \hat{\psi}(\cdot, t)\|_{L^2}$ is $\mathcal{O}(h^{3/4})$ but not $\mathcal{O}(h)$ as in the previous experiment.

FIGURE 13. From initial data (10.3), we have snapshots of the numerical solution, with 800 cells, at different times. The parts of the \hat{v}_i which are not revealed in \hat{u} but may be revealed in $\hat{\psi}$ are colored in red.



We also note that the bound for $\sup_{t \in [0, T]} \|\bar{u}(\cdot, t) - \hat{u}(\cdot, t)\|_{L^1}$ decreases much more slowly than anticipated. This can be understood as follows:

One major source of position uncertainty of shocks is potential velocity errors during time intervals when it is not clear whether ‘boundary’ shocks have collided in $\hat{\psi}$. The length of these time intervals of uncertainty does not show the scaling behavior we expect. We attribute this to the strong time dependence of our bounds on the position error of shocks. Indeed, if we plot Δ_{inner} we see that for any fixed t we have $\Delta_{inner}(t) = \mathcal{O}(h^{1/4})$ but the constant grows quickly in time.

In order to understand how this time-dependence leads to the observed behavior of the lengths of the time intervals of uncertainty mentioned above, let us consider, as an heuristic example, the time when two shocks actually collide in $\hat{\psi}$ compared to the time when our code concludes that a *collision might have happened*. Remark this is a subset of the length of time during which the code is uncertain whether or not a collision has occurred in $\hat{\psi}$. Suppose the initial position difference of the shocks is b and their speed difference is the constant value a . Then they collide at time $\frac{b}{a}$ in the exact solution. Heuristically, we suppose a and b are reproduced accurately by our code and we will ignore any errors in this regard in the current discussion. If our bounds on position errors of shocks were independent of time, then the time t^* , when the code concludes that a collision might have

happened is (approximately) determined as the solution of

$$(10.5) \quad b = at^* + c(h),$$

where $c(h)$ denotes our bound on the sum of the position errors of the two shocks. Then, $t^* = \frac{b-c(h)}{a}$ and thus the length of the time between when the code determines a collision might have occurred, and when it actually does occur in $\hat{\psi}$ is given by

$$\frac{b}{a} - \frac{b-c(h)}{a} = \frac{c(h)}{a},$$

i.e. a quantity that will exactly reproduce the scaling behaviour of $c(h)$.

In contrast, suppose that our bounds on position errors of shocks depend on time linearly. Then t^* is given as the solution of

$$(10.6) \quad b = at^* + c(h)t^*$$

i.e., $t^* = \frac{b}{a+c(h)}$.

Thus, in this case the length of time between when the code determines a collision might have occurred in $\hat{\psi}$, and when it actually occurs in $\hat{\psi}$, is given by

$$\frac{b}{a} - \frac{b}{a+c(h)} = \frac{bc(h)}{a+c(h)}.$$

This quantity shows the same behavior as $c(h)$ when $c(h)$ is small (compared to a) but not when $c(h)$ is not small: in the latter (pre-asymptotic) case the quantity from (10.6) decays much more slowly than $c(h)$. Analogous considerations apply when the time dependence is nonlinear.

In our numerical experiments, the length of the interval of collision uncertainty is clearly still in the pre-asymptotic regime, where its experimental convergence rate is less than that of $c(h)$. The argument above shows that asymptotically for $h \rightarrow 0$ (where also $c(h) \rightarrow 0$) we can expect the length of the time interval of uncertainty to behave like $c(h)$, i.e., to be $\mathcal{O}(h^{1/4})$.

The long computing times of our code and the low convergence rate of Δ_{inner} have convinced us not to pursue computations where the asymptotic behavior of our estimate for $\sup_{t \in [0, T]} \|\bar{u}(\cdot, t) - \hat{u}(\cdot, t)\|_{L^1}$ can be seen.

#cells	$\max_{\alpha} \Upsilon_{\alpha}$	EoC	Γ	EoC	Δ_{inner}	EoC
3200	0.099	—	0.213	—	0.292	—
6400	0.073	0.44	0.156	0.45	0.249	0.23
12800	0.050	0.55	0.106	0.56	0.206	0.27
25600	0.036	0.47	0.075	0.50	0.174	0.24

TABLE 2. Observed values of $\max_{\alpha} \Upsilon_{\alpha}$, Γ , and Δ_{inner} for the example with one rapidly decreasing piece.

$\#cells$	$\ \hat{u} - \hat{u}_{\text{fine}}\ _{L^1}$	EoC	$\ \bar{u} - \hat{u}\ _{L^1}$	EoC	$\ \bar{u} - \hat{\psi}\ _{L^2}$	EoC
3200	$1.07 \cdot 10^{-3}$	—	2.61	—	$2.6 \cdot 10^{-3}$	—
6400	$4.97 \cdot 10^{-4}$	1.1	2.55	0.03	$1.5 \cdot 10^{-3}$	0.79
12800	$2.40 \cdot 10^{-4}$	1.0	2.47	0.05	$9.1 \cdot 10^{-4}$	0.72
25600	$1.22 \cdot 10^{-4}$	1.0	2.38	0.05	$5.4 \cdot 10^{-4}$	0.75

TABLE 3. Error estimator results for the example with one rapidly decreasing piece: estimates on $\|\bar{u} - \hat{u}\|_{L^1}$ and $\|\bar{u} - \hat{\psi}\|_{L^2}$. We also include the values of $\|\hat{u} - \hat{u}_{\text{fine}}\|_{L^1}$.

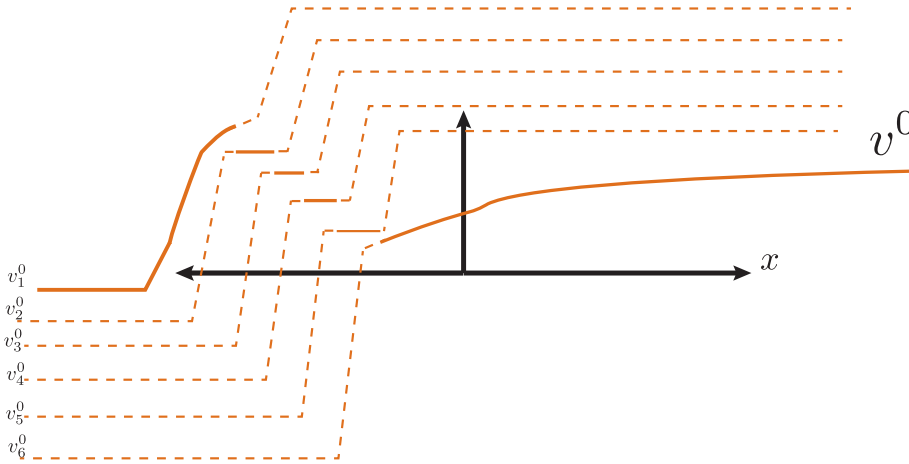


FIGURE 14. Given a function $v^0 \in \mathcal{S}_d^\epsilon$, in the present paper we create piecewise-linear artificial extensions defined on \mathbb{R} . In this diagram, the extensions are denoted by dotted lines (note the diagram is not to scale).

APPENDIX A.

A.1. **Defining the extensions to make the v_i^0 .** We use the process of creating artificial extensions as given in [34]. However, we modify the procedure given in [34]. Unlike in [34], we want the artificial extensions to have a pointwise lower bound on their difference (see (A.19), below). We also want our extensions to be C^1 , at least in regions where we expect the extensions might be revealed (however, even with the extensions constructed in this section, it is still possible that nondifferentiable points, i.e. kinks, are revealed, see the discussion in Section 9). See Figure 14.

Consider initial data $v^0 \in \mathcal{S}_d^\epsilon$ (see (2.2)).

We use the $N \in \mathbb{N}$ and $-\infty = x_0 < x_1 < \dots < x_N < x_{N+1} = +\infty$ from within the context of (2.2).

We also define the one-sided derivatives

$$(A.1) \quad \frac{d^\pm}{dx} v^0(x) := \lim_{y \rightarrow x^\pm} \frac{v^0(y) - v^0(x)}{y - x}.$$

Claim. For $i = 1, \dots, N$, the one-sided derivatives $\frac{d^\pm}{dx} v^0(x_i)$ exist by the definition of \mathcal{S}_d^ϵ . *Proof of Claim.* Let x_i be the left (right) endpoint of a small open interval $I \subset \mathbb{R}$. By the definition of \mathcal{S}_d^ϵ , $(v^0)'$ is uniformly continuous on I . Thus, the derivative (uniquely) extends to a uniformly continuous function $D: \bar{I} \rightarrow \mathbb{R}$. Then by L'Hôpital's rule,

$$(A.2) \quad \frac{d^\pm}{dx} v^0(x_i) = \lim_{y \rightarrow x_i^\pm} \frac{v^0(y) - v^0(x_i)}{y - x_i} = \lim_{y \rightarrow x_i^\pm} \frac{(v^0)'(y)}{1} = D(x_i),$$

with $+$ for the left endpoint and $-$ for the right endpoint. ■

Define the slope

$$(A.3) \quad M := \max \left\{ 1, \max_{k=0, \dots, N} \text{Lip}[v^0 \upharpoonright_{(x_k, x_{k+1})}] \right\}.$$

If v^0 contains at least one discontinuity, we define

$$(A.4) \quad v_1^0(x) := \begin{cases} v^0(x), & \text{if } x < x_1, \\ v^0(x_1-) + (x - x_1) \frac{d^-}{dx} v^0(x_1), & \text{if } x_1 < x < x_I^1, \\ v^0(x_1-) + (x_I^1 - x_1) \frac{d^-}{dx} v^0(x_1) + (x - x_I^1)M, & \text{if } x_I^1 < x < x_R^1, \\ \max \left\{ v^0(x_1-) + (x_I^1 - x_1) \frac{d^-}{dx} v^0(x_1), \right. \\ \left. \sup_{x \in (x_1, \infty)} v^0(x) + \sum_{k=1}^N (v^0(x_k-) - v^0(x_k+)) \right. \\ \left. + \sum_{k=2}^N \left((x_I^k - x_k) \left| \frac{d^-}{dx} v^0(x_k) \right| \right) \right\}, & \text{if } x_R^1 < x, \end{cases}$$

where the x_i are as in (2.2). The number x_I^1 is defined as

$$(A.5) \quad x_I^1 := x_1 + \min \left\{ 1, \frac{v^0(x_1-) - v^0(x_1+)}{2 \left(M + \left| \frac{d^-}{dx} v^0(x_1) \right| \right)} \right\}.$$

If

$$(A.6) \quad \sup_{x \in (x_1, \infty)} v^0(x) + \sum_{k=1}^N (v^0(x_k-) - v^0(x_k+)) \\ + \sum_{k=2}^N \left((x_I^k - x_k) \left| \frac{d^-}{dx} v^0(x_k) \right| \right) < v^0(x_1-) + (x_I^1 - x_1) \frac{d^-}{dx} v^0(x_1)$$

then we define $x_R^1 := x_I^1$. Otherwise, we let x_R^1 be defined as the solution to

$$(A.7) \quad v^0(x_{1-}) + (x_I^1 - x_1) \frac{d^-}{dx} v^0(x_1) + (x_R^1 - x_I^1) M = \sup_{x \in (x_1, \infty)} v^0(x) + \sum_{k=1}^N (v^0(x_{k-}) - v^0(x_{k+})) + \sum_{k=2}^N \left((x_I^k - x_k) \left| \frac{d^-}{dx} v^0(x_k) \right| \right).$$

Similarly, for $i = 2, \dots, N$, we also define

$$(A.8) \quad v_i^0(x) := \begin{cases} \min \left\{ v^0(x_{i-1+}) + (x_J^i - x_{i-1}) \frac{d^+}{dx} v^0(x_{i-1}), \right. \\ \left. \inf_{x \in (-\infty, x_{i-1})} v^0(x) - \sum_{k=1}^{i-1} (v^0(x_{k-}) - v^0(x_{k+})) \right. \\ \left. - \sum_{k=3}^i \left((x_J^{k-1} - x_{k-2}) \left| \frac{d^+}{dx} v^0(x_{k-2}) \right| \right) \right\}, & \text{if } x < x_L^i, \\ v^0(x_{i-1+}) + (x_J^i - x_{i-1}) \frac{d^+}{dx} v^0(x_{i-1}) + (x - x_J^i) M, & \text{if } x_L^i < x < x_J^i, \\ v^0(x_{i-1+}) + (x - x_{i-1}) \frac{d^+}{dx} v^0(x_{i-1}), & \text{if } x_J^i < x < x_{i-1}, \\ v^0(x), & \text{if } x_{i-1} < x < x_i, \\ v^0(x_{i-}) + (x - x_i) \frac{d^-}{dx} v^0(x_i), & \text{if } x_i < x < x_I^i, \\ v^0(x_{i-}) + (x_I^i - x_i) \frac{d^-}{dx} v^0(x_i) + (x - x_I^i) M, & \text{if } x_I^i < x < x_R^i, \\ \max \left\{ v^0(x_{i-}) + (x_I^i - x_i) \frac{d^-}{dx} v^0(x_i), \right. \\ \left. \sup_{x \in (x_i, \infty)} v^0(x) + \sum_{k=i}^N (v^0(x_{k-}) - v^0(x_{k+})) \right. \\ \left. + \sum_{k=i+1}^N \left((x_I^k - x_k) \left| \frac{d^-}{dx} v^0(x_k) \right| \right) \right\}, & \text{if } x_R^i < x. \end{cases}$$

We define $\sum_{\alpha}^{\beta} := 0$, for any indices $\beta < \alpha$.

The number x_J^i is defined as

$$(A.9) \quad x_J^i := x_{i-1} - \min \left\{ 1, \frac{v^0(x_{i-1-}) - v^0(x_{i-1+})}{2 \left(M + \left| \frac{d^+}{dx} v^0(x_{i-1}) \right| \right)} \right\}.$$

The number x_I^i is defined as

$$(A.10) \quad x_I^i := x_i + \min \left\{ 1, \frac{v^0(x_{i-}) - v^0(x_{i+})}{2 \left(M + \left| \frac{d^-}{dx} v^0(x_i) \right| \right)} \right\}.$$

If

$$(A.11) \quad \sup_{x \in (x_i, \infty)} v^0(x) + \sum_{k=i}^N (v^0(x_{k-}) - v^0(x_{k+})) + \sum_{k=i+1}^N \left((x_I^k - x_k) \left| \frac{d^-}{dx} v^0(x_k) \right| \right) < v^0(x_{i-}) + (x_I^i - x_i) \frac{d^-}{dx} v^0(x_i)$$

then we define $x_R^i := x_i$. Otherwise, we let x_R^i be defined as the solution to

$$(A.12) \quad v^0(x_i-) + (x_I^i - x_i) \frac{d^-}{dx} v^0(x_i) + (x_R^i - x_i) M = \\ \sup_{x \in (x_i, \infty)} v^0(x) + \sum_{k=i}^N (v^0(x_k-) - v^0(x_k+)) \\ + \sum_{k=i+1}^N \left((x_I^k - x_k) \left| \frac{d^-}{dx} v^0(x_k) \right| \right).$$

If

$$(A.13) \quad \inf_{x \in (-\infty, x_i)} v^0(x) - \sum_{k=1}^{i-1} (v^0(x_k-) - v^0(x_k+)) \\ - \sum_{k=3}^i \left((x_J^{k-1} - x_{k-2}) \left| \frac{d^+}{dx} v^0(x_{k-2}) \right| \right) > v^0(x_{i-1}+) + (x_J^i - x_{i-1}) \frac{d^+}{dx} v^0(x_{i-1})$$

then we define $x_L^i := x_J^i$. Otherwise, we let x_L^i be defined as the solution to

$$(A.14) \quad v^0(x_{i-1}+) + (x_J^i - x_{i-1}) \frac{d^+}{dx} v^0(x_{i-1}) + (x_L^i - x_J^i) M = \\ \inf_{x \in (-\infty, x_i)} v^0(x) - \sum_{k=1}^{i-1} (v^0(x_k-) - v^0(x_k+)) - \sum_{k=3}^i \left((x_J^{k-1} - x_{k-2}) \left| \frac{d^+}{dx} v^0(x_{k-2}) \right| \right).$$

Finally, we define

$$(A.15) \quad v_{N+1}^0(x) := \begin{cases} \min \left\{ v^0(x_N+) + (x_J^N - x_N) \frac{d^+}{dx} v^0(x_N), \right. \\ \left. \inf_{x \in (-\infty, x_N)} v^0(x) - \sum_{k=1}^N (v^0(x_k-) - v^0(x_k+)) \right. \\ \left. - \sum_{k=3}^{N+1} \left((x_J^{k-1} - x_{k-2}) \left| \frac{d^+}{dx} v^0(x_{k-2}) \right| \right) \right\}, & \text{if } x < x_L^N, \\ v^0(x_N+) + (x_J^N - x_N) \frac{d^+}{dx} v^0(x_N) + (x - x_J^N) M, & \text{if } x_L^N < x < x_J^N, \\ v^0(x_N+) + (x - x_N) \frac{d^+}{dx} v^0(x_N), & \text{if } x_J^N < x < x_N, \\ v^0(x), & \text{if } x > x_N. \end{cases}$$

The number x_J^N is defined as

$$(A.16) \quad x_J^N := x_N - \min \left\{ 1, \frac{v^0(x_N-) - v^0(x_N+)}{2 \left(M + \left| \frac{d^+}{dx} v^0(x_N) \right| \right)} \right\}.$$

If

$$(A.17) \quad \inf_{x \in (-\infty, x_N)} v^0(x) - \sum_{k=1}^N (v^0(x_{k-}) - v^0(x_{k+})) \\ - \sum_{k=3}^{N+1} \left((x_J^{k-1} - x_{k-2}) \left| \frac{d+}{dx} v^0(x_{i-2}) \right| \right) > v^0(x_{N+}) + (x_J^N - x_N) \frac{d+}{dx} v^0(x_N)$$

then we define $x_L^N := x_J^N$. Otherwise, we let x_L^N be defined as the solution to

$$(A.18) \quad v^0(x_{N+}) + (x_J^N - x_N) \frac{d+}{dx} v^0(x_N) + (x_L^N - x_N) M = \\ \inf_{x \in (-\infty, x_N)} v^0(x) - \sum_{k=1}^N (v^0(x_{k-}) - v^0(x_{k+})) \\ - \sum_{k=3}^{N+1} \left((x_J^{k-1} - x_{k-2}) \left| \frac{d+}{dx} v^0(x_{i-2}) \right| \right).$$

Note that by construction, the v_i^0 are Lipschitz-continuous, satisfy $\inf_x \partial_x v_i^0 \geq \inf_x \partial_x v^0$, and verify

$$(A.19) \quad v_i^0(x) - v_{i+1}^0(x) \geq \frac{1}{2} (v^0(x_{i-}) - v^0(x_{i+}))$$

for $i = 1, \dots, N$ and all $x \in \mathbb{R}$.

Finally, if v^0 contains no discontinuities, then $N = 0$ and we define $v_1^0 := v^0$.

A.2. Proof of Lemma 4.3. We now prove (4.17).

We perform a similar derivation as outlined in [35, Lemma 3.2].

Note that \hat{u}_1 is Lipschitz and so we have the exact equalities,

$$(A.20) \quad \partial_t(\hat{u}_1(x, t)) + \partial_x(A(\hat{u}_1(x, t))) = R_1(x, t),$$

$$(A.21) \quad \partial_t(\eta(\hat{u}_1(x, t))) + \partial_x(q(\hat{u}_1(x, t))) = \eta'(\hat{u}_1(x, t))R_1(x, t).$$

Recall (3.3), i.e. $A(u|\hat{u}_1) := A(u) - A(\hat{u}_1) - A'(\hat{u}_1)(u - \hat{u}_1)$. In particular, $A(u|\hat{u}_1)$ is locally quadratic in $u - \hat{u}_1$.

Fix any positive, Lipschitz-continuous test function $\phi: \mathbb{R} \times [0, T) \rightarrow \mathbb{R}$ with compact support. Then, we use that \hat{u}_2 satisfies the entropy inequality in a distributional sense:

$$(A.22) \quad \int_0^T \int_{-\infty}^{\infty} \left[\partial_t \phi(\eta(\hat{u}_2(x, t))) + \partial_x \phi(q(\hat{u}_2(x, t))) \right] dx dt + \int_{-\infty}^{\infty} \phi(x, 0) \eta(\hat{u}_2^0(x)) dx \\ \geq - \int_0^T \int_{-\infty}^{\infty} \phi \eta'(\hat{u}_2(x, t)) R_2(x, t) dx dt.$$

We also view (A.21) as a distributional equality:

$$(A.23) \quad \int_0^T \int_{-\infty}^{\infty} \left[\partial_t \phi(\eta(\hat{u}_1(x, t))) + \partial_x \phi(q(\hat{u}_1(x, t))) \right] dx dt + \int_{-\infty}^{\infty} \phi(x, 0) \eta(\hat{u}_1^0(x)) dx \\ = - \int_0^T \int_{-\infty}^{\infty} \phi \eta'(\hat{u}_1(x, t)) R_1(x, t) dx dt.$$

To get (A.23), we do integration by parts on (A.21).

We subtract (A.23) from (A.22), to get

$$(A.24) \quad \int_0^T \int_{-\infty}^{\infty} [\partial_t \phi \eta(\hat{u}_2(x, t) | \hat{u}_1(x, t)) + \partial_x \phi q(\hat{u}_2(x, t); \hat{u}_1(x, t))] dx dt \\ + \int_{-\infty}^{\infty} \phi(x, 0) \eta(\hat{u}_2^0(x) | \hat{u}_1^0(x)) dx \\ \geq - \int_0^T \int_{-\infty}^{\infty} \left(\partial_t \phi \eta'(\hat{u}_1(x, t)) [\hat{u}_2(x, t) - \hat{u}_1(x, t)] \right. \\ \left. + \partial_x \phi \eta'(\hat{u}_1(x, t)) [A(\hat{u}_2(x, t)) - A(\hat{u}_1(x, t))] \right) dx dt \\ - \int_{-\infty}^{\infty} \phi(x, 0) \eta'(\hat{u}_1^0(x)) [\hat{u}_2^0(x) - \hat{u}_1^0(x)] dx \\ + \int_0^T \int_{-\infty}^{\infty} \phi \left[\eta'(\hat{u}_1(x, t)) R_1(x, t) - \eta'(\hat{u}_2(x, t)) R_2(x, t) \right] dx dt$$

The function \hat{u}_2 is an entropy solution to the scalar conservation law. Thus, for every Lipschitz-continuous test function $\Phi: \mathbb{R} \times [0, T] \rightarrow \mathbb{R}$ with compact support,

$$(A.25) \quad \int_0^T \int_{-\infty}^{\infty} \left[\partial_t \Phi \hat{u}_2 + \partial_x \Phi A(\hat{u}_2) \right] dx dt + \int_{-\infty}^{\infty} \Phi(x, 0) \hat{u}_2^0(x) dx = - \int_0^T \int_{-\infty}^{\infty} \Phi R_2(x, t) dx dt.$$

We also can rewrite (A.20) in a distributional way,

$$(A.26) \quad \int_0^T \int_{-\infty}^{\infty} \left[\partial_t \Phi \hat{u}_1(x, t) + \partial_x \Phi A(\hat{u}_1(x, t)) \right] dx dt + \int_{-\infty}^{\infty} \Phi(x, 0) \hat{u}_1^0(x) dx \\ = - \int_0^T \int_{-\infty}^{\infty} \Phi R_1(x, t) dx dt.$$

To prove (A.26), we again do integration by parts twice. Then, we can choose

$$(A.27) \quad \Phi = \phi \eta'(\hat{u}_1)$$

and subtract (A.26) from (A.25). This yields,

$$(A.28) \quad \int_0^T \int_{-\infty}^{\infty} \left[\partial_t [\phi \eta'(\hat{u}_1(x, t))] [\hat{u}_2(x, t) - \hat{u}_1(x, t)] \right. \\ \left. + \partial_x [\phi \eta'(\hat{u}_1(x, t))] [A(\hat{u}_2(x, t)) - A(\hat{u}_1(x, t))] \right] dx dt \\ + \int_{-\infty}^{\infty} \phi(x, 0) \eta'(\hat{u}_1^0(x)) [\hat{u}_2^0(x) - \hat{u}_1^0(x)] dx \\ = \int_0^T \int_{-\infty}^{\infty} \phi \eta'(\hat{u}_1(x, t)) \left[R_1(x, t) - R_2(x, t) \right] dx dt.$$

Recall \hat{u}_1 is a classical solution and verifies (A.20). Thus,

$$(A.29) \quad \partial_t (\eta'(\hat{u}_1(x, t))) = \partial_t \hat{u}_1(x, t) \eta''(\hat{u}_1(x, t)) \\ = \left(-\partial_x \hat{u}_1(x, t) [A'(\hat{u}_1(x, t))] + R_1(x, t) \right) \eta''(\hat{u}_1(x, t)) \\ = R_1(x, t) \eta''(\hat{u}_1(x, t)) - \partial_x \hat{u}_1(x, t) \eta''(\hat{u}_1(x, t)) A'(\hat{u}_1(x, t)).$$

Thus, by (A.29) and the definition of the relative flux in (3.3),

$$(A.30) \quad \partial_t (\eta'(\hat{u}_1(x, t))) [\hat{u}_2(x, t) - \hat{u}_1(x, t)] + \partial_x (\eta'(\hat{u}_1(x, t))) [A(\hat{u}_2(x, t)) - A(\hat{u}_1(x, t))] \\ = \partial_x \hat{u}_1(x, t) \eta''(\hat{u}_1(x, t)) A(\hat{u}_2(x, t)) \hat{u}_1(x, t) + R_1(x, t) \eta''(\hat{u}_1(x, t)) [\hat{u}_2(x, t) - \hat{u}_1(x, t)].$$

We combine (A.24), (A.28), and (A.30) to get (4.17).

REFERENCES

- [1] Alberto Bressan. *Hyperbolic systems of conservation laws. The one-dimensional Cauchy problem*, volume 20. Oxford: Oxford University Press, 2000.
- [2] Alberto Bressan, Maria Teresa Chiri, and Wen Shen. A posteriori error estimates for numerical solutions to hyperbolic conservation laws. *Arch. Ration. Mech. Anal.*, 241(1):357–402, 2021.
- [3] Alberto Bressan, Graziano Crasta, and Benedetto Piccoli. Well-posedness of the Cauchy problem for $n \times n$ systems of conservation laws. *Mem. Amer. Math. Soc.*, 146(694):viii+134, 2000.
- [4] Alberto Bressan and Marta Lewicka. A uniqueness condition for hyperbolic systems of conservation laws. *Discrete Contin. Dynam. Systems*, 6(3):673–682, 2000.
- [5] Geng Chen, Sam G. Krupa, and Alexis F. Vasseur. Uniqueness and weak-BV stability for 2×2 conservation laws. *Arch. Ration. Mech. Anal.*, 246(1):299–332, 2022.
- [6] Elisabetta Chiodaroli, Camillo De Lellis, and Ondřej Kreml. Global ill-posedness of the isentropic system of gas dynamics. *Comm. Pure Appl. Math.*, 68(7):1157–1190, 2015.
- [7] Bernardo Cockburn. Continuous dependence and error estimation for viscosity methods. *Acta Numerica*, 12:127–180, 2003.
- [8] Andres A. Contreras Hip and Xavier Lamy. On the L^2 stability of shock waves for finite-entropy solutions of Burgers. *J. Differential Equations*, 301:236–265, 2021.
- [9] Constantine M. Dafermos. The second law of thermodynamics and stability. *Arch. Rational Mech. Anal.*, 70(2):167–179, 1979.
- [10] Constantine M. Dafermos. Stability of motions of thermoelastic fluids. *Journal of Thermal Stresses*, 2(1):127–134, 1979.
- [11] Constantine M. Dafermos. *Hyperbolic conservation laws in continuum physics*, volume 325 of *Grundlehren der Mathematischen Wissenschaften [Fundamental Principles of Mathematical Sciences]*. Springer-Verlag, Berlin, fourth edition, 2016.
- [12] Camillo De Lellis, Felix Otto, and Michael Westdickenberg. Minimal entropy conditions for Burgers equation. *Quart. Appl. Math.*, 62(4):687–700, 2004.
- [13] Camillo De Lellis and László Székelyhidi, Jr. On admissibility criteria for weak solutions of the Euler equations. *Arch. Ration. Mech. Anal.*, 195(1):225–260, 2010.
- [14] Andreas Dedner and Jan Giesselmann. A posteriori analysis of fully discrete method of lines discontinuous Galerkin schemes for systems of conservation laws. *SIAM J. Numer. Anal.*, 54(6):3523–3549, 2016.
- [15] Andreas Dedner, Charalambos Makridakis, and Mario Ohlberger. Error control for a class of Runge-Kutta discontinuous Galerkin methods for nonlinear conservation laws. *SIAM J. Numer. Anal.*, 45(2):514–538, 2007.
- [16] Ronald J. DiPerna. Uniqueness of solutions to hyperbolic conservation laws. *Indiana Univ. Math. J.*, 28(1):137–188, 1979.
- [17] Lawrence C. Evans. *Partial differential equations*, volume 19 of *Graduate Studies in Mathematics*. American Mathematical Society, Providence, RI, second edition, 2010.
- [18] Eduard Feireisl, Mária Lukáčová-Medvid’ová, and Hana Mizerová. Convergence of finite volume schemes for the Euler equations via dissipative measure-valued solutions. *Found. Comput. Math.*, 20(4):923–966, 2020.
- [19] Ulrik Skre Fjordholm, Kjetil Olsen Lye, Siddhartha Mishra, and Franziska Weber. Statistical solutions of hyperbolic systems of conservation laws: numerical approximation. *Math. Models Methods Appl. Sci.*, 30(3):539–609, 2020.
- [20] Jan Giesselmann, Charalambos Makridakis, and Tristan Pryer. A posteriori analysis of discontinuous Galerkin schemes for systems of hyperbolic conservation laws. *SIAM J. Numer. Anal.*, 53(3):1280–1303, 2015.
- [21] Jan Giesselmann and Aleksey Sikstel. A-posteriori error estimates for systems of hyperbolic conservation laws. *arXiv e-prints*, page arXiv:2305.01340, May 2023.

- [22] Edwige Godlewski and Pierre-Arnaud Raviart. *Numerical approximation of hyperbolic systems of conservation laws*, volume 118. New York, NY: Springer, 1996.
- [23] William Golding. Unconditional regularity and trace results for the isentropic Euler equations with $\gamma = 3$. *arXiv e-prints*, page arXiv:2207.05821, July 2022.
- [24] William Golding, Sam G. Krupa, and Alexis F. Vasseur. Sharp a-contraction estimates for small extremal shocks. *arXiv e-prints*, page arXiv:2012.09261, December 2020. To appear in *Journal of Hyperbolic Differential Equations*.
- [25] Laurent Gosse and Charalambos Makridakis. Two a posteriori error estimates for one-dimensional scalar conservation laws. *SIAM J. Numer. Anal.*, 38(3):964–988, 2000.
- [26] Ralf Hartmann and Paul Houston. Adaptive discontinuous Galerkin finite element methods for the compressible Euler equations. *J. Comput. Phys.*, 183(2):508–532, 2002.
- [27] Jan S. Hesthaven. *Numerical methods for conservation laws. From analysis to algorithms*, volume 18. Philadelphia, PA: Society for Industrial and Applied Mathematics (SIAM), 2018.
- [28] Carl Johan Peter Johansson and Riccardo Tione. T_5 configurations and hyperbolic systems. *Communications in Contemporary Mathematics*, 0(0):2250081, 2023.
- [29] Moon-Jin Kang and Alexis F. Vasseur. Criteria on contractions for entropic discontinuities of systems of conservation laws. *Arch. Ration. Mech. Anal.*, 222(1):343–391, 2016.
- [30] Dietmar Kröner. *Numerical schemes for conservation laws*. Chichester: Wiley; Stuttgart: Teubner, 1997.
- [31] Dietmar Kröner and Mario Ohlberger. A posteriori error estimates for upwind finite volume schemes for nonlinear conservation laws in multi dimensions. *Math. Comput.*, 69(229):25–39, 2000.
- [32] Sam G. Krupa. Criteria for the a-contraction and stability for the piecewise-smooth solutions to hyperbolic balance laws. *Commun. Math. Sci.*, 18(6):1493–1537, 2020.
- [33] Sam G. Krupa and László Székelyhidi, Jr. Nonexistence of T_4 configurations for hyperbolic systems and the Liu entropy condition. *arXiv e-prints*, page arXiv:2211.14239, November 2022.
- [34] Sam G. Krupa and Alexis F. Vasseur. On uniqueness of solutions to conservation laws verifying a single entropy condition. *J. Hyperbolic Differ. Equ.*, 16(1):157–191, 2019.
- [35] Sam G. Krupa and Alexis F. Vasseur. Stability and uniqueness for piecewise smooth solutions to a nonlocal scalar conservation law with applications to Burgers-Hilbert equation. *SIAM J. Math. Anal.*, 52(3):2491–2530, 2020.
- [36] Stanislav Nikolaevich Kruzhkov. First order quasilinear equations in several independent variables. *Mat. Sb. (N.S.)*, 81 (123):228–255, 1970. English transl. in *Math. USSR, Sb.*, 10:217–243, 1970.
- [37] Marc Laforest. A posteriori error estimate for front-tracking: Systems of conservation laws. *SIAM J. Math. Anal.*, 35(5):1347–1370, 2004.
- [38] Marc Laforest. An a posteriori error estimate for Glimm’s scheme. In *Hyperbolic problems. Theory, numerics and applications. Proceedings of the 11th international conference on hyperbolic problems, Ecole Normale Supérieure, Lyon, France, July 17–21, 2006*, pages 643–651. Berlin: Springer, 2008.
- [39] Philippe G. LeFloch. *Hyperbolic systems of conservation laws*. Lectures in Mathematics ETH Zürich. Birkhäuser Verlag, Basel, 2002. The theory of classical and nonclassical shock waves.
- [40] Nicholas Leger and Alexis F. Vasseur. Relative entropy and the stability of shocks and contact discontinuities for systems of conservation laws with non-BV perturbations. *Archive for Rational Mechanics and Analysis*, 201(1):271–302, 2011.
- [41] Randall J. LeVeque. *Finite volume methods for hyperbolic problems*. Cambridge: Cambridge University Press, 2002.
- [42] Andrew Lorent and Guanying Peng. On the rank-1 convex hull of a set arising from a hyperbolic system of Lagrangian elasticity. *Calc. Var. Partial Differential Equations*, 59(5):Paper No. 156, 36, 2020.
- [43] Charalambos Makridakis. Space and time reconstructions in a posteriori analysis of evolution problems. *ESAIM, Proc.*, 21:31–44, 2007.
- [44] Ol’ga Arsen’evna Oleĭnik. Discontinuous solutions of non-linear differential equations. *Uspehi Mat. Nauk (N.S.)*, 12(3(75)):3–73, 1957. English transl. in *Amer. Math. Soc. Transl. (2)*, 26:95–172, 1963.

- [45] Evgueni Yu. Panov. Uniqueness of the solution of the Cauchy problem for a first order quasilinear equation with one admissible strictly convex entropy. *Mat. Zametki*, 55(5):116–129, 159, 1994. English transl. in *Mathematical Notes*, 55(5):517–525, 1994.
- [46] Denis Serre. *Systems of conservation laws. 1*. Cambridge University Press, Cambridge, 1999. Hyperbolicity, entropies, shock waves. Translated from the 1996 French original by I. N. Sneddon.
- [47] Denis Serre and Alexis F. Vasseur. L^2 -type contraction for systems of conservation laws. *J. Éc. polytech. Math.*, 1:1–28, 2014.
- [48] Stefan Ulbrich. A sensitivity and adjoint calculus for discontinuous solutions of hyperbolic conservation laws with source terms. *SIAM J. Control Optim.*, 41(3):740–797, 2002.
- [49] Alexis F. Vasseur. Time regularity for the system of isentropic gas dynamics with $\gamma = 3$. *Comm. Partial Differential Equations*, 24(11-12):1987–1997, 1999.
- [50] Alexis F. Vasseur. Recent results on hydrodynamic limits. *Handbook of Differential Equations: Evolutionary Equations*, 4:323 – 376, 2008.
- [51] Qiang Zhang and Chi-Wang Shu. Error estimates to smooth solutions of Runge-Kutta discontinuous Galerkin method for symmetrizable systems of conservation laws. *SIAM J. Numer. Anal.*, 44(4):1703–1720, 2006.

(Jan Giesselmann)

DEPARTMENT OF MATHEMATICS, TECHNISCHE UNIVERSITÄT DARMSTADT
64293 DARMSTADT, GERMANY

Email address: `giesselmann@mathematik.tu-darmstadt.de`

(Sam G. Krupa)

MAX PLANCK INSTITUTE FOR MATHEMATICS IN THE SCIENCES,
04103 LEIPZIG, GERMANY

Email address: `Sam.Krupa@mis.mpg.de`